# FLEXURAL BEHAVIOR OF BUILT-UP I-BEAMS MADE FROM HYBRID-FIBER SIFCON PLATES

By

MARKO IVAN LYSZYK

A thesis submitted to the

Graduate School-New Brunswick

Rutgers, The State University of New Jersey

In partial fulfillment of the requirements

For the degree of

Master of Science

Graduate Program in Civil and Environmental Engineering

Written under the direction of

Dr. Husam Najm

And approved by

_____

_____

_____

New Brunswick, New Jersey

January 2017

ABSTRACT OF THE THESIS

Flexural Behavior of Built-up I-beams Made from Hybrid-Fiber SIFCON Plates

by MARKO IVAN LYSZYK

Thesis Director:

Dr. Husam Najm

Flexural members such as beams are typically made from wood, concrete, prestressed concrete, steel, and FRP. Built-up I-beams made from thin fiber reinforced plates are another group of beams that can provide an alternative to steel and reinforced concrete beams for various uses. The purpose of this research is to evaluate the potential of using built-up I-beams made of thin SIFCON plates in structural applications such as beams, lintels, and others. Several built-up I-beams were prepared and tested in flexure. The thin SIFCON plates were made with straight fibers (brass coated microfibers), hooked fibers, and a hybrid using both fibers. The plates were connected using organic epoxy resin with and without thin aluminum angles and with basalt fabrics using an inorganic epoxy. The built-up I-beams were tested in flexure to evaluate bending strength and their failure modes such flange yielding, lateral torsional buckling, and web shear failure. The built-up I-beams were also strengthened using in tension using basalt fabrics to improve their tensile strength. The results showed that the use of basalt fabrics increases the flexural capacity of the built-up beams and can be used for retrofitting of these beams. The results of this study showed that these beams can be fabricated and can be used as structural members subjected to bending. The study also provided test data and information on the

feasibility of these types of beams, methods of connecting plate components, their performance in flexure and their failure modes.

ACKNOWLEDGEMENTS

The author would like to acknowledge various individuals whose contribution was beneficial to this study. I would like to thank Dr. Husam Najm for helping and guiding me through the research process; Alaa Abd Ali for showing me the proper procedure for SIFCON mixing, beam fabrication with concrete plates and basalt fiber sheet attachment; Sam Boukaram, Jaslin Singh, Konrad Kosiak and Helen He for helping make molds, concrete samples and test; David Caronia and Adi Abu Obaidah for answering questions relating to concrete casting and general research procedure; Joseph Pluta and Craig Nowlen for constructing the steel simply supported system for the flexural testing; my parents for the love and support.

TABLE OF CONTENTS

ABSTRACT OF THE THESIS: ..... ii

ACKNOWLEDGEMENTS ..... iv

TABLE OF CONTENTS ..... v

LIST OF TABLES ..... ix

LIST OF FIGURES ..... x

CHAPTER 1 – INTRODUCTION ..... 1

CHAPTER 2 – LITERATURE REVIEW ..... 4

2.1 Concrete Reinforced with Steel Fibers ..... 4

2.2 Mechanical Properties of SIFCON ..... 10

2.3 Applications of SIFCON ..... 13

2.4 Aluminum Plates as External Shear Reinforcement ..... 16

2.5 Basalt Fibers as External Flexural Reinforcement ..... 17

CHAPTER 3 – EXPERIMENTAL PROGRAM ..... 20

3.1 Glossary and Abbreviations ..... 21

3.2 Construction of Plate Molds ..... 22

3.3 Concrete Material and Mixing Procedure ..... 24

3.3.1 Concrete Materials ..... 24

3.3.2 Batching of Materials ..... 25

3.3.3 General Mixing Procedure ..... 29

3.3.4 Mixing Procedure with Premixed Fibers ..... 33

3.4 Casting and Demolding ..... 37

3.4.1 Plate Casting ..... 37

3.4.2 Plate Demolding....41
3.4.3 Cylinder Casting....43
3.4.4 Cylinder Demolding....45
3.5 Beam Fabrication....46
3.5.1 Overview....46
3.5.2 Shear Reinforcement Design....50
3.5.3 Aluminum Angle Preparation....51
3.5.4 Epoxy Mixing Procedure....52
3.5.5 Applying Epoxy to Concrete Plates....54
3.5.6 First Flange – Web Attachment....56
3.5.7 Second Flange – Web Attachment....57
3.5.8 Application of FRP as Shear Reinforcement....57
3.5.8.1 Preparation of FRP....57
3.5.8.2 Batching and Mixing of Nano-Inorganic Composite....58
3.5.8.3 Application of FRP onto Concrete Surface....59
3.5.9 Decision on Shear Reinforcement Material....62
3.5.10 Post-beam Fabrication Aluminum Angle Attachment....63
3.5.11 Application of FRP to Bottom of Tension Flange....64
3.6 Testing....66
3.6.1 Compression Test....66
3.6.2 Elastic Modulus Test....68
3.6.2.1 Overview....68
3.6.2.2 Placement of Elastic Modulus Cage onto Cylinder....68

3.6.2.3 Elastic Modulus Test Procedure ....70
3.6.3 Flexural Test ....72
3.6.3.1 Beam Preparation....72
3.6.3.2 Test Setup....72
3.6.3.3 First Group Test Procedure....73
3.6.3.4 First Group Flexural Test Observations....74
3.6.3.5 Second Group Test Procedure ....75
3.6.3.6 Third Group Test Procedure ....75
3.7 Tension Test & Three-Dimensional Mold Attempts ....79
3.7.1 Tension Test....79
3.7.1.1 First Method for Tension Samples....79
3.7.1.2 Second Method for Tension Samples (with wooden grips) ....80
3.7.1.3 Third Method for Tension Samples ....81
3.7.1.4 Fourth Method for Tension Sample (proposed, not implemented) ....85
3.7.2 Three Dimensional Mold and Beam ....86
3.7.2.1 Background ....86
3.7.2.2 Construction of Mold....86
3.7.2.3 Beam Casting....88
3.7.2.4 Beam Demolding ....90
3.7.2.5 Comments ....91

CHAPTER 4 - RESULTS....93
4.1 Compressive Strength....93
4.2 Elastic Modulus in Compression....95
4.3 Flexural Behavior....97
4.3.1 Beams without External Flexural Reinforcement Tested to Failure....98
4.3.2 Beams Tested to First Crack vs. to Failure with External Flexural Reinforcement....113
4.3.3 Beams with External Flexural Reinforcement Tested to Failure....126
4.3.4 Beams with and without External Flexural Reinforcement Tested to Failure....141
4.3.5 Flexural Behavior Summary....147
CHAPTER 5 - DISCUSSION....152
5.1 Compression Tests....152
5.2 Flexural Tests....156
5.2.1 Beams without External Flexural Reinforcement....157
5.2.2 Beams with External Flexural Reinforcement....159
5.2.3 Load-deformation Curves of Beams with and without External Flexural Reinforcement....161
5.2.4 Effect of External Flexural Reinforcement....163
CHAPTER 6 – CONCLUSIONS AND RECOMENDATIONS....165
6.1 Conclusions....165
6.2 Recommendations for Future Research....166
REFEREENCES....167

LIST OF TABLES

Table 3-1: Mix design.....24

Table 4-1: Compressive Strength of Concrete Cylinders with Various Fibers .....94

Table 4-2: Compressive Elastic Modulus of Concrete Cylinders with Various Fibers ....96

Table 4-3: Mechanical Properties Summary of Beams without External Flexural Reinforcement..... 111-112

Table 4-4: Area under Load-Deformation Curves of Beams without External Flexural Reinforcement.....113

Table 4-5: Mechanical Properties Summary of Beams with External Flexural Reinforcement..... 139-140

Table 4-6: Area under Load-Deformation Curves of Beams with External Flexural Reinforcement.....141

Table 4-7: Elastic Limit – Ultimate Load Ratio and Maximum Deformation .....148

Table 4-8: Effect of External Flexural Reinforcement on Ultimate Load.....149

Table 4-9: Effect of External Flexural Reinforcement on Area under Load-Deformation Curve.....151

LIST OF FIGURES

Figure 3-1: Wooden plate molds....24

Figure 3-2: Batching cement....26

Figure 3-3: Weighing required amount of sand....27

Figure 3-4: Weighing required amount of superplastizer....28

Figure 3-5 Adding sand into mixing bowl....30

Figure 3-6: Adding cement into mixing bowl....30

Figure 3-7: Premixing superplastizer with water....31

Figure 3-8: Creating voids prior for liquid to penetrate prior to wet mixing....32

Figure 3-9: Hand mixing of mortar mix....33

Figure 3-10: Adding steel fibers to mixing bowl....34

Figure 3-11: Adding small amount of superplastizer-water solution....36

Figure 3-12: Placing 50 mm hooked end fibers in wooden molds prior to mixing....38

Figure 3-13: Casting plate molds....39

Figure 3-14: Trowel used to provide a smooth finish of the plate sample....40

Figure 3-15: Demolding plate molds....42

Figure 3-16: Removing plate sample by hand....43

Figure 3-17: Adding 50 mm steel fibers into cylinder....44

Figure 3-18: Concrete plates in curing room....46

Figure 3-19: Concrete plate samples in temperature controlled lab environment....47

Figure 3-20: Delamination of nano-inorganic composite evident at right end of beam....47

Figure 3-21: Marked lines indicating area of epoxy application....49

Figure 3-22: Steel brush producing a rough surface on the concrete plate....50

Figure 3-23: Grinding of aluminum angle .....51
Figure 3-24: Batching of two components of epoxy .....52
Figure 3-25: Mixing two components of epoxy together .....53
Figure 3-26: Applying epoxy to concrete plate .....55
Figure 3-27: First flange to web attachment .....56
Figure 3-28: Bricks and wood blocks stabilizing beam configuration .....57
Figure 3-29: Lines and tape applied to basalt fiber.....58
Figure 3-30: Adding materials into blender.....59
Figure 3-31: Brushing nano-inorganic composite onto basalt fiber .....60
Figure 3-32: Applying slight downward pressure on basalt fiber.....61
Figure 3-33: Applying epoxy to flange for aluminum angle attachment.....63
Figure 3-34: Holding the aluminum angle in place for 30 seconds .....64
Figure 3-35: Roller removing excess nano-inorganic composite from basalt fiber.....65
Figure 3-36: Aligning basalt fiber in the middle of the bottom flange .....66
Figure 3-37: Concrete cylinder in compression machine cage .....67
Figure 3-38: Attachment of elastic modulus cage .....69
Figure 3-39: Cylinder in compression cage with elastic modulus cage.....71
Figure 3-40: Simply supported system with two point supports .....73
Figure 3-41: Positioning of beam onto point supports.....74
Figure 3-42: First Group after failure .....75
Figure 3-43: Extent of cracking for first phase of testing .....76
Figure 3-44: Shear and flexural cracks present in beam during testing.....77
Figure 3-45: Using a knife to cut the basalt fiber on bottom flange .....78

Figure 3-46: Removing a strip of basalt fiber ..... 79
Figure 3-47: Intermediate grip made out of wood ..... 80
Figure 3-48: Design of wooden intermediate grips ..... 81
Figure 3-49: Design of tension samples for third method ..... 82
Figure 3-50: Molds for tension samples in third method ..... 83
Figure 3-51: Failure occurred near grips for third method of tension test ..... 84
Figure 3-52: Analog load display of tension machine ..... 85
Figure 3-53: Three dimensional mold sketch ..... 87
Figure 3-54: Placing concrete in top flange and web ..... 89
Figure 3-55: Removing screws and brackets from end of web ..... 90
Figure 3-56: Misaligned web with bottom flange ..... 91
Figure 3-57: Cracks that occurred during dry curing ..... 92
Figure 4-1: Average Compressive Strengths of Cylinders ..... 95
Figure 4-2: Average Elastic Moduli of Cylinders in Compression ..... 97
Figure 4-3: Beams Tested to Failure without External Flexural Reinforcement ..... 99-101
Figure 4-4: Load-Deformation Curves of Beams with 6 mm, 30 mm and 6 mm & 30 mm Steel Fibers ..... 102
Figure 4-5: Load-Deformation Curves of Beams with 13 mm, 50 mm and 13 mm & 50 mm Steel Fibers ..... 103
Figure 4-6: Load-Deformation Curves of Beams with Straight Steel Fibers ..... 104
Figure 4-7: Load-Deformation Curves of Beams with Hooked End Steel Fibers ..... 105
Figure 4-8: Load-Deformation Curves of Beams with Hybrid Steel Fibers ..... 106
Figure 4-9: Load-Deformation Curves of Beams with 6 mm, 50 mm and 13 mm &

50 mm Steel Fibers .....108

Figure 4-10: Load-Deformation Curves of Beams with 30 mm, 13 mm and 13 mm & 50 mm Steel Fibers .....109

Figure 4-11: Load-Deformation Curves of Beams with 13 mm, 50 mm and 6 mm & 30 mm Steel Fibers .....110

Figure 4-12: 6MM-0323-FRP6 Tested to First Crack ..... 114-115

Figure 4-13: Load-Deformation Curves of Beam with 6 mm Steel Fibers Tested to First Crack and to Failure with the Addition of External Flexural Reinforcement.....116

Figure 4-14: 30MM-1124-AL6 Tested to First Crack ..... 116-117

Figure 4-15: Load-Deformation Curves of Beam with 30 mm Steel Fibers Tested to First Crack and to Failure with the Addition of External Flexural Reinforcement.....118

Figure 4-16: 6&30MM-0323-AL4 Tested to First Crack ..... 118-119

Figure 4-17: Load-Deformation Curves of Beam with 6 mm & 30 mm Steel Fibers Tested to First Crack and to Failure with the Addition of External Flexural Reinforcement.....120

Figure 4-18: 13MM-0317-FRP4 Tested to First Crack ..... 120-121

Figure 4-19: Load-Deformation Curves of Beam with 13 mm Steel Fibers Tested to First Crack and to Failure with the Addition of External Flexural Reinforcement.....122

Figure 4-20: 50MM-1008-AL4 Tested to First Crack ..... 122-123

Figure 4-21: Load-Deformation Curves of Beam with 50 mm Steel Fibers Tested to First Crack and to Failure with the Addition of External Flexural Reinforcement.....124

Figure 4-22: 13&50MM-0318-AL6 Tested to First Crack ..... 124-125

Figure 4-23: Load-Deformation Curves of Beam with 13 mm & 50 mm Steel Fibers Tested to First Crack and to Failure with the Addition of External Flexural Reinforcement ..... 126
Figure 4-24: Beams Tested to Failure with External Flexural Reinforcement ..... 127-129
Figure 4-25: Load-Deformation Curves of Externally Reinforced Beams with 6 mm, 30 mm and 6 mm & 30 mm Steel Fibers ..... 130
Figure 4-26: Load-Deformation Curves of Externally Reinforced Beams with 13 mm, 50 mm and 13 mm & 50 mm Steel Fibers ..... 131
Figure 4-27: Load-Deformation Curves of Externally Reinforced Beams with Straight Steel Fibers ..... 132
Figure 4-28: Load-Deformation Curves of Externally Reinforced Beams with Hooked End Steel Fibers ..... 133
Figure 4-29: Load-Deformation Curves of Externally Reinforced Beams with Hybrid Steel Fibers ..... 134
Figure 4-30: Load-Deformation Curves of Externally Reinforced Beams with 6 mm, 50 mm and 13 mm & 50 mm Steel Fibers ..... 135
Figure 4-31: Load-Deformation Curves of Externally Reinforced Beams with 13 mm, 30 mm and 13 mm & 50 mm Steel Fibers ..... 137
Figure 4-32: Load-Deformation Curves of Externally Reinforced Beams with 13 mm, 50 mm and 6 mm & 30 mm Steel Fibers ..... 138
Figure 4-33: Load-Deformation Curves of Beams with 6 mm Steel fibers with and without External Reinforcement ..... 142

Figure 4-34: Load-Deformation Curves of Beams with 30 mm Steel fibers with and without External Reinforcement .....143
Figure 4-35: Load-Deformation Curves of Beams with 6 mm & 30 mm Steel fibers with and without External Reinforcement .....144
Figure 4-36: Load-Deformation Curves of Beams with 13 mm Steel fibers with and without External Reinforcement .....145
Figure 4-37: Load-Deformation Curves of Beams with 50 mm Steel fibers with and without External Reinforcement .....146
Figure 4-38: Load-Deformation Curves of Beams with 13 mm & 50 mm Steel fibers with and without External Reinforcement .....147

# CHAPTER 1: INTRODUCTION

Girders in bridge superstructures are typically made of steel, concrete, or prestressed concrete. Each material has its advantages and disadvantages and engineer needs to take that into design consideration. In some cases, choosing whether the girders are made out of steel or concrete also at times may rely on the desire of the client. Compared to concrete, steel can save more time in terms of fabrication as structural members do not need time to cure unlike their concrete girder counterparts. It is well-known that the composition of steel girders is more homogenous than concrete girders, with taking account the rebar, and this may attribute to its isotropic properties. The quality control of steel girder fabrication tends to be better than that of concrete girders as steel girders, as concrete girders require more on-site labor. It is easier to achieve longer spans with steel as a longer girder can be fabricated as well as splicing onsite.

Unlike concrete, steel can be recycled and reused to become a structural member again without losing much quality. Steel tends to be lighter than concrete as its cross sectional dimensions are smaller than that of concrete. Conversely, concrete has certain attributes that make it superior to steel. Though concrete can be mixed on site, back log may exist with steel manufacturers and therefore construction delays are possible. Concrete has greater resistance to high temperatures and fire, whereas steel is susceptible to both. Unlike steel, different shapes and forms of concrete can be fabricated depending on the shape of the formwork. Concrete tends to be more economic than steel. In this study, an alternate material is proposed. This material is known as slurry-infiltrated concrete or SIFCON for short. Although relatively a new material when compared to conventional concrete and steel, SIFCON has the potential to be made into structural

members whose cross-sections closely resemble that of rolled steel. Structural members composed of conventional reinforced concrete and prestressed concrete require clear covers, and such structural members have thicknesses much larger than steel structural members in order to fit in rebar and prestressing tendons. Conversely, SIFCON does not necessarily require rebar or prestressing strands as the fibers dispersed throughout the mix are the main contributors to the its tensile strength.

Due to the fact that SIFCON does not necessarily require rebar or prestressing strands leads to the notion utilizing structural members out of SIFCON forgoes facilitates construction as no rebar cage may be required, as well as cost of such labor and material is reduced, if not entirely eliminated. Furthermore, it may be easier to replace a damaged steel structural member with one made of SIFCON whose cross-sectional dimensions are similar to the steel structural member rather than with one made of conventional reinforced concrete or prestressed concrete. Having the cross-sectional dimensions closer in size to steel girders rather than conventional concrete girders and not requiring as much rebar, if any, allows structural members made out of SIFCON to be lighter than conventional concrete, while being less costly than steel. In this study, Beams and cylinders were tested to further delve the potential developments of utilizing structural members made out of SIFCON. The objectives are as follows:

- Compare the flexural behavior of built-up beams with varying steel fiber combinations.
- Compare the compressive strengths and elastic moduli in compression of cylinders with varying steel fiber combinations.

- Investigate the effect of external basalt fiber flexural reinforcement on cracked beams. This is done to emulate beam rehabilitation that may be done on site.
- Investigate the effect of using different types of external shear reinforcement.

# CHAPTER 2: LITERATURE REVIEW

## 1. Concrete Reinforced with Steel Fibers

Though a relatively new topic within the realm of concrete, extensive research has been conducted on fiber reinforced concrete. One of the most commonly-used materials for fibers is steel. Caggiano et al. (2012) investigated the effect of concrete reinforced with mixed steel fibers of different sizes in concrete specimens tested in compression and flexure, and the results were compared to plain concrete specimens. Cube specimens were used to determine the compressive strengths of the concrete with and without various mixed fiber combinations. It was evident from the compressive strengths that the specimens' strength with fibers did not differ greatly from those specimen without fibers. The 150 x 150 x 600 mm beams consisted of both 0.5% and 1% volume of various combinations of 33 mm and 50 mm hooked end steel fibers. A notch with a depth of 45 mm was made on the bottom of the concrete beams. The beams were then placed on two point supports with two concentrated loads being applied on top. The beams were loaded at a rate of 0.005 mm/min, and dedicated displacement transducers measured the displacements on both sides of the notch. It was evident that the amount of fibers influenced the first crack strength and entire post-cracking behavior (Caggiano et al., 2012). The results showed that the greater the percent volume of fibers, the greater the first crack load would be enhanced. Due to the fact the two of fibers were close in geometry and material, the fiber combination had little effect on the behavior of the concrete (Caggiano et al., 2012). It was suggested that future research is needed to investigate mixing fibers of different materials and geometry (Caggiano et al., 2012).

Shahidan et al. (2015) tested fiber reinforced concrete cubes with 0.5%, 1% and 1.5% volume of hooked end steel fibers. The cubes measured 100 x 100 x 100 mm, and

the sizes of steel fibers included those with lengths of 33 mm and 50 mm. The concrete cubes were tested after 7, 14 and 28 days of moist curing. It was concluded that the specimen with 1% volume of 33 mm fibers at 28 days had the highest compressive strength. The specimens with 33 mm fibers overall had higher compressive strengths than the specimens with 50 mm fibers. This was most likely due to the fact that the smaller fibers were more able to occupy voids and it was easier for the concrete to compact (Shahidan et al., 2015). The highest compressive strength out of the specimens with 50 mm steel fibers required the fibers to occupy 0.5% of the volume.

Pajak and Ponikiewski (2013) observed the comparison between self-compacting concrete reinforced with steel fibers and normally vibrated concrete. Seventeen beams of square cross sections were cast with fiber volume fractions of 0.5%, 1% and 1.5%. The fibers included 12.5 mm straight steel fibers and 30 mm hooked end steel fibers. Unlike Caggiano et al., the straight steel fibers and hooked end steel fibers were not mixed together. The beams measuring 150 x 150 x 550 mm with a 500 mm span were set on a servo-controlled electrohydraulic machine, and were subjugated to three-point bending. On the bottom of each beam, a 25 mm deep incision was made so that the crack mouth opening displacement could be measured with a clip gauge. LVDT sensors held by a steel frame were used to measure the midspan deflection. Deflection at maximum load was larger for hooked end steel fibers than straight fibers. Another difference between the two fibers was that after the ultimate load was reached, the load-deflection curve of the specimens with straight steel fibers dropped suddenly, whereas the load-deflection curve of the specimens with hooked end steel fibers gradually decreased. An increase of percent volume of fibers indicated an increase of flexural tensile strength. Fracture energy

increases with increase of fibers and is higher for hooked end steel fibers than straight fibers (Pajak and Ponikiewski, 2013).

The effect of steel fibers on high strength concrete was sought after by Kotatkova and Reiterman (2014). Prismatic specimens with dimensions of 100 x 100 x 400 mm were tested in flexure in three-point bending. Cubes were tested to obtain compressive strength and split strength. Eighteen specimens for each test were made with 60 mm hooked end steel fibers, 30 mm hooked end steel fibers, 25 mm hooked end steel fibers and 40 mm flat end steel fibers. The results indicated that 60 mm steel fibers provided the specimens with the greatest toughness and highest fracture energy (Kotatkova and Reiterman, 2014). Conversely, the specimens with 30 mm steel fibers had higher flexural and split strength. Large fibers did not do much to stop the initial cracking, but they prevented the cracks from getting wider (Kotatkova and Reiterman, 2014). Smaller fibers tended to be more effective in preventing initial cracking, but once the crack reaches a certain width, the fibers were no longer effective (Kotatkova and Reiterman, 2014). The specimens with flattened ends proved to be less efficient than the specimens with hooked end steel fibers (Kotatkova and Reiterman, 2014).

Like Kotatkova and Reiterman, Jain and Singh (2013) examined the behavior of concrete in flexure reinforced with different types of steel fibers, however hooked end steel fibers and crimped steel fibers were used. The hooked end steel fibers were 35 mm and 60 mm long whereas the crimped steel fibers were 30 mm and 60 mm long. The fibers occupied 0.75% and 1.5% of the concrete volume. For some of the mixes with crimped steel fibers, the percent volume of fibers at times needed to be reduced to 1% and 1.2% due to difficulties that arose while mixing concrete and the crimped steel fibers

together (Jain and Singh, 2013). Specimens with dimensions of 180 x 180 x 600 mm and a span length of 540 mm were tested in four-point bending. A close-loop servo-controlled UTM was used to test the beams at a displacement rate of 0.1 mm/min until a 0.6 mm midspan deflection was reached, afterwards the displacement rate was increased to 0.25 mm/min. Flexural testing was completed once a midspan deflection of 3.6 mm was reached. In comparison to the crimped steel fibers, the hooked end steel fibers showed greater toughness due to better bonding to concrete than crimped steel fibers (Jain and Singh, 2013). This is relatable to Kotatkova and Reiterman's research where hooked end steel fibers proved to be more effective than flattened end steel fibers.

In the study conducted by Marar et al. (2016), eighty-four beams consisted of hooked end steel fibers with aspect ratios of 65 and 80 that occupied 0.5%, 1% and 1.5% of the volume. The 100 x 100 x 300 mm beams were further divided into two series which differed by the grade of concrete used in each: C30 and C50. The grades of concrete differed only in water-cement ratios. These beams were tested on a four-point system, but since the shear strength was the main focus, the point load and point supports were set up different than that used to study flexural behavior. One of the point supports was at the end of the beam whereas the other point support was just off center of the beam. One of the point loads was at the opposite end of the beam whereas the other point load was just off center of the beam. Furthermore, each beam had an incision 20 mm deep and 3 mm wide on the top and bottom at midspan in order to ensure that shear failure would occur along the vertical plane intersected by these two incisions, and so that the cracks at both notches would propagate simultaneously (Marar et al., 2016). Based on the results, it was concluded that the higher amount of fiber volume fractions led to a

higher shear strength, and the aspect ratio had negligible effect on shear strength (Marar et al., 2016). Also, the higher the strength and fiber volume fraction, the larger influence the diameter of fibers had on shear strength (Marar et al., 2016).

Ni et al. (2015) examined the relationship between the flexural behavior of fiber reinforced concrete and the varying aspect ratios of hooked end steel fibers. Hooked end steel fibers with different lengths and aspect ratios were kept to 0.7% volume along with polypropylene fibers which accounted for 0.2% of the volume. Steel fibers with 60 mm length and 100 aspect ratio, 60 mm length and 67 aspect ratio, 35 mm length and 64 aspect ratio and 35 mm length and 39 aspect ratio were used. The polypropylene fibers had a length of 18 mm and aspect ratio of 692. A marble cutter was used to make an incision 25 mm deep and 3 mm wide at the middle of a vertical face of the beams. The beams, with a span length of 500 mm, were placed on a three-point bending system, and since the beams were to be loaded at a constant deflection rate, a servo-controlled electrohydraulic machine was operated in "closed loop." The test was not halted unless a midspan deflection of 3.5 mm or a load of 5 kN was reached. It was observed that the fracture energy was not influenced by the aspect ratio (Ni et al., 2014). With the sizes and type of steel fibers used in this study in mind, there was no relationship between proportionality limit and aspect ratio (Ni et al., 2014). It is worth to note that the fracture energy was largest when the fiber's aspect ratio was 67.

Uygunoglu (2008) studied the flexural behavior and microstructure of concrete reinforced with hooked end steel fibers. Steel fibers 30 mm and 60 mm in length occupied 0.2%, 0.4%, 0.6% and 0.8% of the volume. The beams measured 100 x 100 x 350 mm and were tested in flexure on a three-point system with a manually-controlled

machine. These beams were loaded until the first crack began to propagate which point the testing halted, and the crack width was measured. Afterwards, the cracked concrete was coated with gold. Part of the concrete was grinded down and glued to a glass slide to a thickness of 30 microns. A LEO VP-1431 scanning electron microscopy was used to visual inspect the steel fiber-cement interface and polarizing microscopy was used to examine the thin concrete pieces. Unlike previous studies where the pull-out test has been utilized, this study allowed for observations of the steel fiber-cement interface to be made while the steel fibers were still embedded within the concrete (Uygunoglu, 2008). Due to a "wavy" appearance on the surface of the steel fibers, it was concluded that the steel fibers and cement bonded well with one another (Uygunoglu, 2008). A larger amount of steel fibers caused a decrease in the first crack development and an increase in flexural strength (Uygunoglu, 2008).

The relationship between steel fibers and several mechanical properties was sought after by Cagatay and Dincer (2010). These mechanical properties included compressive strength, flexural strength, compressive elastic modulus and toughness. In this study, 50 mm and 60 mm long hooked end steel fibers made up 0.5%, 0.75% and 1% of the mix volume. For each fiber type and volume fraction, three cylindrical samples, three cubic samples, and three prism samples were cast. The samples were tested at 7 days and 28 days. The cylinders and cubes were tested in compression whereas the prisms were tested in flexure via four-point bending. A comparator was used to measure strains of concrete cylinders while under compression. Cagatay and Dincer observed that the greater amount of fibers and a larger aspect ratio led to a higher compressive strength and toughness of the concrete samples (Cagatay and Dincer, 2010). While compared to

the plain concrete samples, the steel fibers had greater effect on cylinders' compressive strength at 7 days than 28 days (Cagatay and Dincer, 2010). Based on the results, there does not seem to be a clear relationship between the compressive strength and compressive elastic modulus (Cagatay and Dincer, 2010).

## 2. Mechanical Properties of SIFCON

Unlike fiber reinforced concrete, slurry infiltrated concrete (SIFCON) deals with a wet mixture of cementitious material and sand, which is poured onto preplaced fibers in molds. Rahim et al. (2016) compared the mechanical properties of SIFCON prisms with prisms reinforced with BRC wire mesh. Both specimen types composed of the same mix. The SIFCON prisms were sized 50 x 100 x 500 mm whereas the BRC wire mesh prisms were sized 25 x 100 x 500 mm. The hooked end steel fibers had an aspect ratio of 67 and accounted for 0.5%, 1% and 2% of the volume in the prism samples. Three samples of each type were tested in flexure after 7 days, 14 days and 28 days of moist curing. Overall, the SIFCON prisms were stronger than those with BRC wire mesh due to the volume of the BRC wire mesh being smaller than 0.5% of the prism it occupied (Rahim et al., 2016). The SIFCON prism with 2% volume of steel fibers proved to be the strongest and most ductile specimen with a flexural strength of 19.34 MPa and a maximum deflection of 10.42 mm (Rahim et al., 2016). As the volume of fibers increased, so did the flexural strength, maximum deflection and ductility (Rahim et al., 2016).

Thirugnanam et al. (2001) studied the ductility of SIFCON in the hinging zones of single span beams and as beam-column joints of a multi-story frame. The steel fibers were cut from thin wires resulting in a 60 mm length and diameter of 0.8 mm. Within the slurry, the fibers accounted for 8% of the volume. The fibers were placed random

orientation inside the molds while maintaining a random orientation, and the cement-sand slurry was poured on top until the molds were filled for both the hinging zones of the beams and the beam-column joints of the frames. The remainder of each specimen was cast with conventional concrete. A single point load was applied to five simply-supported beams in numerous loading and unloading cycles in order to observe the cracking behavior and yielding of the beams. The cyclical load was halted once the beams collapsed. A set of hydraulic jacks applied identical cyclical loading to each story. To measure the deflections and strain of the structural components of the frame, LVDTs and Demec strain gauges were used, respectively, and the displacements of the frame foundation was measured by dial gauges. Steel fibers proved to reduce crack size in this experiment (Thirugnanam et al., 2001). With the addition of SIFCON, the energy absorption capacity increased by 50%, the ductility increased by 100% in the single span beams and the first crack load increased by 40% in these beams (Thirugnanam et al., 2001).

Nanni (1992) studied the differences of aramid fibers, polypropylene fibers and steel fibers mixed with a cement-sand slurry. The aramid fibers were braided and impregnated with epoxy. The aramid fibers were 1 in long, the steel fibers were 1.5 in in length and the polypropylene fibers were 1.5 in in length. The percent volume for the aramid fibers, steel fibers and polypropylene fibers ranged from 0.28%-2.20%, 0.46%-1.46% and 0.21%-0.42%, respectively. For each of the beam specimens, which measured 4 x 4 x 14 in, the fibers were added last into the slurry mix. After testing the beams in flexure, it was evident that the fiber content has a direct relationship with flexural strength for the aramid and steel fibers (Nanni, 1992). The first crack proved to be

minimally influenced by fiber content (Nanni, 1992). Results showed that aramid fibers behaved similar to the steel fibers (Nanni, 1992). Aramid fibers are superior to steel in terms of corrosion, but yet is currently less economical than steel.

Thirty six beams with dimensions of 150 x 150 x 700 mm out of SIFCON were constructed by Sashidhar et al. (2011). Binding steel wire with a diameter of 1 mm played the role for fibers and they occupied 6%, 8%, 10% and 12% of the beam volume. The fibers also varied in size as they included aspect ratios of 40, 50 and 60. As is the general procedure with casting SIFCON, the fibers were preplaced in the mold and the cement-sand slurry was then poured on top until the mold was full. The beams were tested on a four-point system in flexure with a clear span of 600 mm until failure. The load came from a proving ring which transferred load to two 16 mm diameter rods 200 mm from one another acting upon the top surface of the beams. The midspan deflections were measured via dial gages. Compared to the reference specimens, the beams composed of SIFCON had smaller values of deflection (Sashidhar et al., 2011). The load carrying capacity and energy absorption had a direct correlation with the aspect ratio and percent volume of the fibers (Sashidhar et al., 2011).

Sharma et al.'s (2008) research involved thirty slab panel specimens that were made out of SIFCON. The dimensions of each panel were 1 x 1 x 0.025 m. The 25 mm fibers used were made out of high strength steel, and composed of 5%, 7%, 8% and 9% volume of the specimens. The fibers were first placed in the mold, and the cement-sand slurry was poured into the mold. Along with the panel specimens, cubes of dimensions 150 x 150 x 150 mm sides, dog bone specimens of dimensions 300 x 100 x 25 mm and cylinders of 150 mm diameter and 300 mm height were cast. A servo-controlled machine

under constant rate was used to test the accompanying specimens. The panels were set on a loading frame such that 16 equally-spaced point loads of identical load magnitude were acting on each panel. This served as a means to equally distribute the load and prevent punching shear failure (Sharma et al., 2008). The 500 kN capacity machine used a pre-calibrated proving ring to transfer the load to the point loads. Load-deformation behavior data was obtained from gages that were placed at the center and mid-third points on the bottom of the panels. Cracking began in the center of the panels and as the load increased, cracks propagated towards to the corners of the panels (Sharma et al., 2008). These multiple cracks were densely packed and the SIFCON panels did not fail suddenly, which was not observed in the plain mix panel (Sharma et al., 2008). In comparison to FRC, there was a substantial increase of the structural properties of SIFCON, specifically the first crack load and ultimate load which increased by 243% and 429%, respectively. It should be noted, however, that the structural properties increased with a greater fiber content, but decreased for the fiber content values greater than 8% (Sharma et al., 2008). It was proposed that this occurred because the greater amount of fibers might have obstructed the cement-sand slurry from infiltrating the fiber bed completely (Sharma et al., 2008).

## 3. Applications of SIFCON

Research has shown that SIFCON can be used to strengthen or enhance certain mechanical properties of structural members made out of conventional concrete. Liu (2014) conducted a study on reinforced concrete beams with SIFCON blocks on the top of beams. One beam was cast each with one SIFCON block, which had the dimensions of 200 x 120 x 70 mm. Three SIFCON blocks were cast and one block was used on the beam at a time. The dimensions of the blocks were chosen in order to completely occupy

the space on the beam where compression yielding would theoretically take place, as well as to ensure that the compressive strength of the blocks would be less than the GFRP bars' tensile strength (Liu, 2014). Hooked end steel fibers with a length of 30 mm were aligned perpendicular to the load, and placed one layer at a time to attain the highest fiber content possible. The placement of a cement-sand slurry followed. Two steel plates separated the SIFCON blocks from the rest of the beam. The beams differed from one another only by the amount of holes along the sides of the SIFCON blocks. A total of two LVDTs were used to measure the midspan deformation at the bottom of the beam and the shortening of the SIFCON block while under compression. The beam was tested with a SIFCON block until the midspan displacement reached 80 mm. At this point, the first block was replaced by the second block, and the test was repeated. The GFRP reinforcement failed before the third block fail could fail as the third block was stronger than the first two blocks. The SIFCON blocks increased the ductility of the beams, and the holes drilled in the blocks ensured that the failure would occur in the blocks rather than in the FRP bars (Liu, 2014).

Twelve beams were cast and subjugated to cyclical loading in Balaji and Thirugnanam's (2013) research. Each beam had dimensions of 100 x 150 x 1700 mm. In order to ensure a flexural failure, each beam consisted of two 8 mm diameter steel rebar for compression and tension reinforcement as well as 6 mm diameter stirrups spaced at 100 mm (Balaji and Thirugnanam, 2013). The beams were divided into four groups: one group had laminate confinement in the bottom face, another group had laminate confinement on the side faces, a third group had laminate confinement on the bottom and side faces, and the fourth group did not have any laminate confinement. The laminates

were made from SIFCON with round crimpled fibers 30 mm in length at 9% volume. The 20 mm laminates were attached to the beams with Isophthalic resin and covered the entire beam face. The beams were loaded and unloaded in cycles in flexure on a four-point system until the ultimate load was reached. Compared to the other specimens, it took longer for the cracks to develop and widen for the beams with laminate confinement on the side faces (Balaji and Thirugnanam, 2013). The number of laminates attached to the beams and a direct relationship with the ultimate loads (Balaji and Thirugnanam, 2013). The ultimate loads of the beam without laminates, with laminates on the bottom face, with laminates on the side faces, and with laminates on the bottom and side faces were 27 kN, 33 kN, 36 kN and 55 kN, respectively. Crushing of the concrete after the yielding of the steel occurred in the control beam, but not in the beams with laminate confinement (Balaji and Thirugnanam, 2013). The results show that the greater amount of SIFCON laminates used on the beams, the greater the load capacity, ductility and energy absorption capacity become (Balaji and Thirugnanam, 2013).

While Balaji and Thirugnanam used SIFCON to increase the flexural capacity of concrete beams, research by Shannag et al. (2001) involved using SIFCON to repair beams to increase shear capacity. Fourteen beams with dimensions of 15 x 20 x 200 cm were tested to failure. The beams had no shear reinforcement in the shear span. Four beams that failed in shear were repaired with SIFCON jackets within the shear span. Hooked end steel fibers 30 mm in length composing of 8% of the volume were dispersed in the formwork, which was set directly on the beams. Once in place, the SIFCON slurry was poured in, and the formwork was removed after 48 hours. The beams were subjugated to three-point bending with a 2000 kN capacity machine, and the deflection

was set at a rate of 0.02 mm/sec. The load, midspan displacement and curvature were measured with LVDTs. The strain in the rebar was measured via electrical strain gauges. The SIFCON jackets increased the shear strength by 25%-55%, and the repaired beams behaved in a ductile manner as opposed to a brittle shear failure (Shannag et al., 2001).

**4. Aluminum Plates as External Shear Reinforcement**

While there has been investigation of utilizing FRP or steel as an external shear reinforcement, the idea of using aluminum is relatively new, and there is a substantially limited corresponding literature. Abu-Obeidah (2012) tested twenty-six shear deficient concrete beams reinforced with aluminum plates. The beams, including control beams, were divided into two groups: Group A consisted of 6 beams and Group B consisted of 20 beams. All of the beams had dimensions of 150 x 250 x 1840 mm. The main difference between the two groups was that Group A had a shear deficiency in both shear spans, and Group B had a shear deficiency in only one shear span. The author denoted the beam length between one point load to the nearest support as the shear span, and the beam length between the two point loads as the zero shear span (Abu-Obeidah, 2012). The beams in Group A were reinforced with 2 mm thick aluminum plates, #8 stirrups at 187.8 mm intervals in the zero shear span, 2 #16 mm steel bars as tension reinforcement, 2 #10 mm steel bars as compression reinforcement, and had a span length of 1690 mm. The beams in Group B were reinforced with 2 mm thick aluminum plates, #8 mm stirrups at 50 mm intervals within one shear span and the zero shear span, 3 #19 mm steel bars as tension reinforcement, 2 #10 steel bars as compression reinforcement, and had a span length of 1550 mm. For each group, various amounts, sizes and orientations of aluminum plates were utilized. The surface of the aluminum plates and concrete that were to be in contact with one another were grinded down to enhance the bond with epoxy (Abu-

Obeidah, 2012). To attach the aluminum plates to the concrete beams, Sikadur-30LP was used. All beams were tested on four-point system 2500 kN INSTRON 8806 Universal Testing Machine. Strain was measured by gauges attached to the aluminum plates. The load rate was set to 10 kN/min, and the beams were tested to failure. The shear capacity was increased by 10%-89% with help of the aluminum plates.

**5. Basalt Fibers as External Flexural Reinforcement**

There has been research conducted in recent years on strengthening the flexural properties of concrete beams by applying basalt fibers to the external surface. Sim et al. (2015) studied the effect of strengthening concrete beams with basalt fiber sheets. Ten concrete beams with dimensions of 240 x 15 x 25 cm were cast. In order to ensure that a flexural failure occurred, D10 stirrups were placed at every 10 cm along the beam length, and the shear span to depth ratio was 3.5 (Sim et al., 2005). On all beams except for the control specimens, basalt fibers sheets were placed on the tension side such that the fibers were parallel with the longitudinal axis of the beams. The specimens were divided by the length of basalt fiber sheets being used, which was 0.8L and 1.0L, and the number of basalt fiber sheet layers used, which ranged from one to three. Two beams were used for each specimen type. The beams were tested on a four-point bending system with a clear span of 200 cm. The deflection and strain were measured with help of LVDTs on the tension side and strain gages on the longitudinal rebar. After being tested to failure, basalt fiber sheets debonded from the concrete for the beams that consisted of three layers of basalt fiber sheets (Sim et al., 2005). Since the specimens with one and two layers of basalt fiber sheets failed without debonding, these layers reached their maximum flexural capacity and thus proved to be more efficient than three layers (Sim et al., 2005). As expected, the more layers of basalt fiber sheets used, the greater the yield strength and

ultimate load were (Sim et al., 2005). The yield strength increased by 15%, 26% and 16% for the beams with one layer, two layers and three layers, respectively. The ultimate strength increased by 0%, 27% and 29% for the beams with one layer, two layers and three layers, respectively. The length of basalt fiber sheets did not seem to matter too much as the beams with varying basalt strengthening lengths differed only slightly (Sim et al., 2005).

Ali et al. (2015) casted four 150 x 300 x 2000 mm reinforced concrete beams were reinforced with basalt fiber reinforced polymer (BFRP) grids, and one beam served as the control beam. The BFRP grids for the various beams were 3 mm, 5 mm and 7 mm in thickness. The beams were further reinforced with 10 mm diameter stirrups at 80 mm intervals in the shear zone to prevent shear failure (Ali et al., 2015). The tension side of the beams were sandblasted, washed and airbrushed to enhance the bond between the epoxy and concrete. On this surface, a thin layer of epoxy was applied and the BFRP grid was placed, followed by another thin layer of epoxy. If there was any excess epoxy, it was scraped off to provide a smooth, finished surface. Four-point configuration was used to test the beams in flexure using a servo-controlled hydraulic actuator, and the clear span was 1860 mm. To measure deflection, three LVDTs were placed at each end and midspan of the compression side. In comparison to the control beam, the cracking load, yielding load and flexural strength with aid of the BFRP grids increased 30-50%, 10-15% and 25-49%, respectively. In contrast to some of the beams reinforced with basalt fiber sheets as in Sim et al.'s study, Ali et al.'s specimens experienced no debonding of the BFRP grids and may prove that BFRP grids are more efficient than basalt fiber sheets (Ali et al., 2015).

Shen et al. (2015) studied the effect of using basalt fibers as additional flexural reinforcement to beams that have already experienced initial cracking. Where Sim et al. and Ali et al. casted beams for their research, Shen et al. used two pre-existing beams from a bridge. These beams had minor flexural cracking at the time they were removed (Shen et al., 2015). Epoxy resin was used as an adhesive to attach two layers of BFRP sheets on the tension side of one of the beams. Both beams were tested to ultimate load. The cracks were more dispersed in the beam with BFRP sheets, whereas the cracks were more concentrated in the control beam (Shen et al., 2015). The beam with BFRP sheets experienced a 27.2% increase in ultimate load.

# CHAPTER 3: EXPERIMENTAL PROGRAM

In this project, a total of 37 beams were tested in flexure. These beams were divided into 3 groups. The first group composed of 2 beams of similar fiber type to see if shear reinforcement was needed. One beam had shear reinforcement and the other beam did not. The second group consisted of 18 beams, which were tested in flexure to determine the ultimate flexural strength. The 18 beams were further divided into 6 sub-groups of similar fiber type with 3 beams in each sub-group. The third group consisted of 17 beams, which were tested in flexure until cracking, then reinforced with FRP, or fiber reinforced polymer, on the bottom tensile flange and tested in flexure to failure. The 17 beams were further divided into 6 sub-groups of similar fiber type with 3 beams in each sub-group apart from 1 sub-group which consisted of 2 beams of similar fiber type. The sub-groups differed from one another by the type and percent volume of fibers present in the beams themselves. The results of both the second and third groups were compared to one another to observe the effect of flexural strength by rehabilitating damaged beams. The beams were in the shape of I-beams of similar size. The depth of the beam was 4-¾ inches, the width was 4 inches and the length was 18 inches. The two flanges and the web had a thickness of ⅜ inch. The 6 sub-groups consisted of a mortar mix with the following combinations of fibers: 5% per volume 50 mm hooked end steel fibers, 3% per volume 30 mm hooked end steel fibers, 2% per volume 6 mm steel fibers, 1% per volume 13 mm steel fibers, 1.8% per volume 30 mm with 2% per volume 6 mm steel fibers, and 1.8% per volume 50 mm with 1% per volume 13 mm steel fibers.

## 1. Glossary and Abbreviations

Within this study, there are certain terms and abbreviations used that may be unknown to the reader. The purpose of this section is to provide the reader with definitions of the terms as well as any abbreviations used throughout the text, whose meaning is not mentioned elsewhere other than this section.

First Group – Two beams composed of 50 mm hooked end steel fibers. One had shear reinforcement and the other did not. Both were tested to determine whether the epoxy was strong enough to prevent delamination and whether shear reinforcement was needed for the remaining beams.

Second Group – Eighteen beams composed of 6 mm, 13 mm, 30 mm and 50 mm steel fibers. Divided into 6 sub-groups of similar fiber type and combination. Beams in this group were tested in flexure to determine ultimate strength.

Third Group – Seventeen beams composed of 6 mm, 13 mm, 30 mm and 50 mm steel fibers. Divided into 6 sub-groups of similar fiber type and combination. Beams in this group were tested to the point of when cracking began, reinforced with basalt fiber on the bottom of the tensile flange, and tested to failure to study effect of rehabilitation on the ultimate flexural strength.

Nano-inorganic composite – Adhesive developed at Rutgers University by researchers to bind fiber reinforced polymers, in this case basalt fiber, to a concrete surface. Made of a solid component and a wet component. Took two weeks to cure.

Sikadur-31 – Two-component epoxy produced by Sika Corporation. The two components are known as Component A and Component B. Component A is white in color and Component B is black in color.

Beam Designation: XMM-MODA-SN or X&YMM-MODA-SN

- X: Fiber length present in beam (for beams with one fiber type present)
- X&Y: Fiber length present in beam (for beams with two fiber types present)
- MM: unit of fiber length (millimeters)
- MODA: month and day of when concrete was cast (i.e. March 7$^{th}$ = 0307)
- S: Shear reinforcement (AL for aluminum angles; FRP for basalt fiber)
- N: Number beam with the fiber type and combination present (i.e. number from 1-6)

**2. Construction of Plate Molds**

The molds for the plate specimens were constructed out of ¾ inch thick plywood and ⅜ inch by ⅜ inch pine hardwood strips. The top surface of the plywood acted as the bottom surface of the wooden plate mold. The hardwood strips were used to enclose a rectangular area that would contain the cast concrete to form the plate specimen. Since the plywood was manufactured in sheets that measured 4 feet by 8 feet, a table wood saw was used to cut the plywood into smaller pieces. The plate specimens, when cast, would be consolidated while situated on a vibrating table. The cuts of plywood for the wooden plate molds needed to be small enough to fit completely onto the vibrating table. In general, the cuts of plywood measured 20 inches by 14 inches. The hardwood strips were also cut since they were manufactured in lengths of 36 inches. The plate specimens that would make up the beams were sized 18 inches by 4 inches with a ⅜ inch thickness. The hardwood strips were cut into four pieces per each mold. Two pieces would be situated along the short dimension of the mold and would be denoted as end pieces. The two other

pieces of the hardwood strips would be situated along the long dimension of the mold and would be denoted as side pieces. The side pieces were cut to a length of 18 inches. Though the end pieces needed to be at least 4 inches long, they were cut such that their length was 5-6 inches. This was done as way to provide a means of demolding the plate specimens. The length of the end pieces included 4 inches for the width of the plate specimen, ¾ inch for the interface with the two side pieces, and ¼ inch to 1 ¼ inch extension to provide leverage so a chisel and hammer would be able to remove the end piece. This method shall be discussed later in Section 4.2. The side piece was first attached to the plywood with two wire nails hammered in the side piece. The location of the wire nails varied from 1 inch to 4 inches from the nearest end of the side piece. The reason for this range is that the grain of the wood at times would obstruct the wire from penetrating the hardwood strip, and a new location nearby would have to be utilized. A pen and tape measure was used to draw a 1 inch long line at a distance of 4 inches from the ends of the side piece. This was done so the second side piece would line up to these two lines while ensuring that the distance between them would be 4 inches. One end piece was positioned such that one end of the large dimension would be flush with the small dimension of the side piece, while the end piece extending a distance of at least 4 inches. Two wire nails were hammered into the end piece at a distance of 1 inch from each end. The second side piece was lined up along the two 1 inch lines and its small dimension was lined up perpendicularly to the long dimension of the end piece. The second side piece was attached to the plywood by hammering two wire nails 1 to 4 inches from each end. The second end piece was lined up such that to enclose the area encompassed by the first three pieces, and the second end piece was hammered in the

plywood with two wire nails positioned at 1 inch from each of its ends. The plate mold can be seen in Figure 1 below.


Figure 1: Wooden plate molds

## 3. Concrete Material and Mixing Procedure

### 3.1 Concrete Materials

The building material being investigated consists of five ingredients: concrete sand, superplasticizer, Type I Portland cement, water, and steel fibers. The mix design, as seen below in Table 1, was predetermined based on previous research.

Table 1: Mix Design

| Material | Percent per Unit Weight |
|---|---|
| Cement | 29.6% |
| Sand | 59.2% |
| Water | 10.7% |
| Superplastizer | 0.6% |

The sand was obtained from Weldon Materials in Berkeley Heights, New Jersey. Prior to pick up, the sand was stored outside and was exposed to the environment. The sand was not heated before batching and mixing to eliminate moisture. Therefore, it is

possible that there is moisture in the sand at the time of pick up, batching and mixing. The sand had a fineness modulus of 2.6. The sand was not sieved prior to batching, however, if there was aggregate larger than ⅜ inch, it was removed by hand. Such aggregate was removed as it was seemed to be a foreign particle that mistakenly made its way in the pile of sand in the quarry. The water was obtained from a hose in the laboratory.

**3.2 Batching of Materials**

The first items to be batched prior to mixing were the cement, sand and water. One 5-gallon plastic bucket each was used to transport and temporarily store the cement, sand. The empty bucket was placed on a scale that would record the weight in pounds to two decimal places with an accuracy of ± 0.05 pounds. The scale was zeroed out while the empty bucket was on it, such that any additional material on the scale, namely the material added to the interior of the bucket, would register on the digital dial as the approximate weight of the material needed. The cement was first added to the empty bucket on the weight scale. Using a round mouth scoop, the cement was added to the bucket until the net weight displayed matched the required cement weight as per the mix design and volume of the mix ± 0.05 pounds. Figure 2 depicts this step.


Figure 2: Batching cement

In the case where the weight of material required was beyond the level of accuracy of the scale, the required weight of that material was rounded up or down according to the following situations. If the required weight of the material had the digit in the hundredths place less than 3, then the required weight was rounded down such that the digit in the hundredths place was 0. If the required weight of the material had the digit in the hundredths place greater than 2 and less than 8, then the required weight was rounded such that the digit in the hundredths place was 5. With any required weight of material outside of the ranges mentioned in the previous two cases, the digit in the hundredths place was rounded to 0, and a 1 was added to the tenths place. Once the correct amount of cement was weighed, the bucket with the cement was removed from the scale and another empty 5-gallon bucket was placed on the scale. The scale was zeroed out while the empty bucket was situated on the scale so that they weight reading would be solely of the material in the bucket. The sand was transported from its storage

location to the bucket with a round mouth scoop. Dry sand was used as much as possible, however, there was a possibility that the sand was not completely dry. The sand was inspected by feel and visually. If the sand was deemed too wet, then the sand would be dried in an oven until there was no moisture content. The sand was added until the net weight displayed matched the required sand weight as per the mix design and volume as seen in Figure 3.

Figure 3: Weighing required amount of sand

Due to the level of accuracy of the scale, the method previously explained regarding rounding the required weight of material was considered. When the required weight of the sand was displayed by the scale, the bucket of sand was removed. Another empty bucket was placed on the scale and the scale was zeroed out. Water was added to the bucket via a hose in the laboratory until the required weight of the water was displayed on the scale dial after taking the weight rounding consideration as previously mentioned. Once the required weight of the water was displayed by the scale dial, the

bucket of water was removed. The next material to be batched was the superplasticizer. Since the amount required of the superplasticizer was relatively small to that of the cementitious material, a scale with that can read and display a recorded weight to the nearest one-tenth of a gram was used. A clean plastic cup was placed on the scale and the scale was zeroed out. The required amount of superplasticizer was poured into the cup. During the pouring of the superplasticizer, the cup was temporarily removed from the scale so that if the superplasticizer would spill, the spilled material would not affect the weight reading on the scale. Once the required amount of superplasticizer was displayed by the dial on the scale, the cup and superplasticizer were removed as seen in Figure 4.

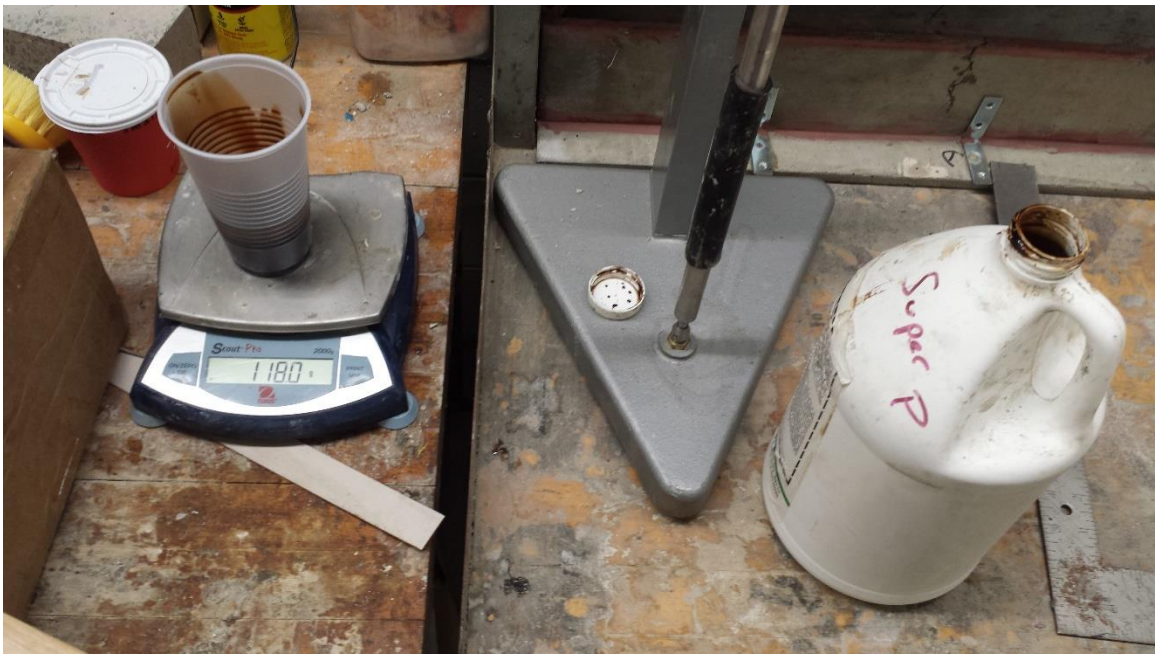


Figure 4: Weighing required amount of superplastizer

A clean, plastic cylindrical mold was used to contain the required amount of steel fibers. Using the same scale as was used for measuring the amount of superplasticizer, the empty cylindrical mold was placed on the scale, and the scale was zeroed out. The required amount of steel fibers were placed into the cylindrical mold until the weight

displayed on the scale dial represented the weight and amount of steel fibers required. The 30 mm and 50 mm fibers were transported from their storage location to the cylindrical mold by hand. However, it was advisable that the 6 mm and 13 mm steel fibers not come into contact directly by hand as a safety precaution. The diameters of the 6 mm and 13 mm steel fibers were relatively small and could puncture the skin even by wearing the necessary gloves. Therefore, a ⅜ inch diameter steel tamping rod was used to help guide the 6 mm and 13 mm steel fibers from their bag directly to the cylindrical mold.

### 3.3 General Mixing Procedure

The buckets of cement, sand, water and cup of superplasticizer were brought to the area where the mixer was located. The materials were placed on a tarp in order to prevent the area from becoming dirty in the case of spillage. The mixer was a Univex SRM12 concrete mortar mixer. The propeller blade was removed as was the mixing bowl. The mixing bowl was placed on the ground next to the batched materials so the act of adding the material to the bowl would be easier. The sand was first added to the bowl. Figure 5 depicts this step.

Figure 5: Adding sand into mixing bowl

The mixing bowl was then attached to the mixer as was the propeller blade, and the mixing bowl was raised to the starting position required for mixing. Cement was then added to the mixing bowl by use of the round mouth scoop. This can be seen in Figure 6.


Figure 6: Adding cement into mixing bowl

It is worth noting that the cement was added to the bowl after raising the mixing bowl to the starting position for two main reasons. If the cement was added into the mixing bowl before the sand, the sand could cause a portion of the cement to plume and exit the mixing bowl upon impact, which would result in a lower amount of cement than designed for. Furthermore, due to the nature of the sand, cement and concrete mortar mixer setup, if both materials were situated in the mixing bowl prior to raising the mixing bowl, there would be difficulty to raise the mixing bowl since the propeller blade could not penetrate the cement and sand. Once in the starting position, the mixer was turned on to the lowest frequency for 1 minute. This was done so that the dry material may be homogenously mixed before the addition of the liquid material. When the 1 minute of dry mixing was complete, the superplasticizer was poured into the bucket of water in a way such that all of the superplasticizer left the cup and none was left on the interior side of the cup. Figure 7 illustrates this step of the mixing procedure.

Figure 7: Premixing superplastizer with water

The bucket of water and superplasticizer was picked up slightly and shaken by hand in order for the water and superplasticizer to become a homogeneous solution. This bucket was poured into the mixing bowl and a ⅜ inch diameter steel tamping rod was used to create voids into the dry material so that the liquid solution could penetrate easier throughout the dry material and to avoid the liquid material from splashing out of the mixing bowl once the mixer would be turned on. This step is shown in Figure 8.

Figure 8: Creating voids prior for liquid to penetrate prior to wet mixing

The material was then mixed for 3 minutes of the lowest frequency. After the 3 minutes, the mixer was stopped and a ⅜ inch diameter steel tamping rod was used to mix the material to provide as much contact as possible between the liquid and solid components. This was essential because due to the setup of the mixer, the propeller blade cannot reach the bottom of the mixing bowl, preventing the components from mixing completely. It was permissible to remove the mixing bowl from the mixer and mix by hand, which is shown in Figure 9.

Figure 9: Hand mixing of mortar mix

This proved to be a more efficient way of mixing rather than using the ⅜ inch diameter steel tamping rod since it was easier to detect whether dry clumps existed in the mixing bowl, in which case they would be broken up by hand. Once it was felt that the mixture had no dry clumps, whether via tamping rod or by hand, the mixing bowl was attached to the mixer and the mortar was mixed for another phase of 3 minutes. In this phase, the intensity was increased every 20-30 seconds by 1 tick mark as displayed on the machine. After this phase, the mixing bowl was removed and the mixing procedure was complete.

### 3.4 Mixing Procedure with Premixed Fibers

The mixing procedure for the 6 mm and 13 mm steel fibers differed from the mixing procedure of the plain mortar mix. Because of their size, the 6 mm and 13 mm steel fibers were small enough to be mixed along with the cement, sand, water and superplasticizer before casting. With all the materials batched, the first step of the mixing

procedure was to add 2 scoops of sand, 1 scoop of cement and a representative amount of steel fibers. The steel fibers were poured from a clean, plastic cylindrical mold. This step is depicted in Figure 10.


Figure 10: Adding steel fibers to mixing bowl

What is meant by the term representative amount, is that the materials present in the dry mix will not be added to the mixing bowl and mixed together simultaneously. Rather, to guarantee homogenous mixing occurs, a smaller portion of the dry material

would be added and mixed before another portion of the dry material would be added and mixed. It was up to the person mixing to visually judge how much steel fibers would be deemed as an appropriate representative amount of steel fibers in order to be proportionate with each addition of sand and cement. Each of the dry materials were added and mixed on the lowest intensity for 30 seconds. This process was followed until all of the dry material had been added and mixed. The superplasticizer was then poured into the bucket of water such that there was little to no superplasticizer remaining on the interior sides of the cup. The bucket of the 2 liquid materials was picked up slightly and shaken by hand to allow the 2 liquid materials to become a homogeneous solution. As was the case of the addition and mixing of the dry material, the liquid solution was added and mixed in smaller portions rather than all at the same time. A plastic container was used to transport a small portion of the liquid solution from the bucket to the mixing bowl. This was done for 2 reasons. When a small portion of the liquid solution was introduced to the dry material, the nature of the mixture with a low moisture content would cause the material to clump, creating voids that would allow access to the bottom of the mixing bowl as seen in Figure 11.


Figure 11: Adding small amount of superplastizer-water solution

With each addition of the liquid solution, the liquid solution was poured in these deep voids so the material at the bottom could come into contact with moisture. This method is preferred over adding the entire liquid solution at one moment of the mixing procedure because the mortar mix with small steel fibers should not be mixed by hand as was the case in the plain mortar mix procedure explained previously. Due to the diameter of the small steel fibers, it was fairly easy for the fibers to become lodged into the human

skin. Furthermore, because the sand was not completely dry before mixing, it was possible that the mixture would have contained too much moisture if the entire amount of liquid solution was added. To ensure that the mixture was not too moist, small portions of the liquid were added and mixed for 30 seconds on the next higher frequency. It was up to the visual observation and judgement of the person in charge of mixing to decide whether more liquid solution was needed or no. This was also to prevent segregation of the material.

## 4. Casting and Demolding

### 4.1 Plate Casting

Before the concrete was placed, a releasing agent was applied to the wooden molds so that the concrete would not bond with the wooden surface and therefore it would be easier for demolding. To do so, WD-40 was applied on all interior sides of the mold wherever the concrete would be in contact the mold. The mixing bowl of concrete was removed from the mixer and placed next to the vibrating table. The size of the vibrating plate allowed two plates to be cast at a time. The wooden plate molds were placed in close proximity to the vibrating table to minimize the lag time between removing cast plates from the vibrating table and mounting empty molds onto the vibrating table. Due to their larger size compared to the 6 mm and 13 mm steel fibers, the 30 mm and 50 mm steel fibers were preplaced in the molds before the placement of concrete, rather than added during the mixing procedure. Other than physically preplacing the 30 mm and 50 mm fibers, the plate casting procedure was the same for all mix types. The 30 mm and 50 mm steel fibers were added to the wooden plate molds after the application of the WD-40 lubricant. After the wooden plate molds were placed

onto the vibrating table and the WD-40 was applied, the 30 mm and 50 mm steel fibers were placed by hand in such a way the fibers were uniformly distributed throughout the mold while maintaining a random orientation. This is illustrated in Figure 12.

Figure 12: Placing 50 mm hooked end fibers in wooden molds prior to mixing

The vibrating table was turned on to the lowest frequency as to prevent the 30 mm and 50 mm steel fibers from moving out of position. What was observed before implementing this step, was that if the vibration was at a mid-level to high-level frequency, the 30 mm and 50 mm steel fibers tended to gravitate towards one area and align their orientation in the same if not similar direction. A round mouth scoop was used to transport concrete from the mixing bowl and place it into the wooden plate molds which can be seen in Figure 13.


Figure 13: Casting plate molds

Once the majority of the 30 mm and 50 mm steel fibers were in contact with the concrete, the frequency of the vibrating table was increased. It was assumed that weight of the placed concrete would hold the steel fibers in place while the vibrating frequency was increased, and that any possible movement of the preplaced steel fibers would be minimal and have negligible effect. Generally, the concrete was placed along the middle of the mold to allow the concrete to consolidate towards the ends and sides of the mold

during vibration. If the concrete was originally placed along the edge of the mold during consolidation, the concrete might have spilled over the side of the wooden plate mold and be deemed wasted material. A 6 inch trowel was used to assist to distributing the concrete throughout the wooden plate mold and further consolidate the concrete. Having the trowel be 6 inches in width allowed for the trowel to rest on the sides of the mold and ensure that the top surface of the concrete plate would be level with the top of the mold. Figure 14 depicts this step.

Figure 14: Trowel used to provide a smooth finish of the plate sample

Using a brushing-like action, the remaining parts of the mold were filled and the top surface of the concrete plate was leveled with a smooth finish. When the plate molds were filled and level, they were removed and placed on a level table in an environmentally-controlled lab room free of vibration for initial curing. To prevent the concrete from setting and becoming less workable, the concrete was hand mixed with the round mouth scoop until it was visually and physically determined that the concrete had adequate workability. After the casted plate samples were stored, the next wooden plate molds were filled following the same procedure, until all the plates were cast. The plate samples underwent dry-curing for 24 hours ±8 hours as per ACI C31 specification.

**4.2 Plate Demolding**

After the dry-curing phase, the plate samples were demolded. The demolding process required two tools: a hammer and a chisel. Due to the design of the mold itself, the end pieces extended past the 4-inch wide plate specimen and the two ⅜-inch wide side pieces. With the end piece sticking out slightly, the chisel and hammer were used to remove the end piece from the mold entirely, without disrupting the other components of the mold and the plate specimen itself. The flat end of the chisel was in contact with the top surface of the plywood, which was the same surface as the bottom of the wooden plate mold. The angled part of the chisel was faced up and wedged in between the top surface of the plywood and the bottom of the end piece. The direction of which the chisel was hammered was such that the longitudinal axis of the chisel was perpendicular to the wooden plate mold's end piece. Figure 15a illustrates the demolding of the first end piece.

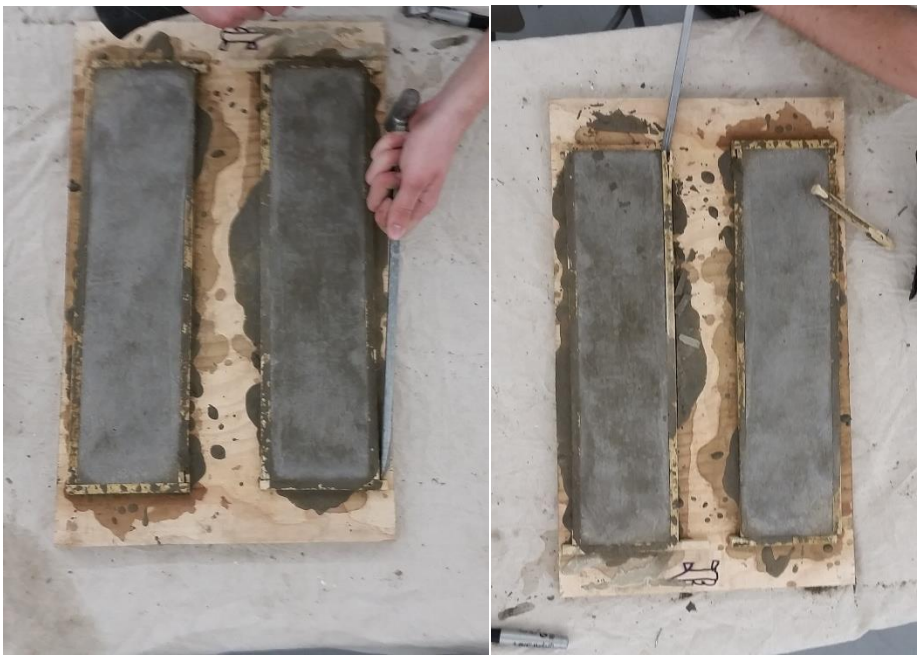

Figure 15: Right (a) Removing first end piece; Left (b) Removing first side piece

Once the end piece was removed, one of the side pieces was removed. It did matter which one, but at least one end piece and one side piece needed to be removed. Having the flat part of the chisel level with the bottom surface of the mold and the angled part facing up, the chisel was wedged between the bottom of the mold and the side piece, and hammered such that the side piece would move up. This is illustrated in Figure 15b. Once it was evident that the one nail connecting the side piece to the bottom of the mold was dislodged, the side piece was further removed by hand. The plate specimen was removed with two hands evenly spaced along the plate specimens' long dimension and lifting up slowly as see in Figure 16.


Figure 16: Removing plate sample by hand

After the plate specimens were removed, one side of the specimens were labeled to identify the type of fibers present in each plate, when the plate was cast and the last name of the researcher responsible. The plates were then placed in a curing room where they would be subjected to wet curing for 28 days. With use a trowel to scrape the bottom and interior sides of the wooden plate mold, any remaining concrete was removed. The end and side pieces that were removed in the demolding process were discarded and replaced with new end and side pieces of similar size. The wooden plate molds were able to be re-used for an additional two times.

**4.3 Cylinder Casting**

The cylinders were cast using 4 inch by 8 inch plastic cylindrical molds. Similar to the wooden plate molds, WD-40 was applied on all interior sides of the plastic cylindrical molds. The cylindrical molds were placed on the vibrating table. With the round mouth scoop, the concrete was transported from the mixing bowl into the

cylindrical mold. The dial on the vibrating plate was set on a mid-level frequency. If the frequency was too low, the concrete would not consolidate sufficiently, and if the frequency was too high, the water would have bled through the top surface of the concrete. Unlike casting the plate specimens, the 30 mm and 50 mm steel fibers were not preplaced simultaneously. Instead, they were added in representative amounts with every scoop of concrete added to ensure that the 30 mm and 50 mm steel fibers were uniformly distributed throughout the concrete cylinder. Figure 17 depicts adding the 50 mm steel fibers into the cylinder.

Figure 17: Adding 50 mm steel fibers into cylinder

If this was not done and the steel fibers would have been preplaced all at once prior to casting, the steel fibers would have been concentrated towards the bottom of the

concrete cylinder. The concrete was added in relatively small portions at a time, after which the 30 mm and 50 mm steel fibers were added. When it became visually evident that the 30 mm and 50 mm steel fibers could not consolidate further into the concrete, the next relatively small portion of concrete was added into the cylindrical mold. This process was repeated until the cylindrical mold was completely filled with concrete. A flat bottom trowel and ⅜ inch diameter steel tamping rod was used to smooth out the top surface of the concrete cylinder. Afterwards, the concrete cylinders were capped and placed on a level table in an environment-controlled lab room free of vibration for initial curing.

**4.4 Cylinder Demolding**

After 24 hours ±8 hours of dry curing, the cylinders were demolded. The cap of the cylindrical mold was removed by hand or by rubber mallet if needed be. The cylinder was then orientated with the bottom surface facing up and the top surface resting on a flat, level surface. A nail was hammered in a pre-manufactured hole in the center of the bottom surface of the cylindrical mold 10-15 times. With the bottom of the cylinder facing up, a pressurized hose was then used to force air into the manufactured hole. The air flowed through the space between the cylindrical mold and concrete cylinder, and the increase in pressure forced the cylindrical mold to be removed from the concrete cylinder. Once demolded, the concrete cylinders were labeled with information detailing the mix type, date of casting, and the last name of the researcher responsible. The cylinders were then placed in a curing room where they would be subjected to wet curing for 28 days. A few of the plate samples are in the curing room in Figure 18.

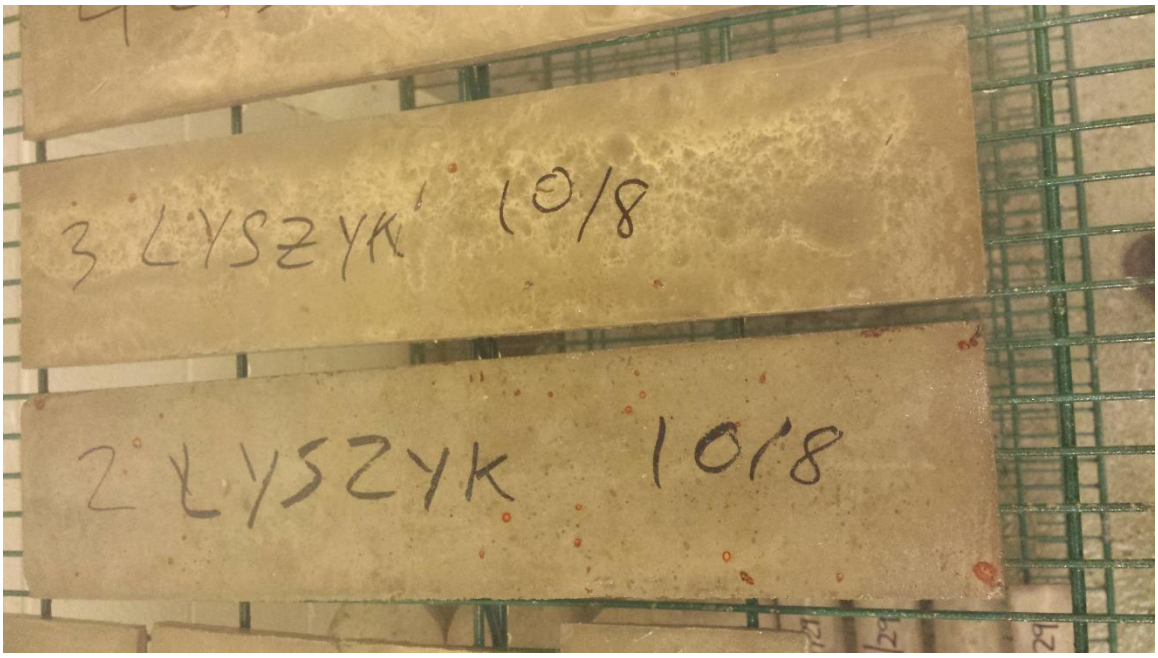


Figure 18: Concrete plates in curing room

## 5. Beam Fabrication

### 5.1 Overview

After 28 days of moist curing, the concrete plates were taken out and placed in a temperature controlled lab environment as seen in Figure 19. The concrete plates remained in this storage facility until the epoxy was obtained. The epoxy acted as an adhesive so that the concrete plates could be connected perpendicular to one another. Originally, it was thought that a nano-inorganic composite would be strong enough to connect the concrete plates together. However, when such a beam was tested in flexure as seen in Figure 20, the bottom flange and web delaminated from one another before any shear or flexure failure could have taken place. Therefore, an epoxy was sought after to prevent delamination.

Figure 19: Concrete plate samples in temperature controlled lab environment

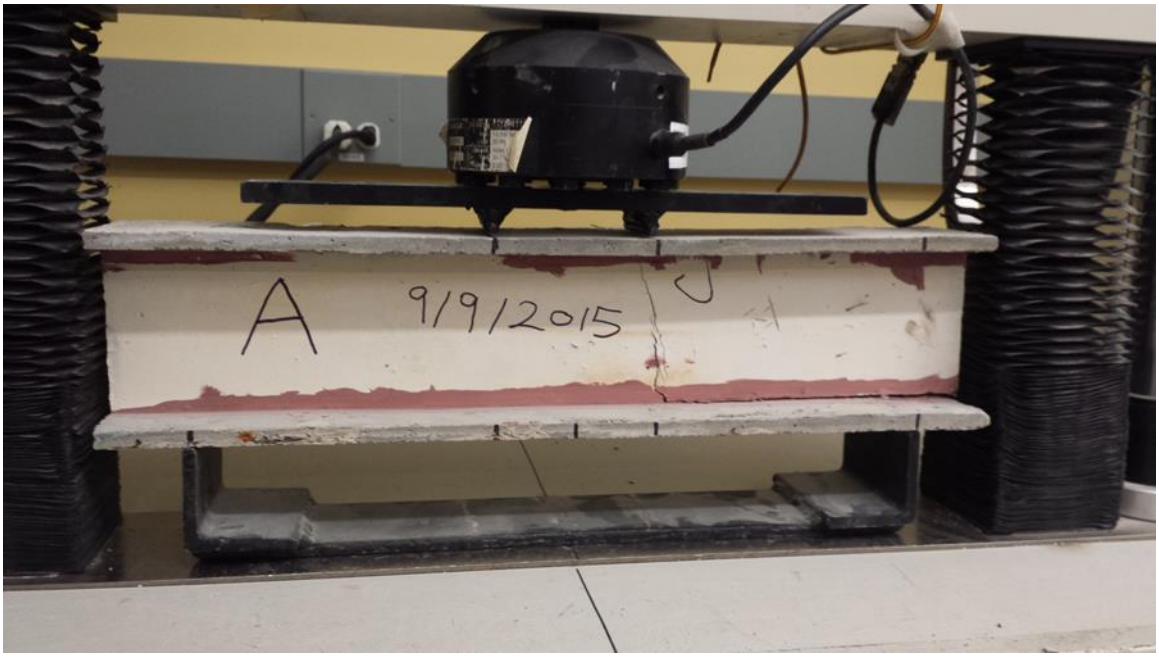


Figure 20: Delamination of nano-inorganic composite evident at right end of beam

Before the concrete plates could be connected, the concrete plates were prepared. This process included assigning which concrete plates would act as the flanges and which concrete plates would act as the webs. The plates that were to be assigned as the webs

were chosen on the basis on whether they could stand on their own completely vertically on a plate acting as a flange. If the plate was able to accomplish this, then it would be designated as a web and the plate it was balancing on would be designated as a flange. The concrete plates were also grouped into beams such that each beam would have been composed of concrete plates of the same mix and age. The next step was to use a black marker to trace the perimeter of the area of the web-flange interface. This perimeter was traced on the interior side of the flanges such that the space in between the two longitudinal lines was ⅜ inch, which corresponded to the thickness of the webs. The two longitudinal lines were produced such that each line was equidistant from the center longitudinal axis of the concrete plate to ensure that the concrete plate acting on the web would be aligned in the center of the flanges. The longitudinal lines were continued along the thickness of the concrete plates acting as the flanges. This was done in foresight because once the epoxy would be applied to the area between the web and flange, the longitudinal lines dictating the area where the web should be aligned would no longer be visible for the epoxy would cover those lines. Having these continue along the flange thickness, where the lines would not have been covered by the epoxy, allowed for the assurance that the flange would be aligned within the two longitudinal lines. For the cases where the beam was to include shear reinforcement consisting of aluminum angles, a black marker was used to draw the border of the aluminum angle onto the flange. This can be seen in Figure 21.

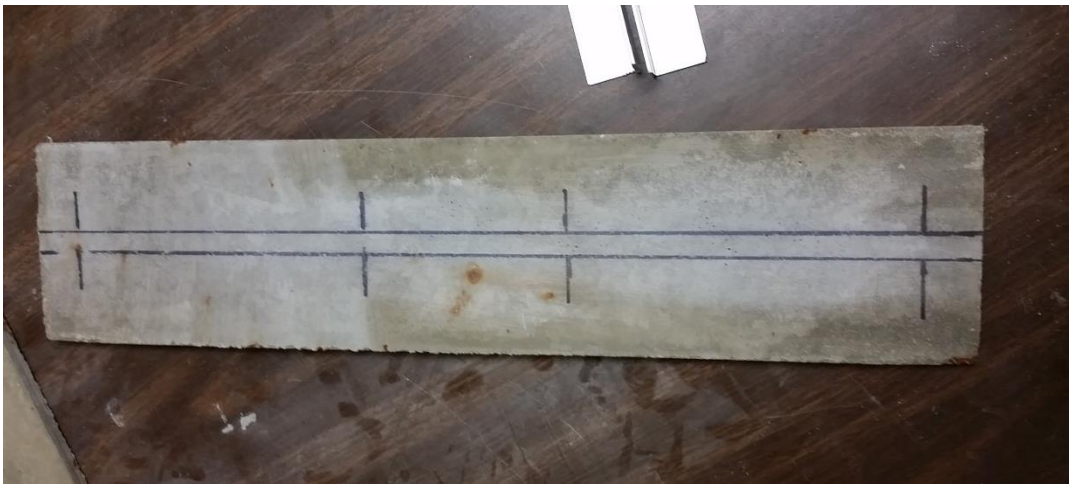

Figure 21: Marked lines indicating area of epoxy application

The area bound by these lines represented the area that would be occupied by the horizontal leg of the aluminum angle. In order for the concrete-epoxy connection to be enhanced, a steel wire brush was used to produce a rough surface along the longitudinal edges of the web, the area of the flanges in between the two longitudinal lines, and the area on the web and flange that was to be in contact with the aluminum angle, if applicable. Figure 22 shows the steel brush producing a rough surface on the concrete. This was done to promote interlocking of the concrete and epoxy such to prevent possible delamination.

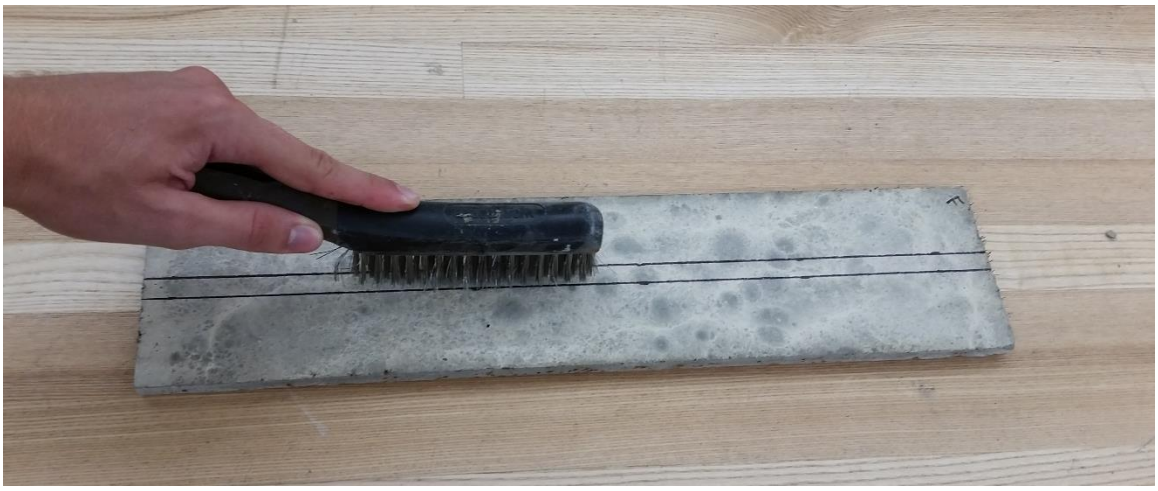

Figure 22: Steel brush producing a rough surface on the concrete plate

Before all of the beams were connected via epoxy, two test beams were constructed to determine whether the epoxy was strong enough so that delamination would not occur through visual inspection. Both beams were composed of 5% volume of 50 mm steel hooked end fibers and had age was 200 days. One beam had aluminum angles as shear reinforcement and the other beam had no shear reinforcement. It is also worth of note that in order to prevent the flange from moving during application of epoxy and attaching the web, the flange of each beam was clamped down to the table.

**5.2 Shear Reinforcement Design**

Not certain whether the concrete beams would fail in shear or flexure, it was decided to include shear reinforcement in order for a flexural failure to occur. Since the beam was 18 inches in length, it was decided to divide the length of the beam in thirds, where the 2 thirds from the ends would include shear reinforcement as that is where shear is the greatest. The middle third would not have shear reinforcement. Therefore, the shear reinforcement zone would exist within 6 inches from each end.

### 5.3 Aluminum Angle Preparation

For one of the initial two beams of the first group, aluminum angles were used as shear reinforcement. The aluminum angle had a thickness of 1/16 inches and each leg was 1 inch long. Since the aluminum angle was manufactured in 6 foot lengths, a chop saw was used to cut the 6 inch lengths. After cutting the aluminum angles in 6-inch lengths, it was observed that there was aluminum become jagged at the location where the cut was. A grinder was used to smooth out the ends so that the aluminum angle would be flush with the corner made by the web and flange. The grinder was also used to produce a rough surface on the sides of the aluminum angle that was to be in contact with the epoxy. The grinding of the aluminum angle and the grinded surface of the aluminum angle are shown in Figure 23a and Figure 23b, respectively.

Figure 23: Left (a) Grinding aluminum angle; Right (b) Grinded aluminum angle

### 5.4 Epoxy Mixing Procedure

The Sikadur-31 epoxy consisted of two components. A plastic container was used to batch and contain both components. The plastic container was placed on a scale and the scale was zeroed out such that any non-zero weight reading on the scale would indicate the weight of additional material other than the plastic container. The two components had a weight ratio of 1:1, meaning for any size mix, each component's weight should be the same as each other. A wooden paint stirrer was used to transport an amount of Component A to the container, and the container was placed onto the scale. The weight of the material was noted and Component B was added to the plastic container on top of the Component A via a 2 inch wide plastic spatula until the weight reading on the scale doubled the weight of the white component which is shown in Figure 24.

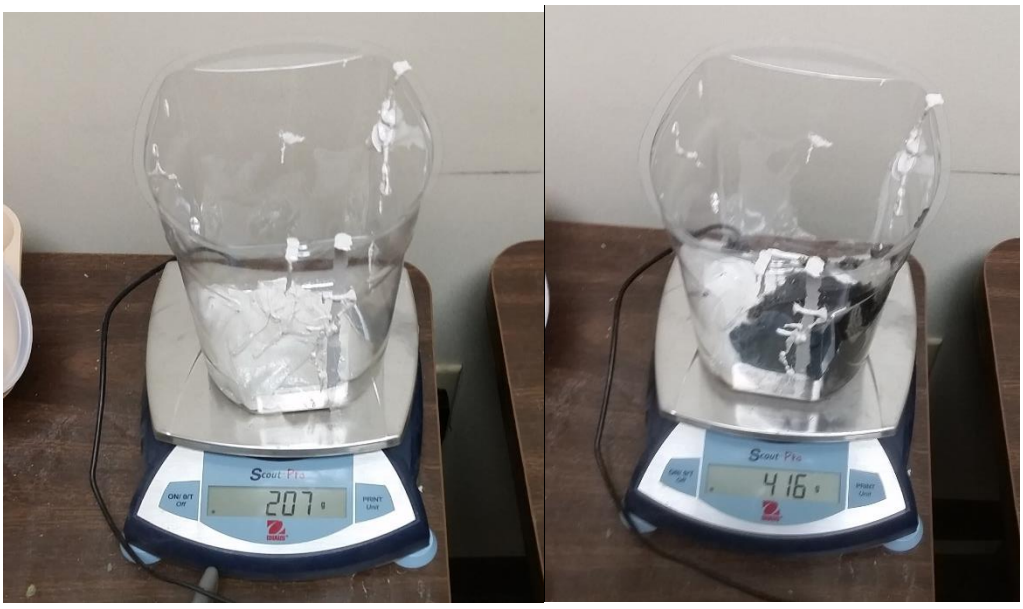


Figure 24: Batching of two components of epoxy

Another wooden paint stirrer was used to mix the two components by hand until the epoxy formed a uniform gray color and no white or black was visible, indicating a

homogeneous mix. Depending on the size of the mix and intensity of mixing, the duration of hand mixing with the stirring tool generally was between 2-5 minutes. This step is depicted in Figure 25.

Figure 25: Mixing two components of epoxy together

It should be noted that there was no specific reason why a wooden paint stirrer and a 2 inch plastic spatula were used, but it should be emphasized that three separate tools should be used to batch each component and mixing them together for two reasons. The first reason is to prevent one component on the batching tool from coming into contact with the other component in the storage container, and if this were to happen, the components could begin to react with each other in the storage container. The second

reason is to prevent excess component on the batching tool from coming into contact with the already-batched material in the plastic container for mixing. Once the material was properly batched, no more material was added. However, if the same tool was used for batching and mixing, then the individual component still on the tool might disrupt the 1:1 ratio in the plastic container.

### 5.5 Applying Epoxy to Concrete Plates

Once the epoxy was homogenously mixed, a wooden or metal spatula is used to transport the epoxy from the plastic container and place it onto the concrete plate. The epoxy was applied in the area encompassed by the lines that were previously drawn and the area of the web that was to be in contact with the flange. As mentioned before, the area bound by these lines represented the area where the web and flange were to be connected. It was made sure that the layer of epoxy was not too thick otherwise shrinking of the epoxy would have a negative impact on the connection. Therefore, the wooden or metal spatula was used to smooth and distribute the epoxy throughout the area dictated by the previously drawn lines and the area of the web that was to be in contact with the flange until the layer of epoxy was relatively small as seen in Figure 26.

Figure 26: Applying epoxy to concrete plate

There was no means of measuring the thickness of the epoxy layer, so visual inspection and judgement were used to determine whether the thickness of the epoxy layer was sufficient. Due to the fact that one of the first two beams to be tested had shear reinforcement consisting of aluminum angles, the aluminum angles needed to be in contact with the epoxy as well. The vertical leg of the aluminum angle was to be attached the web whereas the horizontal leg was to be attached to the flange. The epoxy was applied to one side of the vertical leg of the aluminum angle, yet the epoxy, that was to be in contact with the horizontal leg of the aluminum angle and flange, was applied directly on the flange. The reason that the epoxy was applied to one leg of the aluminum angle was to facilitate the placement of the aluminum angle which would not have been the case if the epoxy was applied on both legs of the aluminum angle prior to placement. The application of the epoxy in the area that was to be occupied by the horizontal leg of the

aluminum angle followed the same procedure for the application of the epoxy for the web-flange connection.

**5.6 First Flange - Web Attachment**

With the epoxy applied on the web and flange, the web was placed onto the flange such that the areas of the web and flange covered by epoxy would coincide with one another. Pressure was briefly applied downward onto the web by hand and the position of the web was adjusted such that the angle between the web and flange was 90 degrees. This step is illustrated in Figure 27.

Figure 27: First flange to web attachment

Bricks and/or wood blocks were strategically placed on both sides of the web until the epoxy set to ensure the required perpendicular connection. The epoxy needed at minimum 24 hours to completely set as per Sikadur-31 specifications, so as a conservative rule of thumb, the concrete plates were not disturbed until the next day. It would normally take 48 hours to for a beam to be fabricated, as the second flange would not be attached to the web until the epoxy from the first web-flange connection completely set.

## 5.7 Second Flange – Web Attachment

After checking by hand that the epoxy set, the clamps keeping the flange in place were removed. Mixing and applying the epoxy to the plates followed the same procedure as with attaching the first flange and web together. Similar to the web attachment to the first flange, bricks and/or wood blocks were placed on both sides of the web, however, an additional step was required. Since the web at this stage of the beam configuration was top heavy due to the previously attached flange, paper materials such as index cards were placed between the bottom of the top flange and the top of the bricks and/or wood blocks to hold the top flange in place, and to ensure that the web-flange connection remained perpendicular. To enhance the bond between the web and flange, bricks and/or wood blocks were placed on the top flange to provide downward pressure while the epoxy set. This can be seen in Figure 28.

Figure 28: Bricks and wood blocks stabilizing beam configuration

## 5.8 Application of FRP as Shear Reinforcement

### *5.8.1 Preparation of FRP*

The fiber reinforced polymer, more specifically basalt fiber, used for the shear reinforcement for some of the beams was basalt fiber. A sheet of basalt fiber had lines

drawn on it with a black marker to represent rectangular pieces with dimensions of six inches by seven inches. The dimension of six inches was required to reinforce the beam up to six inches from each end. The dimension of seven inches was required to reinforce the beam in shear by being connected to the top of the bottom flange, side of the web and bottom of the top flange. Figure 29 shows the preparation of the basalt fiber.

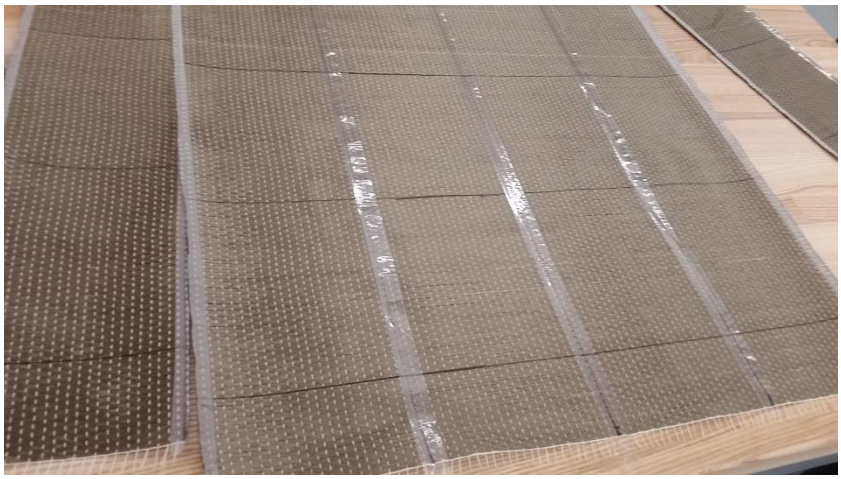

Fiber 29: Lines and tape applied to basalt fiber

Once these lines representing the dimensions were drawn, transparent scotch tape was placed on top of the lines perpendicular to the longitudinal orientation of the basalt fibers. This was done to prevent the fiber from fraying while cutting the basalt fiber with scissors.

*5.8.2 Batching and Mixing of Nano-Inorganic Composite*

The materials to produce the nano-inorganic composite consisted of a solid component and a liquid component. The solid component was previously batched and stored in a plastic bag. The liquid component needed to be batched out 190 grams for each bag of solid component. The solid component was first added to the blender, and then the liquid component followed which can be seen in Figure 30.

Figure 30: Adding materials into blender

The lid was placed on top of the blender and the blender was turned on maximum speed for two minutes. After two minutes, the blender was stopped and a plastic spatula was used to move any unmixed solid component to the bottom of the blender to produce the greatest yield of material. The lid was placed on top of the blender, and the blender was turned on maximum speed for another two minutes.

*5.8.3 Application of FRP onto Concrete Surface*

The nano-inorganic composite was poured into a square plastic container. One piece of the basalt fiber was placed nearby the container containing the nano-inorganic composite on a plastic sheet. A foam brush was dipped into the nano-inorganic composite, and the nano-inorganic composite was brushed onto the basalt fiber in the

direction parallel to the longitudinal axis of the basalt fibers until the color of the basalt fiber would not be visible through the layer of nano-inorganic composite. Figure 31 illustrates brushing the nano-inorganic composite onto the basalt fiber.

Figure 31: Brushing nano-inorganic composite onto basalt fiber

The piece of basalt fiber was then flipped over, and the process of applying the nano-inorganic composite was repeated. However, after the nano-inorganic composite was applied to the second side of the basalt fiber, a plastic roller with ridges was used to remove any excess nano-inorganic composite that may have been present. The piece of basalt fiber was flipped to its initial side where the nano-inorganic composite was applied with the foam brush and as with the second side, the use of the plastic roller was required. The beam was positioned on its side such that the flanges were vertical and the web was horizontal. The nano-inorganic composite was applied to the area of shear reinforcement along the beam. This area included parts the web, bottom of the top flange and top of the bottom flange that were within six inches from each end. Afterwards, the basalt fiber was placed on top of this designated area and downward pressure was applied by hand to

minimize the space between the concrete surface and basalt fiber. This is shown in Figure 32.

Figure 32: Applying slight downward pressure on basalt fiber

The foam brush was further used to apply additional nano-inorganic composite to the top surface of the basalt fiber, and a roller was used to remove any excess nano-inorganic composite. The process of applying the basalt fiber was repeated to the opposite end of the beam. The other side of the beam had basalt fiber applied to its ends after the nano-inorganic composite dried, which typically was assumed to be eight hours or overnight to be conservative.

### 5.9 Decision on Shear Reinforcement Material

The question that arose was whether aluminum angles or the basalt fiber be used as the shear reinforcement. The benefit of using aluminum angles was that epoxy and aluminum was readily available, and it only took two days for the beams to be ready for testing. There was a concern that the shear strength might not be great enough due to the fact that the previously dried epoxy protruded out and prevented the aluminum angles being flush with the corners at the web-flange connection. Whereas this would pose a potential problem for the rigid aluminum angles, the relatively flexible basalt fiber would not be significantly affected. The basalt fiber, would simply follow the contours of the web and flange. The issue with the basalt fiber was that it required the nano-inorganic composite. The nano-inorganic composite was produced by researchers at Rutgers University and was not necessarily readily available, and the nano-inorganic composite required a minimum of two weeks to completely set. Nevertheless, the basalt fiber was chosen in favor to the aluminum angles. After applying the basalt fiber to eight of the beams, six beams consisting of 13 mm steel fibers and two beams consisting of 6 mm steel fibers, more material to produce the nano-inorganic composite was required. Due to unforeseen delays in obtaining the required amount of material to produce the nano-inorganic composite, it was decided that the aluminum angles should play the role as shear reinforcement. The decision was reinforced with the fact that the type of shear reinforcement would not have a significant effect on the results of the flexural tests because the objective of the shear reinforcement was to ensure that the beams would fail in flexure and not in shear.

### 5.10 Post-beam Fabrication Aluminum Angle Attachment

After it was evident that waiting for more material for the nano-inorganic composite would result in substantial delay as discussed in Section 5.9, it was decided that the remaining beams would have aluminum angles serving as their shear reinforcement. The issue with attaching the aluminum angles at this stage was that the epoxy used to attach the web and flanges together was dry, and protruding out of the web-flange connections. At times, these protrusions prevented the rigid aluminum angles to be flush with the corners of where the web and flange met. This created spaces between the surface of the aluminum angle and the concrete. To compensate for this, the amount of epoxy was increased in order to fill up these voids. Using a clean, wood or metal spatula, epoxy was applied to the web in area bounded by 1 inch from the web and 6 inches from the end of the beam. This is depicted in Figure 33.


Figure 33: Applying epoxy to flange for aluminum angle attachment

This area was also the same size area as one leg of the aluminum angle. The metal spatula was used to apply epoxy also onto the vertical leg of the aluminum angle. The aluminum angle was then positioned such that the entire horizontal leg made contact with

the already-placed epoxy and the vertical leg made contact with the web of the beam. After the aluminum angle was set on the desired location, slight pressure was applied by hand towards the flange and web for 30 seconds to ensure the bond between the aluminum angle and concrete was strong as possible, and the epoxy would be essentially forced into any voids caused by the dry epoxy protrusions. Figure 34 shows how the aluminum angle was held in place.

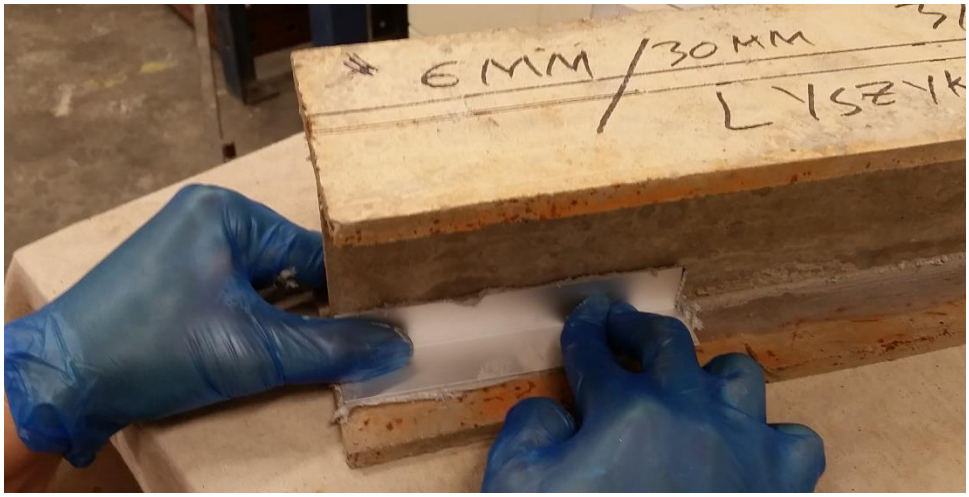


Figure 34: Holding the aluminum angle in place for 30 seconds

Due to the set time of the epoxy, aluminum angles were only attached to the bottom half of the beam on a given day. It was not until the following day that the beam was turned over, and four more aluminum angles were attached to the beam.

**5.11 Application of FRP to Bottom of Tension Flange**

In order to strengthen the bottom flange after cracking, basalt fiber was applied. A sheet of basalt fiber had lines drawn on it with a black marker to represent rectangular pieces with dimensions of 3 inches by 18 inches. The dimension of 3 inches was chosen to ensure that the flexural strength was enhanced while simultaneously not too strong in flexure such that a shear failure would be prevented. The dimension of 18 inches ensured

that the basalt fiber covered the entire length of the bottom flange. Once these lines representing the dimensions were drawn, transparent scotch tape was placed on top of the lines perpendicular to the longitudinal orientation of the basalt fibers. This was done to prevent the fiber from fraying while cutting the basalt fiber with scissors. The batching, mixing and application of the nano-inorganic composite followed the same procedure as in Sections 5.8.2 and 5.8.3, respectively. Figure 35 illustrates how the roller was used to remove excess nano-inorganic composite from the basalt fiber.

Figure 35: Roller removing excess nano-inorganic composite from basalt fiber

The beam was positioned such that the bottom flange was facing up and parallel with the surface of the table. The nano-inorganic composite was applied in an area 3 inches in width and ½ inch from each side of the flange since the 3-inch wide basalt fiber fabric was to be placed in the middle of the bottom flange as depicted in Figure 36.

Figure 36: Aligning basalt fiber in the middle of the bottom flange

Afterwards, the basalt fiber was placed on top of this designated area and downward pressure was applied by hand to minimize the space between the concrete surface and basalt fiber. The foam brush was further used to apply additional nano-inorganic composite to the top surface of the basalt fiber, and a roller was used to remove any excess nano-inorganic composite.

## 6. Testing

### 6.1 Compression Test

After undergoing 28 days of moist curing, the cylinders were removed from the curing room. Three cylinders of each mix type were tested to obtain the compressive strength. The equipment used was a Forney compression machine. The cylinder had steel caps placed on each of its ends, and the cylinder was placed directly onto the testing platform in the compression cage as see in Figure 37.


Figure 37: Concrete cylinder in compression machine cage

The plate providing the compression force was lowered onto the top of the cylinder until the plate was barely touching the cylinder yet at the same time holding the cylinder in place via compression. At this point, the load reading was zeroed out. The compression machine was set on ‘Metered Advance’ and the load rate was controlled by hand using a dial situated on the machine. The load rate generally was between 200 lb/sec and 400 lb/sec. The test was concluded until the ultimate load was reached and the cylinder broke.

## 6.2 Elastic Modulus Test

### *6.2.1 Overview*

After undergoing 28 days of moist curing, the cylinders were removed from the curing room. The cylinders were to be tested to obtain the elastic modulus in compression. An elastic modulus cage was used to measure the axial deformation. An issue arose with the elastic modulus cage in which the spring connecting the top and bottom yokes was too loose, and would prevent the top yoke from being parallel to the bottom yoke. There was a delay in testing as it took time for the manufacturer of the elastic modulus cage to send a new spring. By the time the spring arrived and was fitted onto the elastic modulus cage, another issue arose. Due a prior commitment, the researcher in charge of testing was to be away for a period of time. Although the some of the earlier-cast cylinders could have been tested on Day 35 instead of Day 28, the later-cast cylinders would could not have been tested having a similar age since the researcher would not be present to test the cylinders. Therefore, it was decided that the elastic modulus testing should commence after the researcher returned such that all the cylinders would be tested with the same age. Even though the age of the cylinders on the day of testing was 70 days rather than 28 days, it was assumed that since the rate of increase of the compressive strength of concrete typically slows down dramatically after 28 days, the older age of the cylinders would not have much effect in the compressive elastic modulus.

### *6.2.2 Placement of Elastic Modulus Cage onto Cylinder*

Unlike the previous compressive tests where the metal caps were placed on both ends of the cylinder, the size of the elastic modulus cage prevented the metal caps from

fitting onto the cylinder. Instead of metal caps, both ends of the cylinder being tested were dipped into liquid sulfur. With sulfur caps in place, the elastic modulus cage was able fit onto the cylinder. The total height of the elastic modulus cage was 6 ½ inches and the cylinders were 8 inches in height. Being that the optimal position for elastic modulus cage was to be as symmetric to the cylinder as possible, the bottom yoke of the elastic modulus cage was placed on a two separate pieces of medium density fiberboard with a thickness of ¾ inch. Figure 38 illustrates the elastic modulus cage resting on the two separate pieces of medium density fiberboard during attachment.

Figure 38: Attachment of elastic modulus cage

This allowed for the bottom yoke to be level during attachment to the cylinder, and for the cylinder to be placed symmetrically along the longitudinal axis of the cylinder by having ¾ inch of clear space between the yokes and ends of the cylinder. The screws on the bottom yoke were attached first, and they were turned such that they would reach

the surface of the cylinder simultaneously to prevent eccentricity. The attachment of the middle yoke followed, as did the top yoke. While attaching all three yokes, it was important that the pin holding up one side of the top yoke remained completely vertical and the axial deformation pin was centered on the pin's required platform. It was made sure that the screws were symmetric in how far they were turned so that the cross section of the cylinder was concentric with that of the yokes. Once all the screws were secured and the elastic modulus cage was in optimal position, the braces holding the yokes together were removed.

*6.2.3 Elastic Modulus Test Procedure*

Using a Forney compression machine, the cylinder with the elastic modulus cage was placed directly onto the testing platform in the compression cage. The machine was turned on, and the plate providing the compressive force was lowered onto the top of the cylinder until the plate was barely touching the cylinder yet at the same time holding the cylinder in place through compression. At this point, the deformation measuring device on the elastic modulus cage and the load cell on the compression machine were zeroed out. The compression machine was set on 'Metered Advance' and the load rate was controlled by hand using a dial situated on the machine. Though the setup of the compression machine prevented the load rate from being constant, the load rate was typically 200 lb/sec. It should be noted that the load rate was below the range of that specified in ASTM C469 due to the fact that the researcher needed to control the load rate dial manually and record simultaneously, so a lower load rate allowed enough time for the researcher to observe when the load cell reached a 1000 pound interval and record what the axial deformations were. The axial deformation measurements were recorded at

every 1000 pounds until 40% of the cylinder's ultimate load was reached as per ASTM C469 Specifications.


Figure 39: Cylinder in compression cage with elastic modulus cage

Despite the fact that the cylinders used for elastic modulus testing were not used for compressive strength tests, the ultimate load of the cylinders were assumed to be the same as cylinders of the same mix tested previously. This was done in order to estimate when the load was to about to exceed the elastic limit. If anything, the assumed elastic

limit at 28 days was more conservative, as a 70-day old cylinder would require a greater load to exceed the elastic limit. Once the cylinder was tested to 40% of its assumed ultimate load, it was removed from the compression machine and placed on a nearby table. The elastic modulus cage was removed from and refitted on the cylinder to be tested again. This procedure was repeated one more time until the elastic modulus readings were recorded twice as per ASTM C469 Specifications.

## 6.3 Flexural Test

### *6.3.1 Beam Preparation*

A black marker was used to draw lines along the outer surface and thickness of the top and bottom flange. Lines were drawn across the width of the beams at a distance of 1 inch from the beam's ends, and this line was continued onto the side of the flanges. This line was made to assist in proper placement of the beam on the point supports, and to ensure there was a 1 inch overhang towards each end. Lines were also drawn across the width of the beams at a distance of 7 inches from the beam's ends, and this line was continued onto the side of the flanges. This line was made to ensure the two point loads would be symmetric placed onto the beam.

### *6.3.2 Test Setup*

The beam was situated on two point supports. The apices of the two point supports were 16 inches from each other to provide one inch overhang to prevent slipping. The simply supported system, as seen in Figure 40, was made of ¼ inch thick steel plate with dimensions of 6 inches by 22 long inches, and two ⅛ inch thick steel angles with dimensions of 2 inches by 2 inches. The angles were cut to a length of 5 inches to allow enough room for the width of the 4 inch wide beam. Two point loads

consisted of two ¼ inch thick rods three inches in length. The point loads were separated 4 inches apart from one another.

Figure 40: Simply supported system with two point supports

*6.3.3 First Group Test Procedure*

The beam was placed on the point supports such that the lines on the bottom flange one inch from each end coincided with the apices of the point supports. Next, the point loads were aligned with the lines on the top flange seven inches from each end. Because the point supports were five inches wide compared to the four inch width of the beam, the beam was centered in the middle of the point support. Due to the fact that the width of the beam was larger than the lengths of the rods acting as the point loads, the beam was also positioned such that the center of the width of the point loads coincided with the longitudinal axis of the beam. This is illustrated in Figure 41.

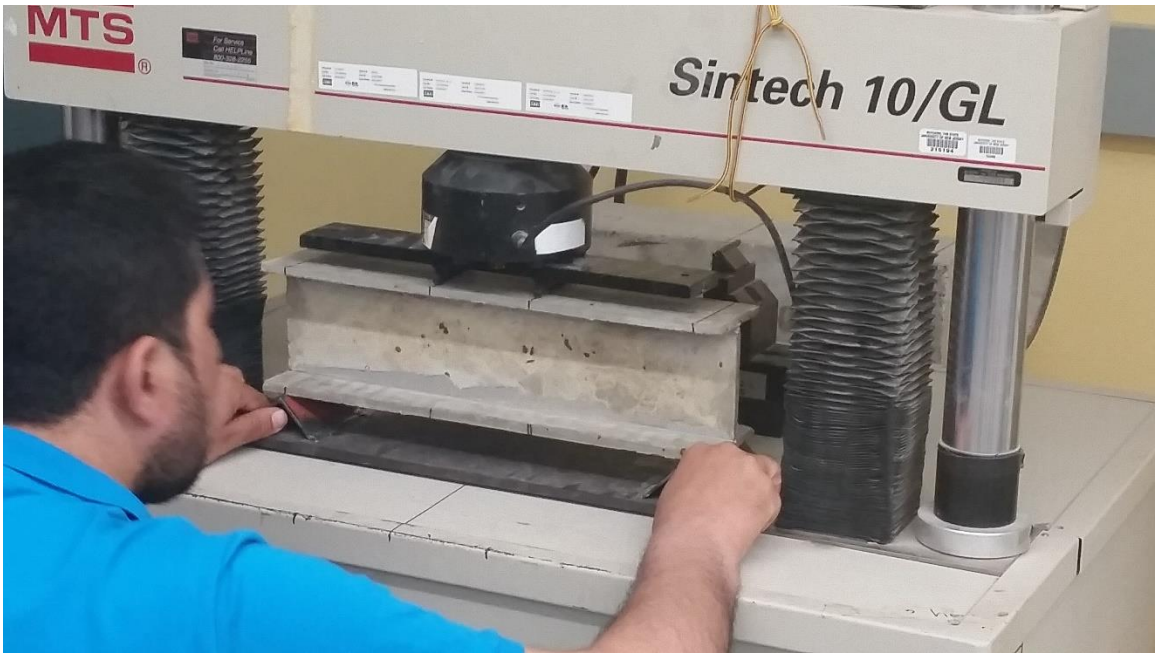


Figure 41: Positioning of beam onto point supports

This was to ensure the load acting on the beam was not eccentric. Once in position, the fine adjustment knob on the MTS machine was used to lower the point load onto the beam until the point loads were barely touching the top flange and the measured load was 10 to 15 pounds. Even though the load was not zeroed out prior to testing, the 10 to 15 pound offset was deemed to have negligible effect since the failure load was predicted to be two order of magnitudes larger than the load offset and the load offset was kept consistent with all beam specimens. The deflection reading was zeroed out, and the MTS flexure machine automatically applied the load, while recording the load and deflection. The beam was tested beyond failure until it was evident that the load was relatively constant while the deflection continued to increase.

*6.3.4 First Group Flexural Test Observations*

After the testing the two beams of the first group, one beam with aluminum angles for shear reinforcement and one beam without shear reinforcement, it was

concluded that the epoxy was strong enough to serve its purpose since it was evident that no delamination had taken place. The beam without shear reinforcement failed in shear, whereas the beam with shear reinforcement failed in flexure as seen in Figure 42.

Figure 42: First Group after failure

It was decided that the remaining beams would require shear reinforcement since the objective of the project is to study the flexural strength rather than the shear strength.

*6.3.5 Second Group Test Procedure*

The second group was tested using the same procedure as the first group described in Section 6.3.3. The second group was tested in flexure in strength with only shear reinforcement to determine the ultimate flexural strength of the beams.

*6.3.6 Third Group Test Procedure*

The third group was tested using the same procedure as the first and second group, except the test to beginning of cracking was stopped until it was visually evident that cracking began, and the beams were removed from the MTS flexural machine and

placed in a secure temporary storage location. Figure 43 shows how much a crack would typically propagate before stopping the first phase of testing.


Figure 43: Extent of cracking for first phase of testing

Basalt fiber was attached to the bottom of the tensile flange as described in Section 5.10. After two weeks of the nano-inorganic composite curing, the beams were tested to failure using the same procedure as discussed in Section 6.3.3.

When the sixth beam (first beam in the 6 mm steel fibers sub-group) was tested in flexure, both flexural cracks and shear cracks were present. Not sure at the time whether the occurrence of shear cracks was due to the beam's properties or the flexural strength with the addition of the basalt fiber on the bottom flange was too great, it was decided that two more beams would be tested to see if shear cracks develop. If this was case, the basalt fiber on the bottom flange would have had to be reduced. Two beams (both beams in the 13 mm steel fibers sub-group) were tested, and they both developed flexural cracks and shear cracks. One such beam is depicted in Figure 44.


Figure 44: Shear and flexural cracks present in beam during testing

It was concluded since the issue occurred with beams of a different sub-group that shear cracks developed due to the increase of flexural strength. It should be noted that the beams with the first five beams tested in the third group (30 mm steel fibers and 50 mm steel fibers) alone had no issue with shear cracking. A possible reason for this is that the flexural strength of these beams were less than that of the beam of the other sub-groups. It was advised to reduce the width of the basalt fiber along the bottom of the tensile flange for the remaining beams. The basalt fiber was reduced to 2 inches in order to lower the flexural strength while simultaneously providing enough basalt fiber to see an increase in flexural strength.

Since the width of the remaining beams' basalt fiber was to be reduced to 2 inches, a strip ½ inch in width was removed from each side. A tape measure and black marker was used to indicate ½ inch from both sides of the FRP. A sharp-bladed knife was used to cut through the dried nano-inorganic composite and basalt fiber along the lines

made by the black marker. The ½ inch strips were lifted up with the knife on one end and pulled off by hand. After having the width of the basalt fiber reduced, the remaining beams were tested to failure using the procedure described in Section 6.3.3. Figure 45 and Figure 46 show cutting the basalt fiber with a knife and removing the strip of basalt fiber, respectively.

Figure 45: Using a knife to cut the basalt fiber on bottom flange

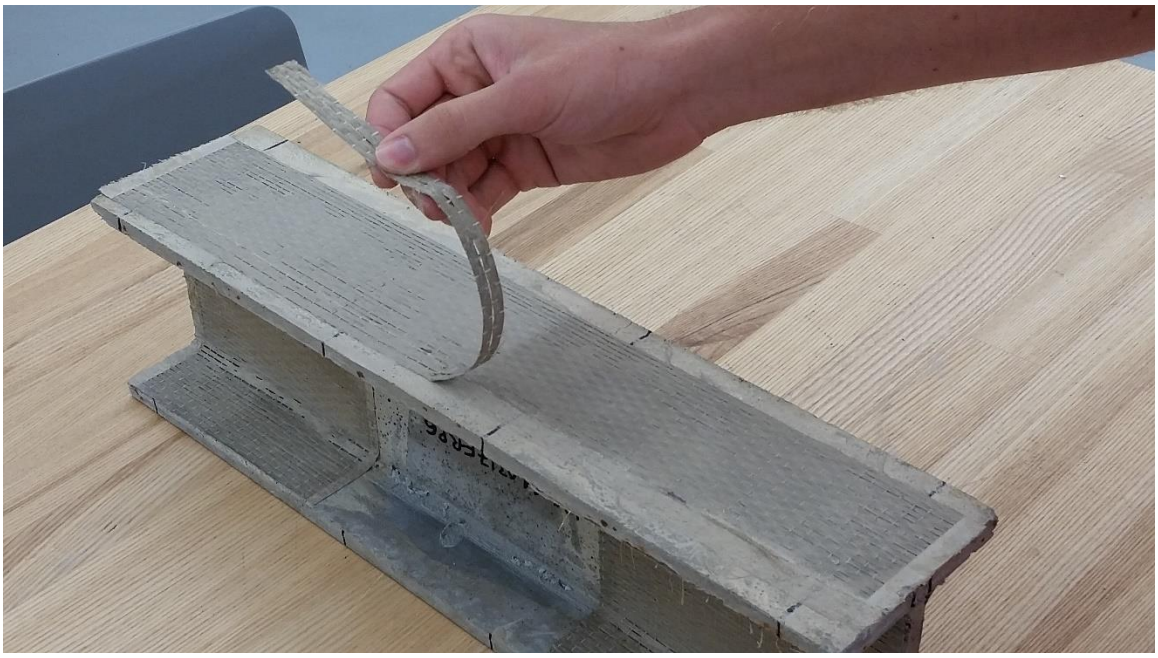

Figure 46: Removing a strip of basalt fiber

## 7. Tension Test & Three-Dimensional Mold Attempts

### 7.1 Tension Test

#### *7.1.1 First Method for Tension Samples*

In order to determine the tensile strength and tensile elastic modulus of the concrete, plate samples were to be made to be tested in tension. The elastic modulus was to be determined by recording the strain via strain gage directly attached onto the concrete. The first method's proposed design was a concrete specimen with dimensions 2 inches by 8 inches and a thickness of ⅜ inch. The molds and casting for the tension samples followed the same procedure as described in Sections 2 and 4.1, respectively. After 28 days of moist curing, the tension samples were removed from the curing room. It was then realized that the distance between the grips of the tension machine was greater than the length of the tension samples.

*7.1.2 Second Method for Tension Samples (with wooden grips)*

The next proposed method of performing the tension samples was to use 4 inches by 18 inches plate samples with a thickness of ⅜ inch. The focus on using this size of a plate sample to test in tension was that a set of intermediate grips needed to be constructed as seen in Figure 47.

Figure 47: Intermediate grip made out of wood

There were two reasons why a set of intermediate grips needed to be constructed. The first reason was to prevent contact and potential slipping of the concrete with metal grips of the machine. The second reason was to provide a means of fitting a 4 inch wide plate sample to fit on the tension machine's 2-inch wide grips. Therefore, a proposed design required one end of the intermediate grips to be 4 inches in width to match the width of the plate sample, and the width of the intermediate grips would have a width to match the width of the metal grips present on the tension machine. Wood was chosen as the material for the intermediate grips because it had a relatively low cost, was readily available, and was easy to cut. The challenge that came with choosing wood as the material to fabricate the intermediate grips was that it was difficult to get perfectly

straight lines required for the grips. Figure 48 illustrates the design of the intermediate grips.

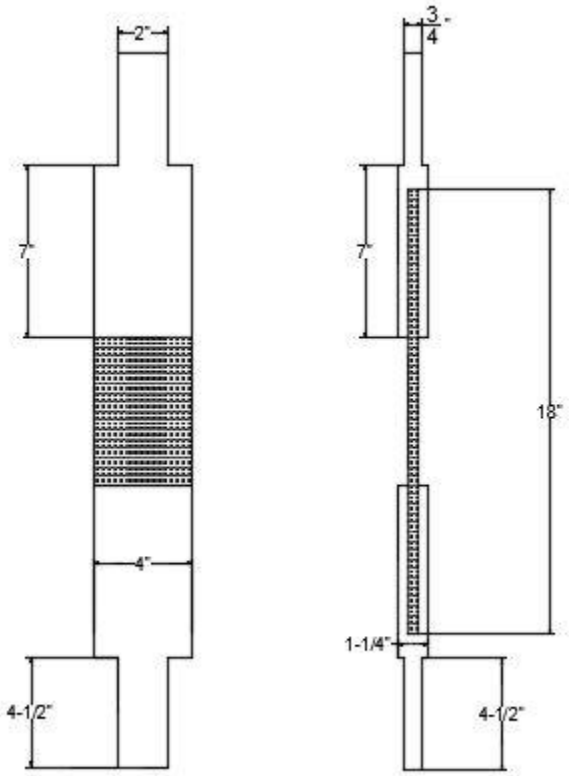


Figure 48: Design of wooden intermediate grips

*7.1.3 Third Method for Tension Samples*

Due to the fact that the wooden grips were able to be correctly fabricated, the idea was proposed to design a concrete sample such that that maximum width would completely fit the machine's metal grips, yet have a narrowed cross section in the middle so that the failure would be guaranteed to take place in the middle of the specimen, away from the grips. Figure 49 displays the design of the plate mold for the third method tension samples.

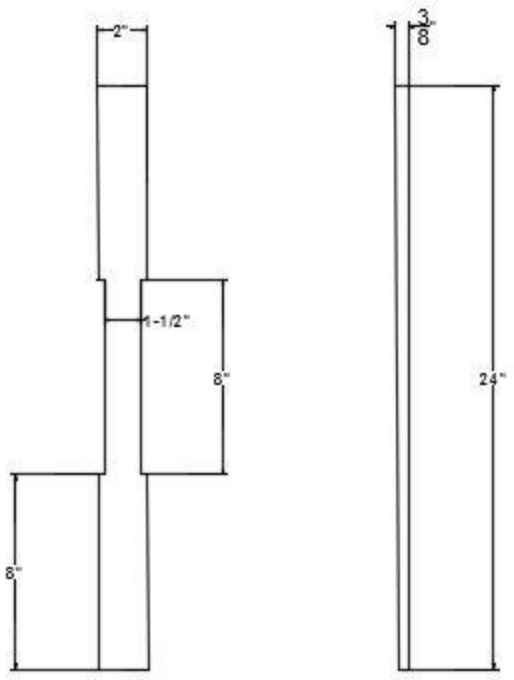


Figure 49: Design of tension samples for third method

The mold fabrication and placement of concrete of the tension samples followed the same procedure as described in Sections 2 and 4.1, except for two changes in the mold fabrication. The mold was constructed such that the interior dimensions were 2 inches by 24 inches. Furthermore, two 8-inch pieces of hardwood strips with a cross section of ¼ inch by ¼ inch were glued together and attached along the interior perimeter of the middle third of the side piece with duct tape. The molds for the tension samples can be seen in Figure 50.


Figure 50: Molds for tension samples in third method

This was done on the other side piece as well so that the concrete sample would narrow in the middle third. Once the concrete samples spent 28 days of moist curing in the curing room, the concrete samples were taken out and let to dry. A strain gage was attached in to the middle of the tension sample. The strain gage was attached to the middle third such that the both the center and longitudinal axis of the strain gage coincided with the center and longitudinal axis of the tensile specimen. A small amount of 200 Catalyst-C was applied onto the location where the strain gage was to be situated.

After 30 seconds, the accompanying M-bond 200 Adhesive was placed in this location, followed by the strain gage. After 3 minutes of constant downward pressure by hand onto the strain gage, the sample was ready for testing. The concrete tensile sample was set in the tensile machine. During the test, the failure occurred in the bottom third of the tension sample, near the grips as see in Figure 51.

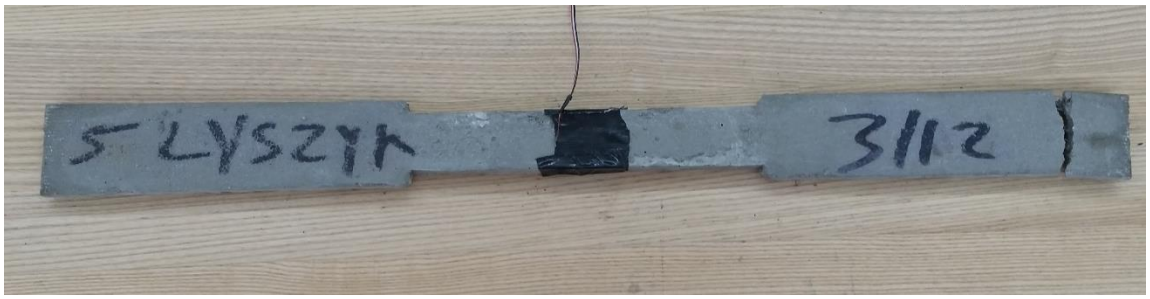

Figure 51: Failure occurred near grips for third method of tension test

This was not a desired outcome. It was discovered that the cross section of the middle third of the specimen was in fact larger than the bottom and top thirds. Although the width of the middle third was smaller than the remainder of the specimen, the thickness happened to be too large and thus created a larger cross section than that of the bottom and top thirds of the specimen. This could have resulted due to two possible reasons. One possible reason is the width of the middle third of the tension specimen was smaller than the length of the 50 mm steel hooked-end fibers that were placed. This relatively small width could have could have caused the steel fibers to be stuck in between the two sides of the mold, preventing concrete from consolidating entirely, and causing the concrete to build up on top, exceeding the desired thickness. The second possible reason is that because concrete in the middle third was level to ensure a thickness of ½ inch rather than ⅜ inch. This was due to the two ¼ inch thick hardwood strips being stacked on top of each other, resulting in a thickness of ½ inch. Since

consolidation during concrete placement was aided by using a steel trowel, the width of the middle third was too small to allow the steel trowel to level the concrete in the middle third to a thickness of ⅜ inch, and the two ¼ inch pieces of hardwood strips dictated the thickness of the middle third of the tension specimen. Furthermore, it was deemed that the load cell of the tension machine was too high for the tension samples since the tension sample failed around 500 to 600 pounds, whereas the tension machine had a capacity of 60,000 pounds. Figure 52 displays the analog load display of the tension machine.

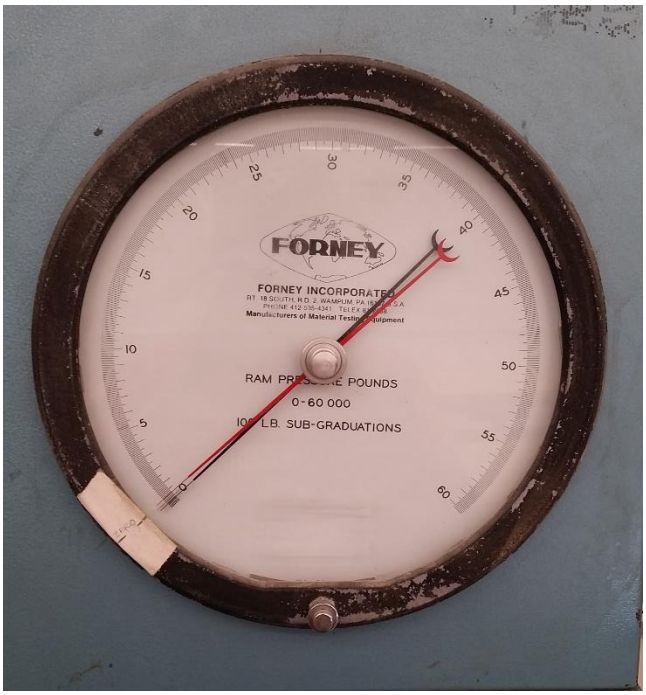


Figure 52: Analog load display of tension machine

*7.1.4 Fourth Method for Tension Sample (proposed, not implemented)*

Based on the previous methods to perform a direct tensile test, the next method followed closely to that of the first method. The tensile specimen would roughly be the same size as that described in the first method of performing the tensile test. The difference in this method was the machine used. Instead of the tension machine, the MTS machine that normally was used for flexural tests would be utilized. Using the MTS

machine, the computer program Test Works would be able to record the instantaneous load, deformation and plot this information on a graph. What was needed was a set of tension grips that could be temporary installed on the MTS machine. Due to delay and time constraint of obtaining the tension grips, it was decided to forgo this method. Out of the methods attempted in this project to determine the tensile properties, both elastic modulus and uniaxial strength, this method is recommended for future researchers to pursue if documenting such characteristics of their concrete is desired.

## 7.2 Three Dimensional Mold and Beam

### *7.2.1 Background*

An attempt was made to fabricate a concrete I-beam using a three-dimensional mold. If this method were to be successfully implemented, it would forgo the step of attaching the concrete plates together via epoxy. Wood was used to construct the three-dimensional wood as it was relatively inexpensive and readily available. It was decided to used 6 mm steel fibers premixed in the concrete. This was done to maintain the desired random orientation of the steel fibers, which would have not been possible with the larger steel fibers since they would have tended to align parallel to the longitudinal axis of the beam within the ⅜ inch thick web.

### *7.2.2 Construction of Mold*

The mold composed of three main parts: the bottom and edges of the bottom flange, the web and interior surfaces of the top and bottom flanges, and the top and edges of the top flange. These parts shall be named Section A, Section B, and Section C, respectively. Section A was constructed using the same procedure as for the plate sample molds described in Section 2, however, the plywood was 4-¾ inches wide and 18-¾

inches long, and the hardwood strips consisted of two pieces 18-¾ inches in length and two pieces 4 inches in length. Section B consisted of three sub-sections that eventually were attached to each other. Figure 53 shows the design of the three dimensional mold.

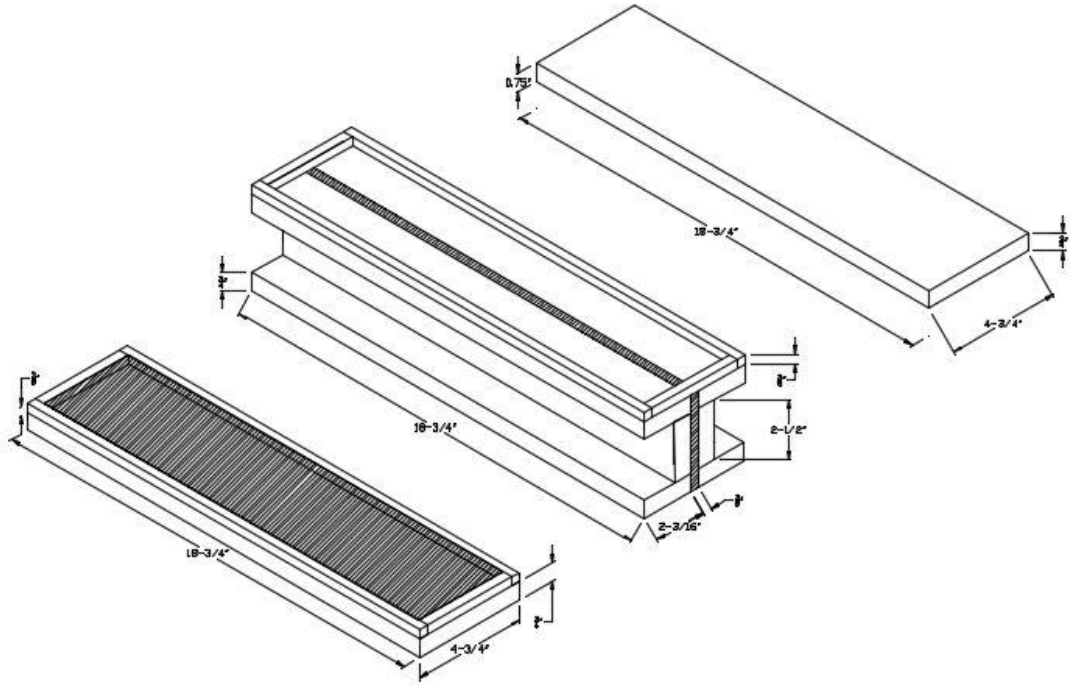

Figure 53: Left – Section A; Middle – Section B; Right – Section C

The first sub-section was made up two pieces of plywood with a width of 2-½ inches and four pieces of plywood with a width of 2-$^{3}/_{16}$ inches. All six pieces were of 18-¾ inches long. Each 2-½ inch wide piece were placed orthogonally between two 2-$^{3}/_{16}$ inch wide pieces and attached with brackets and screws. The second sub-section composed of two pieces of wood that were attached to the ends of the beam along the web. This sub-section was a piece of plywood measuring 4 inches in height and 2 inches wide. A 4 inch long hardwood strip was attached to one end to fit inside the end of the mold to ensure the ⅜ inch thickness was retained throughout the entire web. The second sub-section was attached to the first sub-section via brackets and screws. The third sub-section was made up of two hardwood strips measuring 18-¾ inches in length and two

hardwood strips measuring 4 inches in length. All four pieces were hammered on top of the second sub-section similar to that of Section A. Section C composed of the same size plywood as Section A.

*7.2.3 Beam Casting*

The plate mold for the bottom flange was placed on a vibrating table and WD-40 was sprayed into the interior surface of Section A, B and C. With the vibrating table turned on, concrete was placed into the mold with a scoop and a 6 inch wide steel trowel was used to smooth the top surface of the concrete. Section B was placed on top of Section A such that the perimeters of both sections would coincide with one another. Clamps were placed to hold Section A and Section B together. Due to the limited amount of clamps, one clamp was used on each side of the bottom flange. The clamps were positioned such that they were equidistant from both each other and the ends of the beams to prevent eccentricity. Concrete was placed into the web and into the top flange as seen in Figure 54.

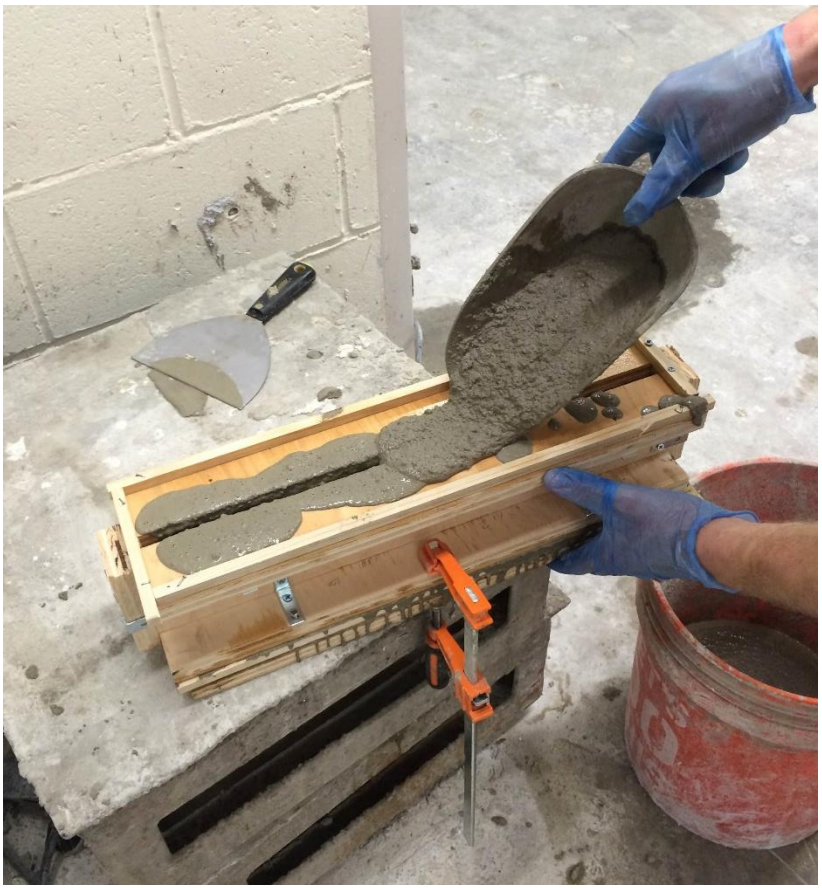

Figure 54: Placing concrete in top flange and web

A 6 inch wide steel trowel was used to smooth the top surface of the concrete. Section C was placed on top of Section B such that the perimeters of each section would coincide with another. Clamps were placed to hold Section B and Section C together. As stated before, due to the limited number of clamps, the clamps were positioned similar to that of the clamps on the bottom flange. The casted beam was placed on top of a bucket during dry curing since the clamps would have prevented the casted beam from curing on a flat, level surface such as the floor or table. The beam spent 24 hours of dry curing in an environmentally stable lab before being demolded.

*7.2.4 Beam Demolding*

The clamps at the top of the beam were removed as well as the top plank of wood. A hammer and chisel were used to dislodge the ⅜ inch hardwood strips from the top of the beam. It should be noted that the direction of the hammering of the chisel was parallel to the local edge of the flange as to prevent damage to the concrete beam. The screws attaching the ends of the web to the sides of the web were removed as were the wood pieces covering the ends of the web via a ⅜ inch corded drill. This can be seen in Figure 55.

Figure 55: Removing screws and brackets from end of web

The drill was then used to remove the screws and brackets attaching the interior flange wood pieces to the sides of the web. The chisel was positioned at one end of the remaining wood pieces attached to the flange. The hammer forced the wood piece to dislodge from in between the flange and web. This step was repeated to the other remaining wood pieces attached to the flange and web. The order of which the wood pieces were removed was from top to bottom. At this point of the demolding process, the

remaining part of the wooden mold was attached to the bottom and sides of the bottom flange. This resembled the setup for concrete plate samples. The ⅜ inch hardwood strips were removed using the same procedure as described in Section 4.2. The beam was removed from the last piece of the wood and placed in the curing room for 28 days.

*7.2.5 Comments*

After spending 28 days in the curing room, observations were made to determine whether the beam was in adequate condition to be tested and whether this method of beam fabrication should be pursued in this project. Observations included: concrete leaking during casting, web and flanges were not lined up and cross section was not symmetric, cracks easily formed from misaligned flange and web. Figure 56 and Figure 57 show the misalignment that occurred with utilizing the three dimensional mold and the cracks that occurred during dry curing in the mold, respectively.

Figure 56: Misaligned web with bottom flange

Figure 57: Cracks that occurred during dry curing

Evidently it was decided not to pursue this method. The underlying culprit was the choice of material for the mold: wood. With wood as the main material for the three-dimensional mold, it was hard to get mold perfectly shaped, and the concrete seemed to stick to wood even if release lubricant was used.

# CHAPTER 4: RESULTS

This chapter discusses the results of the experimental program conducted on SIFCON plates. The test results include compression test results on fiber concrete and hybrid fiber concrete specimens as well results from modulus of elasticity test on concrete cylinders. However, most of the test results and discussions reported in this chapter will focus on I-beam test results in flexure.

## 1. Compressive Strength Tests

Compressive tests were conducted on fiber concrete cylinders with variable fiber content and fiber types. Table 1 shows the results of the compression tests of the various fiber content combinations. The compressive strengths shown in the table are given in pounds per square inch (psi). Three cylinders, labeled ‘A’, ‘B’ and ‘C’, of each fiber content combination were cast and tested using a Forney Compression Machine available in the Civil Laboratory at Rutgers University. The cylinders were tested at 28 days. The average compressive strengths are tabulated in the last row in Table 1. The test results show that the cylinders with hybrid fibers gave the highest compressive strength compared to the cylinders with only one type of fibers. Those cylinders with hybrid fibers including 6 mm brass-coated micro fibers and 30 mm hooked fibers give the highest compressive strength followed by those cylinders with hybrid fibers 13 mm micro fibers and 50 mm hooked steel fibers. The cylinders with only 13 mm brass coated micro straight fibers and only 6 mm brass coated micro straight steel fibers have the lowest compressive strengths. The cylinders with only 50 mm hooked steel fibers and only 30 mm hooked steel fibers have intermediate compressive strengths.

Table 1: Compressive Strength of Concrete Cylinders with Various Fibers

| COMPRESSIVE STRENGTH (psi) | | | | | | |
|---|---|---|---|---|---|---|
| | **6 MM** | **13 MM** | **30 MM** | **50 MM** | **6 MM & 30 MM** | **13 MM & 50 MM** |
| **A** | 9,016 | 8,693 | 8,811 | 8,721 | 10,253 | 9,391 |
| **B** | 8,878 | 7,967 | 8,558 | 9,185 | 10,062 | 9,221 |
| **C** | 7,996 | 7,657 | 9,778 | 8,905 | 10,050 | 9,398 |
| **Average** | 8,630 | 8,106 | 8,685 | 8,953 | 10,121 | 9,337 |

Figure 1 shows the comparison of the average compressive strengths of each of the different fiber content combinations based on three cylinders tested after 28 days. This bar graph provides a visual representation of the average compressive strengths. As with Table 1, the compressive strengths have units in pounds per square inch (psi). The concrete with 6 mm micro fibers and 30 mm hooked steel fibers has the highest compressive strength, whereas the concrete with 13 mm steel fibers has the lowest compresive strength. From the highest strength to the lowest strength, the fiber combinations are as follows: 6 mm & 30 mm steel fibers, 13 mm & 50 mm steel fibers, 50 mm steel fibers, 30 mm steel fibers, 6 mm steel fibers and 13 mm steel fibers.

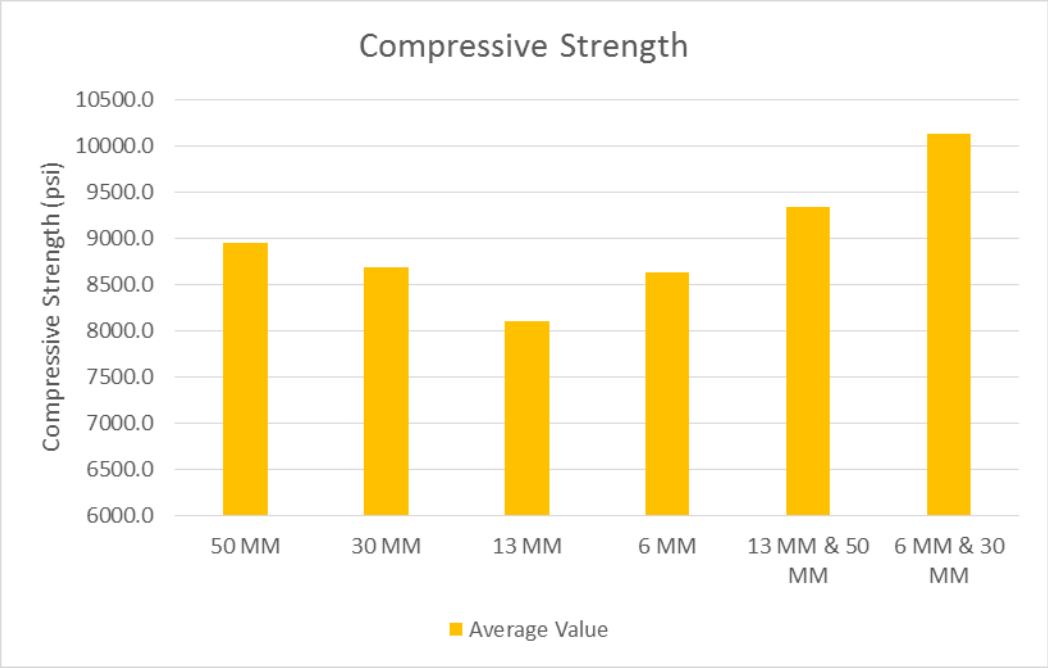


Figure 1: Average Compressive Strengths of Cylinders

**2. Elastic Modulus in Compression**

The measured values of the elastic modulus in compression for the different steel fiber combinations are tabulated in Table 2. Apart from the concrete with only 50 mm hooked steel fibers and only 30 mm hooked steel fibers, three cylinders were tested in compression within the elastic region to determine the elastic modulus. There were only two cylinders for the 50 mm hooked steel fibers and 30 mm hooked steel fibers, however, the two values of elastic modulus are relatively close to one another. The elastic modulus is in units of kips per square inch (ksi). The cylinders with the highest elastic moduli are those made with 13 mm micro fibers and 50 mm hooked steel fibers and those made with 6 mm micro fibers and 30 mm hooked steel fibers. The cylinders with the lowest elastic moduli were those made with 50 mm hooked steel fibers and with only 30 mm hooked steel fibers. The cylinders with elastic moduli between the lowest and highest values are those with 13 mm steel fibers and 6 mm steel fibers.

Table 2: Compressive Elastic Modulus of Concrete Cylinders with Various Fibers

| COMPRESSIVE ELASTIC MODULUS (ksi) | | | | | | |
|---|---|---|---|---|---|---|
| | **6 MM** | **13 MM** | **30 MM** | **50 MM** | **6 MM & 30 MM** | **13 MM & 50 MM** |
| **A** | 4,442 | 4,674 | 4,252 | 4,237 | 4,428 | 4,735 |
| **B** | 4,244 | 4,374 | 4,461 | 4,276 | 4,547 | 4,584 |
| **C** | 4,827 | 4,298 | x | x | 4,681 | 4,341 |
| **Average** | 4,504 | 4,449 | 4,357 | 4,256 | 4,552 | 4,553 |

Figure 2 shows the comparison of the average compressive elastic modulus of multiple cylinders for each of the different fiber content combinations tested after 70 days. This bar graph provides a visual representation of the average compressive elastic moduli. As with Table 2, the compressive strengths have units in ksi. The concrete with 13 mm mircro/50 mm hooked steel fibers has the highest elastic modulus, whereas the concrete with 50 mm steel fibers has the lowest modulus. From the highest elastic modulus to the lowest elastic modulus, the fiber combinations are as follows: 13 mm & 50 mm steel fibers, 6 mm & 30 mm steel fibers, 6 mm steel fibers, 13 mm steel fibers, 30 mm steel fibers and 50 mm steel fibers.

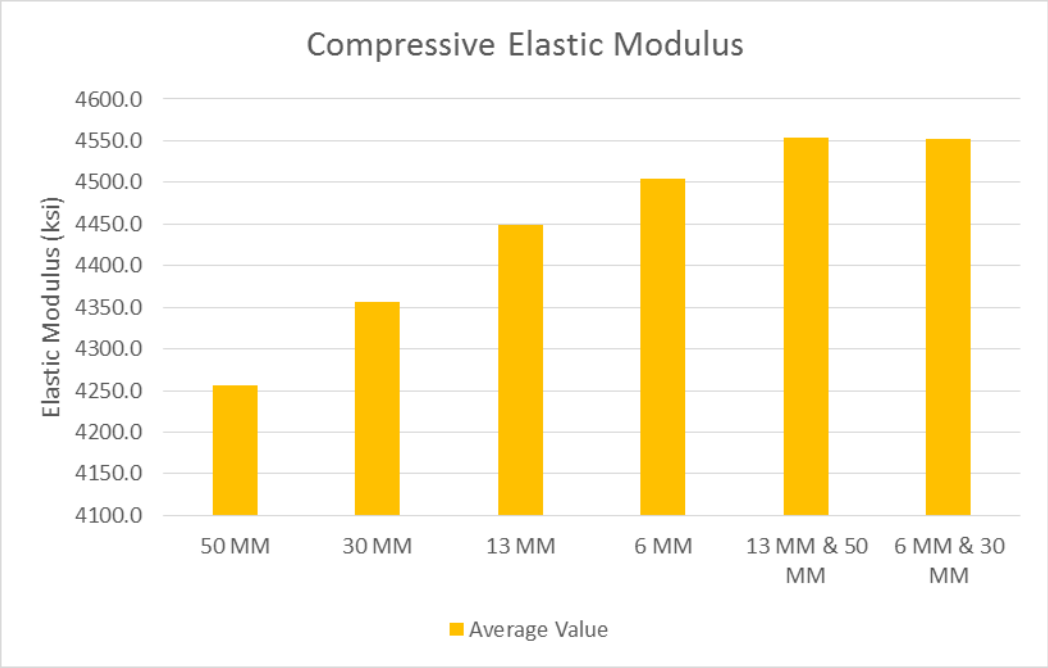


Figure 2: Average Elastic Moduli of Cylinders in Compression

**3. Flexural Behavior**

Although three beams were tested for each sub-group with exception of the 50 mm hooked fiber sub-group, one beam was used to represent its corresponding sub-group to compare its load-deformation curve with that of another beam sub-group. Only one beam was chosen to represent its corresponding sub-group in to reduce congestions in the graphs. The load-deformation curves are divided into three groups to highlight three different attributes: beams that were tested to ultimate load without external basalt fiber flexural reinforcement, beams that were tested to first crack load, and beams that were tested to ultimate load with external basalt fiber flexural reinforcement after having been cracked. Due to the fact that the concrete plates of the different beams were cast at different times of the study, it was a common occurrence that the beams did not have the same age at the time of testing. In order to compare the beams of different fiber combination, it shall be assumed that the strength and elastic modulus of the various

concrete mixes does not change substantially after 28 days. To reinforce this assumption, the compressive elastic moduli and compressive strengths test results indicate that these two mechanical properties generally do not vary greatly among the various concrete mixes. The load-deformation curves of different beams are compared with one another. Data such as ultimate load, midspan deformation at the ultimate load, elastic limit, midspan deformation at the elastic limit, bending stiffness, accumulative area under the curve, area of the elastic region, area under the load-deformation curve between the elastic limit and ultimate load and post-ultimate region area are taken into consideration when drawing comparisons.

### 3.1 Failure of Beams without External Basalt Fiber Flexural Reinforcement

The beams series represented in this section are 6MM-0323-AL2, 13MM-0317-FRP3, 6&30MM-0401-AL1, 13&50MM-0318-AL1, 30MM-1029-AL1 and 50MM-1015-AL1. All beams did not have any external basalt fiber flexural reinforcement, and were tested to failure. Figure 3 shows these beams at end of testing. The age of the beam with 6 mm fibers, 13 mm fibers, 6 mm & 30 mm fibers, 13 mm & 50 mm fibers, 30 mm fibers, and 50 mm fibers were 105 days, 118 days, 96 days, 117 days, 258 days and 272 days, respectively. The following graphs illustrate load-deformation curves generated by the flexure tests. Each graph depicts test results from either two or three beams for comparison.


(a)


(b)

(c)


(d)


(e)


(f)

Figure 3: Beams Tested to Failure without External Flexural Reinforcement (a) 6MM-0323-AL2; (b) 13MM-0317-FRP3; (c) 6&30MM-0401-AL1; (d) 13&50MM-0318-AL1; (e) 30MM-1029-AL1; (f) 50MM-1015-AL1

The load-deformation curves in Figure 4 are of two beams with different fiber types and one beam with both fiber types that are present in the other two beams. Beam 6&30MM-0401-AL1 has the highest ultimate load and 6MM-0323-AL2 has the lowest ultimate load. The midspan deformation at the ultimate load of beam series 6&30MM-0401-AL1 is the highest, whereas the non-hybrid beams' midspan deformations at the ultimate load are relatively close to one another. The load at the elastic limit and the midspan deflection at the elastic limit follows the same trend among the three beams of the same series. The same trend is also observed for the ultimate load and midspan deformation at the ultimate load. The hybrid beam has the highest bending stiffness, and the beam with 6MM-0323-AL2 has the lowest bending stiffness. Beams 6MM-0323-AL2 and 30MM-1029-AL1 show a dip in load right after the elastic limit which is not as evident for 6&30MM-0401-AL1. Around the ultimate, the graph of 6MM-0323-AL2 resembles a parabola, where 30MM-1029-AL1 and 6&30MM-0401-AL1 resemble more

of a point. Before gradually leveling out, all three graphs' post-ultimate slopes are similar to their respective slopes prior the elastic limit. Beam 30MM-1029-AL1 shows a relative sharp decrease in load after the graph's peak which is not present in the other beams. Beam 6&30MM-0401-AL1 and 30MM-1029-AL1 level off longer than 6MM-0323-AL2, and maintain a similar load and maximum deformation, though 6&30MM-0401-AL1's maximum deformation is larger.

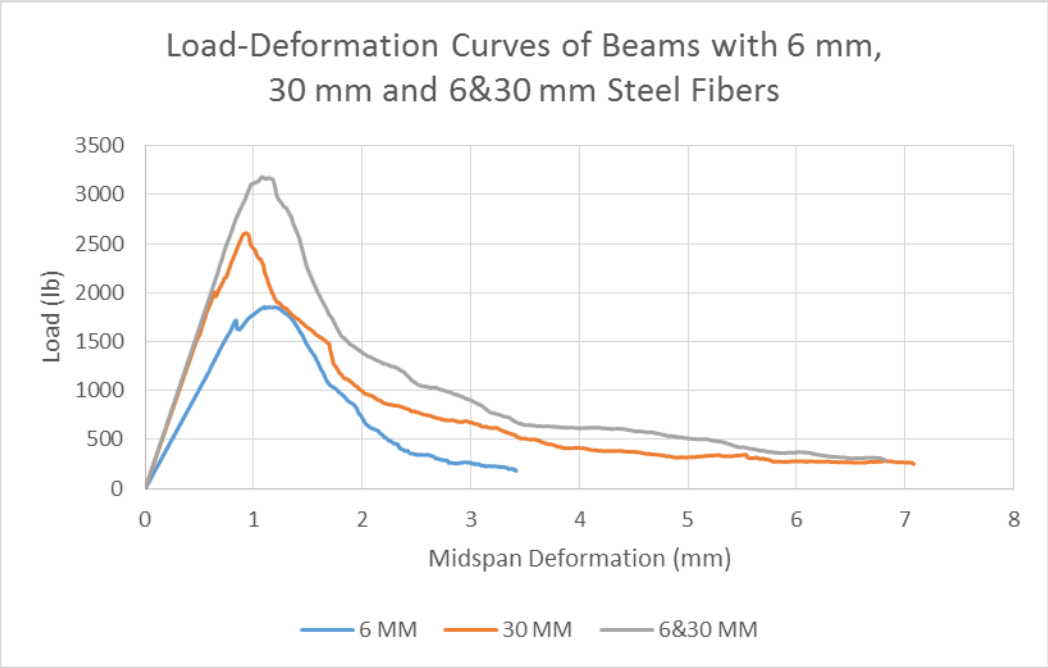


Figure 4: Load-Deformation Curves of Beams with 6 mm, 30 mm and 6 mm & 30 mm Steel Fibers

The load-deformation curves Figure 5 are of two beams with different fiber types and one beam with both fiber types that are present in the other two beams. Beam 50MM-1015-AL1 has the highest ultimate load, 13MM-0317-FRP3 has the lowest ultimate load, and 13&50MM-0318-AL1 has an ultimate load between the highest and lowest value. The midspan deformation at the ultimate load of 13&50MM-0318-AL1 is the greatest, whereas the midspan deformation at the ultimate load of 50MM-1015-AL1 is the least. Beam 50MM-1015-AL1 has the greatest elastic limit and 13MM-0317-FRP3

has the lowest elastic limit. The midspan deformation at the elastic limit of 13&50MM-0318-AL1 is the greatest, whereas the midspan deformation at the elastic limit of 50MM-1015-AL1 is the least. Beam 50MM-1015-AL1 has the highest bending stiffness, and 13&50MM-0318-AL1 has the smallest bending stiffness. All three graphs exhibit a decrease in load just after the elastic limit. After the peak in the graph, 50MM-1015-AL1 decreases at a rate similar to the slope before the elastic limit, whereas the post-ultimate slope of the other two beams are more gradual compared to their respective slopes in the elastic region. Beam 13&50MM-0318-AL1 experienced greatest deformation change between the elastic limit and ultimate load, whereas 50MM-1015-AL1 experienced the least deformation change between the elastic limit and ultimate load. During the last phase of the testing, 13&50MM-0318-AL1 supported the greatest load and deformation, whereas 13MM-0317-FRP3 supported the least load and deformation.

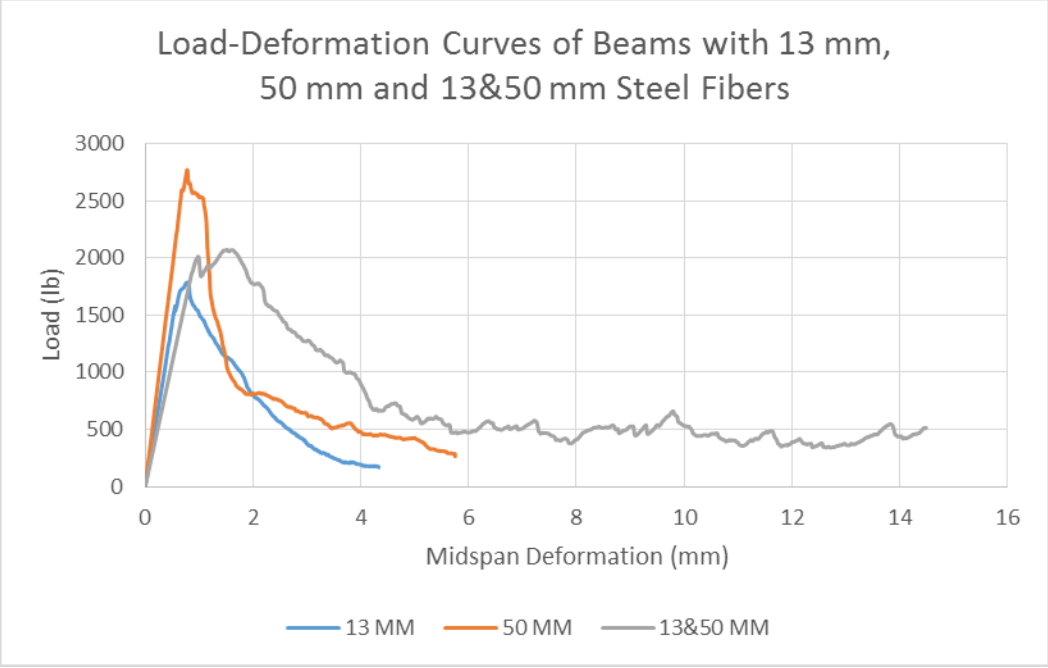


Figure 5: Load-Deformation Curves of Beams with 13 mm, 50 mm and 13 mm & 50 mm Steel Fibers

Figure 6 depicts load-deformation curves of two beams with straight steel fibers. The ultimate load and midspan deformation at the ultimate load of 6MM-0323-AL2 are slightly larger than those of 13MM-0317-FRP3. Beam 6MM-0323-AL2 has a slightly greater elastic limit and corresponding midspan deformation than 13MM-0317-FRP3. Beam 13MM-0317-FRP3 has a greater bending stiffness than 6MM-0323-AL2. Both graphs have a defined decrease in load after the elastic limit, though this is more pronounced with 6MM-0323-AL2. The graph for 6MM-0323-AL2 forms a parabolic shape, and this is not as evident in 13MM-0317-FRP3. After the ultimate load, the slope of the graph for 6MM-0323-AL2 resembles the slope in its elastic region, whereas the post-ultimate slope of the graph for 13MM-0317-FRP3 is more gradual than its corresponding slope in the elastic region. Both graphs maintain a similar load towards the end of the testing, though 13MM-0317-FRP3 reaches a larger deformation in this stage.

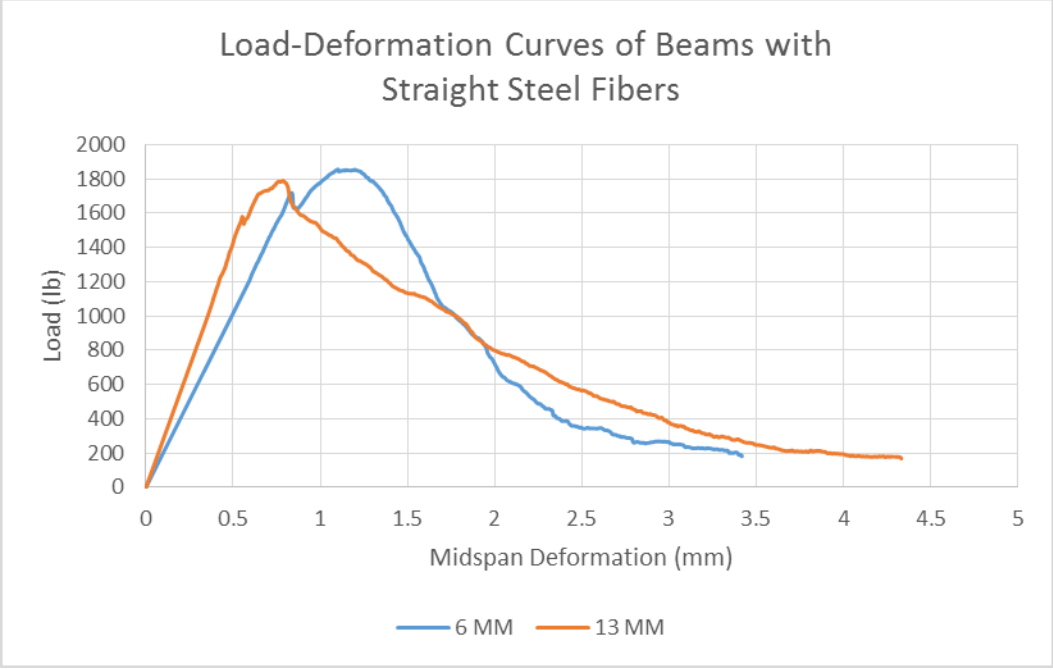


Figure 6: Load-Deformation Curves of Beams with Straight Steel Fibers

Figure 7 depicts load-deformation curves of two beams with hooked end steel fibers. The ultimate is larger for 50MM-1015-AL1 than 30MM-1029-AL1. However, the midspan deformation at the ultimate load is slightly larger for 30MM-1029-AL1 than 50MM-1015-AL1. Beam 50MM-1015-AL1 has a greater elastic limit and slightly larger corresponding midspan deformation than 30MM-1029-AL1. Beam 50MM-1015-AL1 has a greater bending stiffness than 30MM-1029-AL1. There is a small dip in load right after the elastic limit for both beams. Although both ultimate loads are at a part of the graph where a point forms, there is a small load plateau after the ultimate is reached for 50MM-1015-AL1. The post-ultimate slope of 50MM-1015-AL1 is similar to the slope in the elastic region, whereas the post-ultimate slope is more gradual than slope in the elastic region for 30MM-1029-AL1. Towards the end of testing, both beams supported a similar load, yet 30MM-1029-AL1 experienced a greater deformation.

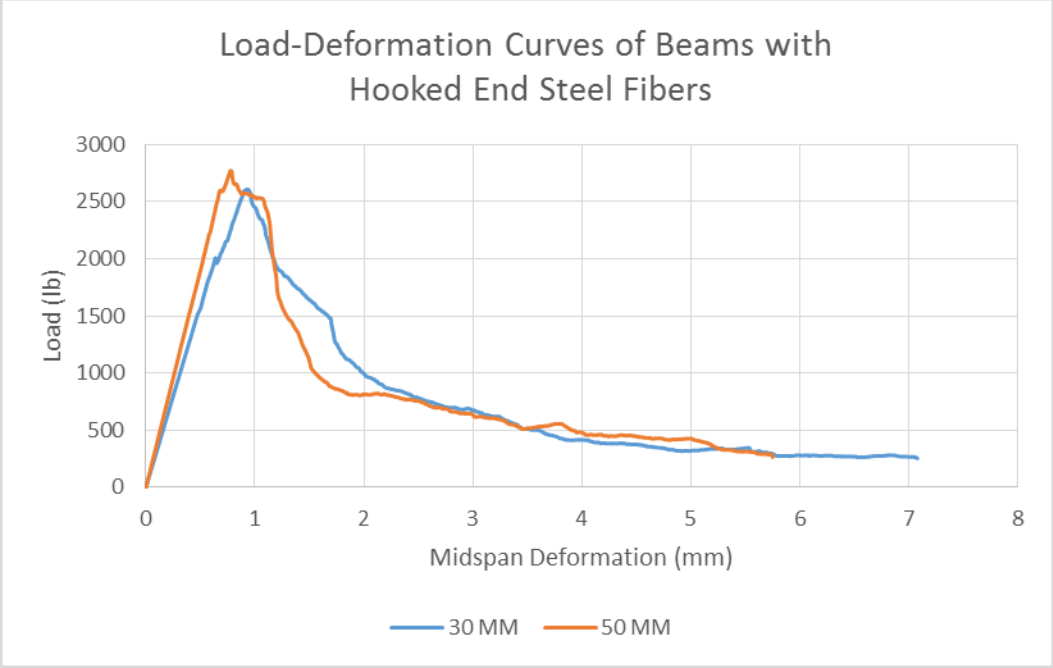


Figure 7: Load-Deformation Curves of Beams with Hooked End Steel Fibers

Figure 8 depicts load-deformation curves of two beams with hybrid or multiple fiber types. The ultimate load is substantially larger for 6&30MM-0401-AL1 than 13&50MM-0318-AL1. The midspan deflection at the ultimate load is larger for 13&50MM-0318-AL1 than 6&30MM-0401-AL1. Beam 6&30MM-0401-AL1 has a greater elastic limit and bending stiffness, yet a smaller corresponding midspan deformation  than 13&50MM-0318-AL1. Around the ultimate load, the graph for 6&30MM-0401-AL1 forms a sharp peak, whereas 13&50MM-0318-AL1's graph resembles a parabola. Beam 13&50MM-0318-AL1shows a distinctive decrease in load after elastic limit is reached. The post-ultimate slope is similar to the slope prior to the elastic limit for 6&30MM-0401-AL1, whereas the post-ultimate slope for 13&50MM-0318-AL1 is more gradual. Both beams support similar loads towards the end of testing, though 13&50MM-0318-AL1 deforms much more.

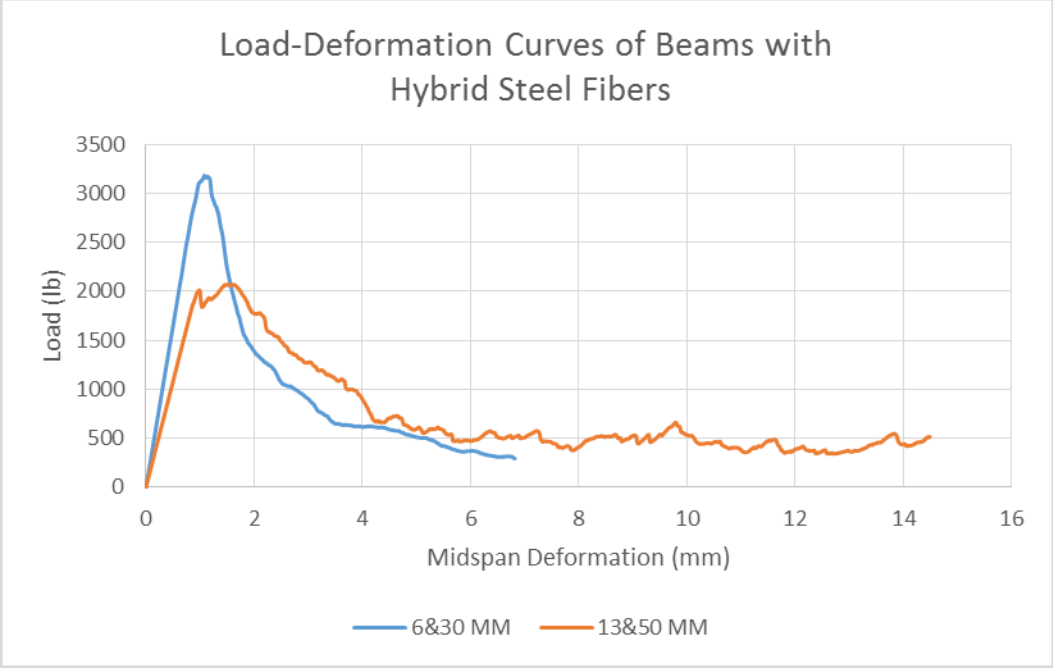


Figure 8: Load-Deformation Curves of Beams with Hybrid Steel Fibers

Load-deformation curves for 6MM-0323-AL2, 50MM-1015-AL1 and 13&50MM-0318-AL1 are shown in Figure 9. Beam 50MM-1015-AL1 has the highest ultimate load, whereas 6MM-0323-AL2 has the lowest ultimate load. Beam 13&50MM-0318-AL1 has the largest midspan deformation at the ultimate load, while beam 50MM-1015-AL1 has the smallest midspan deformation at the ultimate load. Beam 50MM-1015-AL1 has the highest elastic limit, yet the smallest corresponding midspan deformation. Beam 6MM-0323-AL2 has the lowest elastic limit, yet a corresponding midspan deformation that is relatively close to that of 13&50MM-0318-AL1. Beam 50MM-1015-AL1 has the highest bending stiffness, whereas the bending stiffness of the other two beams are relatively close to one another. Beam 6MM-0323-AL2 and 13&50MM-0318-AL1 have a well-defined decrease in load after the elastic limit, and the graphs resemble a parabola around the peak, unlike 50MM-1015-AL1. The width of the curve is smallest for 50MM-1015-AL1 and greatest for 13&50MM-0318-AL1. The post- ultimate slope is similar to the slope in the elastic region for 6MM-0323-AL2 and 50MM-1015-AL1, whereas the post-ultimate slope of 13&50MM-0318-AL1 is more gradual than the slope in the elastic region. At the last phase of testing, 13&50MM-0318-AL1 supports the greatest load and experiences the greatest deformation, whereas 6MM-0323-AL2 supports the least load and deformation at this phase.

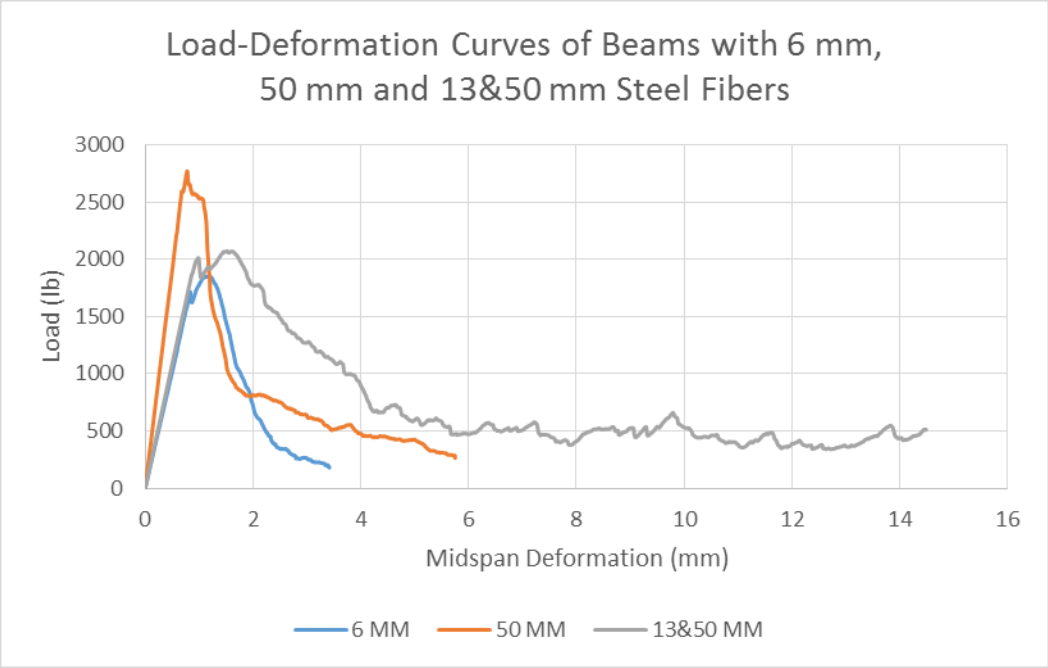


Figure 9: Load-Deformation Curves of Beams with 6 mm, 50 mm and 13 mm & 50 mm Steel Fibers

Load-deformation curves for 30MM-1029-AL1, 13MM-0317-FRP3 and 13&50MM-0318-AL1 are shown in Figure 10. Beam 30MM-1029-AL1 has the highest ultimate load, whereas 13MM-0317-FRP3 has the lowest ultimate load. Beam 13&50MM-0318-AL1 has the largest midspan deformation at the ultimate load, and 13MM-0317-FRP3 has the smallest midspan deformation at the ultimate load. Beam 30MM-1029-AL1 has the highest elastic limit and beam 13MM-0317-FRP3 has the lowest elastic limit. At the elastic limit, 13&50MM-0318-AL1 has the largest corresponding midspan deformation, whereas 13MM-0317-FRP3 has the lowest corresponding midspan deformation. Beam 30MM-1029-AL1 has the highest bending stiffness, and beam 13&50MM-0318-AL1 has the lowest bending stiffness. Beam 13&50MM-0318-AL1 has a well-defined decrease in load after elastic limit. The graphs for 30MM-1029-AL1 and 13MM-0317-FRP3 form a sharp peak around the ultimate load, whereas the graph follows a parabolic shape for 13&50MM-0318-AL1 around the

ultimate load. The post-ultimate slopes for all three beams are less than their corresponding slopes in the elastic region. The width of the curve is largest for is largest for 13&50MM-0318-AL1. When the graphs leveled out towards the end of testing, 13&50MM-0318-AL1 experienced the greatest deformation and was able to support the greatest load at this deformation, whereas 13MM-0317-FRP3 experienced the least deformation and supported the least load at the corresponding deformation.

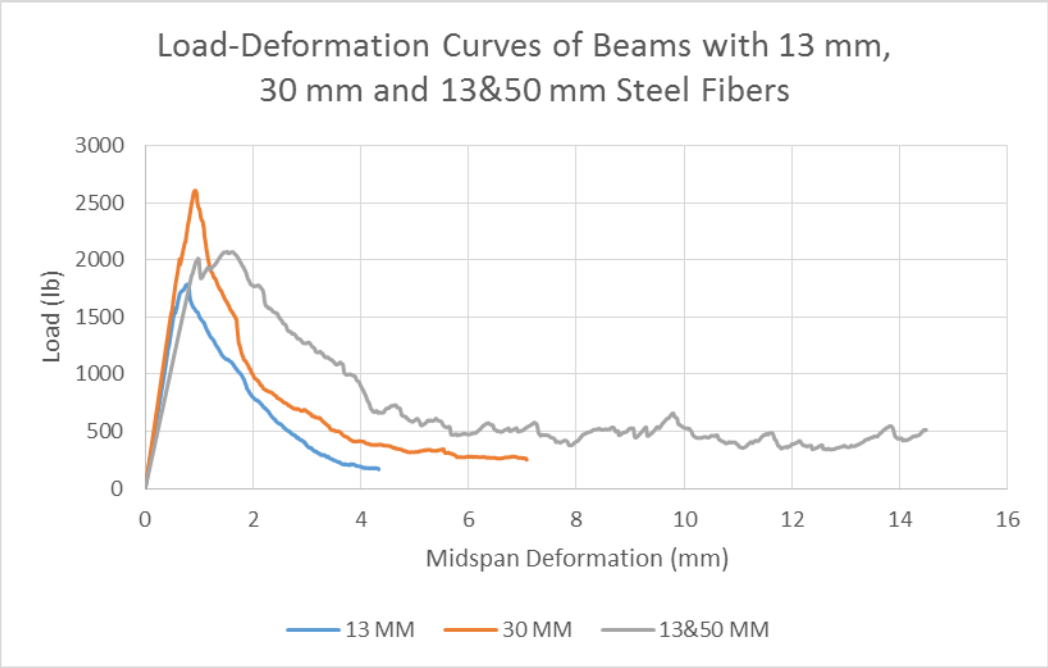


Figure 10: Load-Deformation Curves of Beams with 13 mm, 30 mm and 13 mm & 50 mm Steel Fibers

Load-deformation curves for 6&30MM-0401-AL1, 13MM-0317-FRP3 and 50MM-1015-AL1 are shown in Figure 11. Beam 6&30MM-0401-AL1 has the highest ultimate load, whereas 13MM-0317-FRP3 has the lowest ultimate load. Beam 6&30MM-0401-AL1 has the largest midspan deformation at the ultimate load, and 50MM-1015-AL1 has the smallest midspan deformation at the ultimate load. Beam 6&30MM-0401-AL1 has the highest elastic limit and corresponding midspan deformation, whereas 13MM-0317-FRP3 has the lowest elastic limit and corresponding midspan deformation.

Beam 50MM-1015-AL1 has the highest bending stiffness, whereas 13MM-0317-FRP3 has the lowest bending stiffness. Not all graphs exhibit a significant decrease in load after the elastic limit. Although not all graphs have a sharp peak at the ultimate load, neither graph forms a perfect parabola. The post-ultimate slope of 13MM-0317-FRP3 is more gradual than the slope in the elastic region, whereas the post-ultimate slopes of 50MM-1015-AL1 and 6&30MM-0401-AL1 resemble the slopes of the elastic region before leveling out. Beam 6&30MM-0401-AL1 maintains the greatest load and deformation towards the end of testing, whereas 13MM-0317-FRP3 maintains the least load and deformation at this stage.

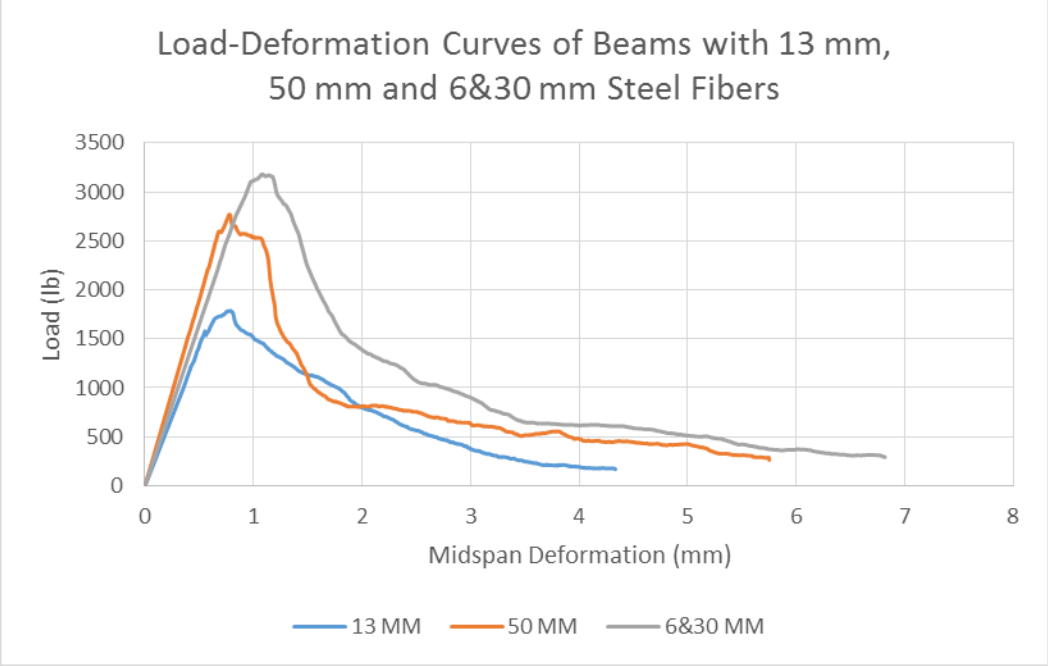


Figure 11: Load-Deformation Curves of Beams with 13 mm, 50 mm and 6 mm& 30 mm Steel Fibers

Table 3 shows a summary of the mechanical properties obtained from the flexural tests for all the beams tested without external flexural reinforcement. The first column tabulates the ultimate load of each beam. The beams that have the greatest ultimate load to the least strength in terms of fiber combinations are as follows: 6 mm & 30 mm steel

fibers, 50 mm steel fibers, 30 mm steel fibers, 13 mm & 50 mm steel fibers, 6 mm steel fibers and 13 mm steel fibers. The second column tabulates the midpan deformation or deflection at the ultimate load of each beam. At the ultimate load, the beams that have the greatest deflection load to the least deflection in terms of fiber combinations are as follows: 13 mm & 50 mm steel fibers, 6 mm & 30 mm steel fibers, 6 mm steel fibers, 30 mm steel fibers, 50 mm steel fibers and 13 mm steel fibers. The third column tabulates the elastic limit of each beam. The beams that have the greatest elastic limit to the least elastic limit in terms of fiber combinations are as follows: 6 mm & 30 mm steel fibers, 50 mm steel fibers, 6 mm steel fibers, 13 mm steel fibers, 13 mm & 50 mm steel fibers, and 30 mm steel fibers. The fourth column tabulates what is the midpan deformation or deflection at the elastic limit of each beam. At the elastic limit, the beams that have the greatest deflection load to the least deflection in terms of fiber combinations are as follows: 6 mm & 30 mm steel fibers, 6 mm steel fibers, 13 mm & 50 mm steel fibers, 50 mm steel fibers, 13 mm steel fibers and 30 mm steel fibers. The fifth column tabulates the bending stiffness each beam. The beams that have the greatest bending stiffness to the least bending stiffness in terms of fiber combinations are as follows: 50 mm steel fibers, 30 mm steel fibers, 6 mm & 30 mm steel fibers, 13 mm steel fibers, 13 mm & 50 mm steel fibers and 6 mm steel fibers.

Table 3: Mechanical Properties Summary of Beams without External Flexural Reinforcement

| Specimen | Ultimate Load (lb) | Deflection at Ultimate (mm) | Elastic Limit (lb) | Deflection at Elastic Limit (mm) | Bending Stiffness (lb/mm) |
|---|---|---|---|---|---|
| 6MM-0401-AL1 | 2,692.1 | 1.059 | 2,448.7 | 0.821 | 2,957.9 |
| 6MM-0323-AL2 | 1,854.6 | 1.102 | 1,718.6 | 0.836 | 2,060.3 |
| 6MM-0323-AL3 | 1,970.6 | 1.424 | 1,835.9 | 1.196 | 1,575.2 |
| 13MM-0317-FRP1 | 2,020.5 | 0.614 | 1,938.7 | 0.582 | 3,351.9 |
| 13MM-0317-FRP2 | 1,339.0 | 0.794 | 9,24.6 | 0.502 | 1,844.3 |

| | | | | | |
|---|---|---|---|---|---|
| 13MM-0317-FRP3 | 1,787.8 | 0.789 | 1,579.6 | 0.553 | 2,847.4 |
| 30MM-1029-AL1 | 2,607.6 | 0.921 | 2,007.7 | 0.638 | 3,161.7 |
| 30MM-1029-AL2 | 2,175.6 | 0.988 | 1,706.0 | 0.588 | 2,906.7 |
| 30MM-1029-AL3 | 3,078.5 | 1.254 | 1,953.3 | 0.674 | 2,907.6 |
| 50MM-1015-AL1 | 2,771.5 | 0.775 | 2,592.3 | 0.676 | 3,811.9 |
| 50MM-1015-AL2 | 2,247.9 | 1.232 | 1,356.4 | 0.577 | 2,341.4 |
| 50MM-1015-AL3 | 2,984.0 | 0.898 | 2,775.9 | 0.737 | 3,899.4 |
| 6&30MM-0401-AL1 | 3,183.1 | 1.077 | 2,924.6 | 0.908 | 3,302.8 |
| 6&30MM-0323-AL2 | 3,737.0 | 1.53 | 3,176.0 | 1.185 | 2,743.7 |
| 6&30MM-0323-AL2 | 1,996.8 | 1.088 | 1,793.7 | 0.835 | 2,229.0 |
| 13&50MM-0318-AL1 | 2,072.8 | 1.521 | 1,987.3 | 0.944 | 2,167.2 |
| 13&50MM-0318-AL2 | 2,060.8 | 1.351 | 1,447.6 | 0.693 | 2,061.3 |
| 13&50MM-0318-AL3 | 2,583.5 | 1.084 | 1,783.1 | 0.664 | 2,675.8 |

Table 4 lists the areas of various regions as well as the accumulative areas of the load-deformation curves obtained from the flexural tests for all the beams tested without external flexural reinforcement. The first column tabulates the area of the elastic region of each beam. In the elastic region, the beams that have the greatest area to the least area in terms of fiber combinations are as follows: 6 mm & 30 mm steel fibers, 6 mm steel fibers, 50 mm steel fibers, 13 mm & 50 mm steel fibers, 30 mm steel fibers and 13 mm steel fibers. The second column tabulates the area under the load-deformation curve between the elastic limit and ultimate load of each beam. Between the elastic limit and ultimate load, the beams that have the greatest area to the least area in terms of fiber combinations are as follows: 13 mm & 50 mm steel fibers, 30 mm steel fibers, 6 mm & 30 mm steel fibers, 50 mm steel fibers, 6 mm steel fibers and 13 mm steel fibers. The third column tabulates the post-ultimate area under the load-deformation curve of each beam. The beams that have the greatest post-ulitmate area to the least post-ultimate area in terms of fiber combinations are as follows: 13 mm & 50 mm steel fibers, 6 mm & 30 mm steel fibers, 50 mm steel fibers, 30 mm steel fibers, 13 mm steel fibers and 6 mm steel fibers. The fourth column tabulates the accumulative area under the load-deformation curve of each beam. The beams with the greatest accumulative area to the

least accumulative area in terms of fiber combinations are as follows: 13 mm & 50 mm steel fibers, 6 mm & 30 mm steel fibers, 30 mm steel fibers, 50 mm steel fibers, 13 mm steel fibers and 6 mm steel fibers.

Table 4: Area under Load-Deformation Curves of Beams without External Flexural Reinforcement

| Specimen | Area of Elastic Region (lb-mm) | Area between Elastic Limit and Ultimate Load (lb-mm) | Area of Post-Ultimate Region (lb-mm) | Accumulative Area (lb-mm) |
|---|---|---|---|---|
| 6MM-0401-AL1 | 1,003.9 | 608.2 | 2,146.7 | 3,758.8 |
| 6MM-0323-AL2 | 714.4 | 463.8 | 1,711.9 | 2,890.1 |
| 6MM-0323-AL3 | 1,127.5 | 434.4 | 1,950.8 | 3,512.6 |
| 13MM-0317-FRP1 | 567.3 | 63.5 | 3,083.7 | 3,714.6 |
| 13MM-0317-FRP2 | 232.1 | 339.4 | 3,589.8 | 4,161.3 |
| 13MM-0317-FRP3 | 434.1 | 400.9 | 2,392.1 | 3,227.0 |
| 30MM-1029-AL1 | 647.1 | 643.8 | 4,121.2 | 5,412.2 |
| 30MM-1029-AL2 | 502.6 | 795.0 | 2,877.9 | 4,175.5 |
| 30MM-1029-AL3 | 660.4 | 1,510.5 | 2,921.8 | 5,092.7 |
| 50MM-1015-AL1 | 872.8 | 262.7 | 3,901.1 | 5,036.6 |
| 50MM-1015-AL2 | 390.6 | 1,239.0 | 3,660.1 | 5,289.7 |
| 50MM-1015-AL3 | 1,057.4 | 461.8 | 2,795.1 | 4,314.4 |
| 6&30MM-0401-AL1 | 1,358.6 | 521.7 | 5,160.9 | 7,041.1 |
| 6&30MM-0323-AL2 | 1,923.9 | 1,225.8 | 4,879.5 | 8,029.2 |
| 6&30MM-0323-AL2 | 774.0 | 485.6 | 6,454.4 | 7,713.9 |
| 13&50MM-0318-AL1 | 963.0 | 1,133.9 | 8,688.6 | 10,785.5 |
| 13&50MM-0318-AL2 | 496.1 | 1,177.5 | 4,829.8 | 6,503.4 |
| 13&50MM-0318-AL3 | 589.3 | 948.0 | 4,546.9 | 6,084.2 |

### 3.2 Beams Tested to First Crack vs. to Failure with External Flexural Reinforcement

The beams represented in this section are 6MM-0323-FRP6, 13MM-0317-FRP4, 6&30MM-0323-AL4, 13&50MM-0318-AL6, 30MM-1124-AL6 and 50MM-1008-AL4. The beams were first tested to the point when cracking started to take place, which in this study is referred to as first crack. At the time of testing to first crack, the age of the beam with 6 mm fibers, 13 mm fibers, 6 mm & 30 mm fibers, 13 mm & 50 mm fibers, 30 mm fibers, and 50 mm fibers were 133 days, 139 days, 133 days, 138 days, 253 days and 300 days, respectively. These beams were then reinforced with basalt fiber and tested to

failure. At the time of testing to failure, the age of the beam with 6 mm fibers, 13 mm fibers, 6 mm & 30 mm fibers, 13 mm & 50 mm fibers, 30 mm fibers, and 50 mm fibers were 153 days, 159 days, 153 days, 158 days, 272 days and 319 days, respectively. It should be noted that due to the fact that some previous beams failed in shear as opposed to flexure, not all the beams had the same width of basalt fiber attached to the tension flange at the time of testing. The basalt fiber attached to 13MM-0317-FRP5, 30MM-1124-AL6 and 50MM-1008-AL4 had a width of 3 inches, whereas the basalt fiber attached to 6MM-0323-FRP6, 6&30MM-0323-AL5 and 13&50MM-0318-AL4 had a width of 2 ½ inches, 2 inches and 2 ½ inches, respectively. All of these six beams failed in flexure, apart from 13MM-0317-FRP5, which failed in shear. Included in this section are graphs used to illustrate load-deformation curves generated by the flexure tests. Each graph depicts test results of one beam having been tested to first crack and to failure after having been externally reinforced with basalt fiber.

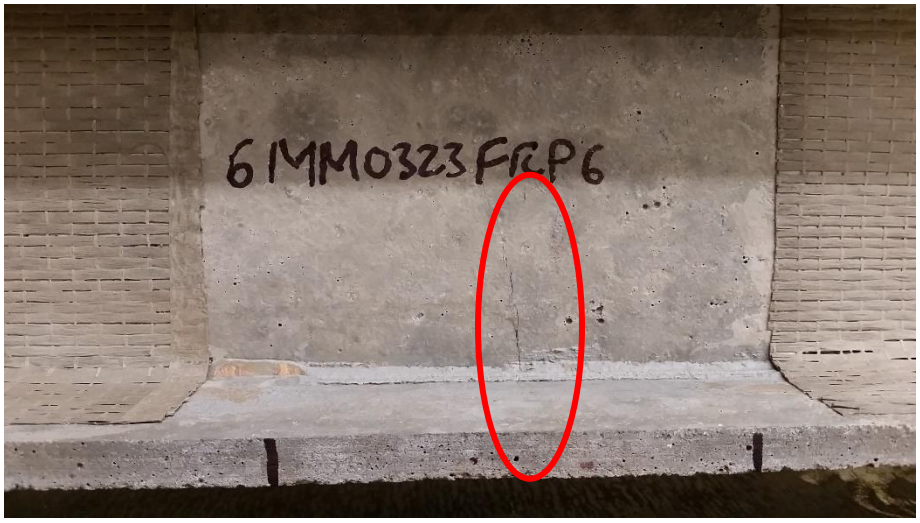


(a)

(b)

Figure 12: 6MM-0323-FRP6 Tested to First Crack (a) Side view; (b) Bottom view

Figure 12 shows the extent of cracking of 6MM-0323-FRP6. The two load-deformation curves represent the results of two tests of one beam composed of 6 mm steel fibers in Figure 13. The rehabilitated beam has a greater bending stiffness, which is denoted by the steeper slope. There is a decrease in load after the elastic limit when the beam was not reinforced with basalt fiber, whereas this not evident when the beam was reinforced with basalt fiber. Specifically, the bending stiffness of the beam while testing just to the point of when cracking started is 2,729 lb/mm and the bending stiffness of the beam after being reinforced with basalt fiber is 4,049 lb/mm. After reinforcing the beam with basalt fiber, it is shown that the elastic limit is increased and occurs at a greater midspan deformation than the elastic limit. The elastic limit for testing to first crack is 1,856 lb and occurred at a midspan deformation of 0.63 mm, whereas after being reinforced with basalt fiber, the elastic limit is 3,387 lb and occurs at a midspan deformation of 0.87 mm.

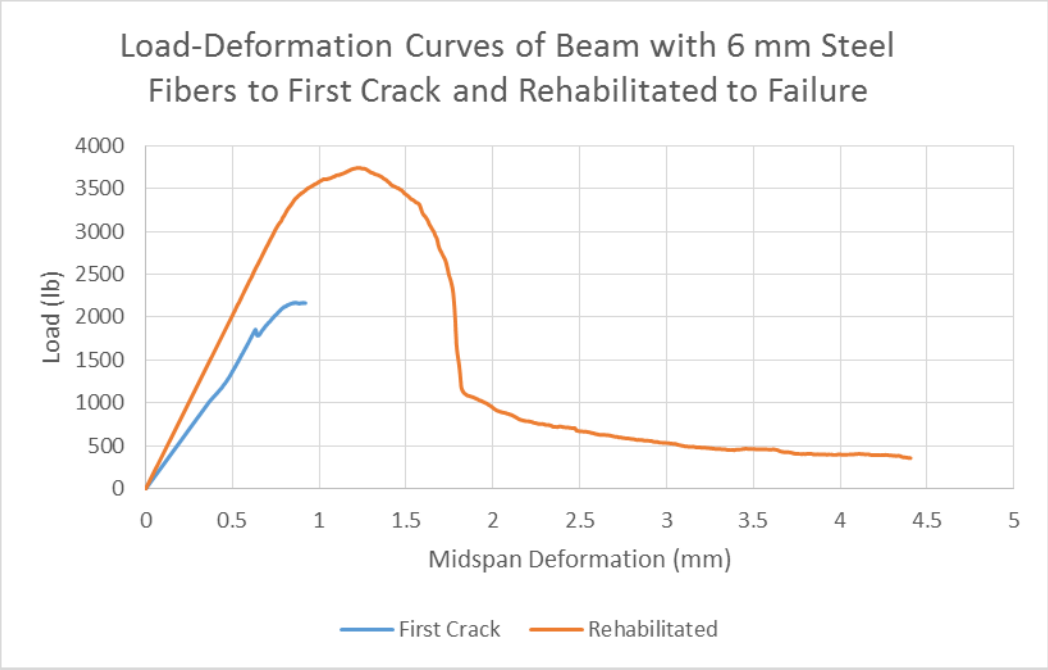


Figure 13: Load-Deformation Curves of Beam with 6 mm Steel Fibers Tested to First Crack and to Failure with the Addition of External Flexural Reinforcement

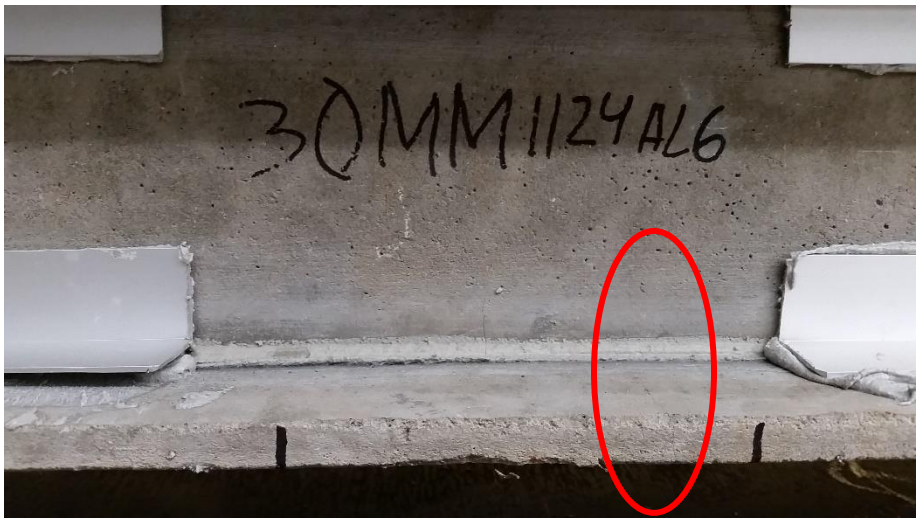


(a)

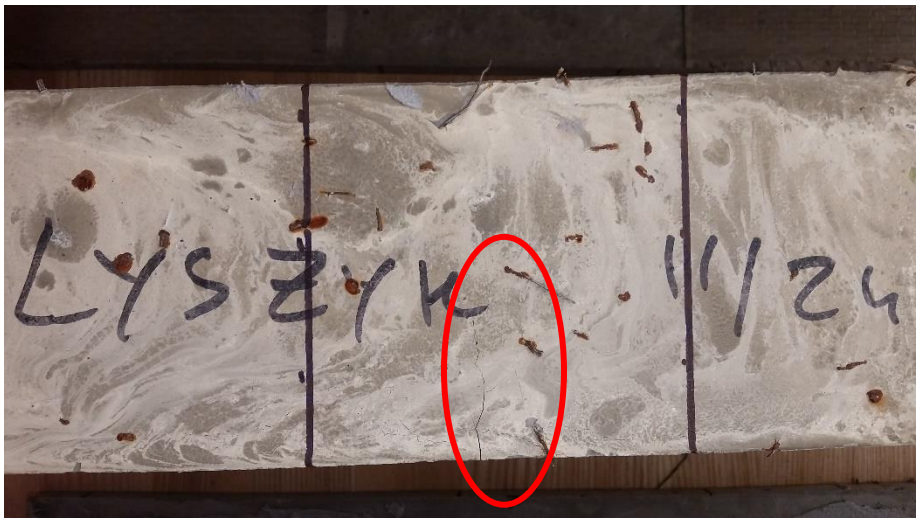

(b)

Figure 14: 30MM-1124-AL6 Tested to First Crack (a) Side view; (b) Bottom view

Figure 14 shows the extent of cracking of 30MM-1124-AL6. The two load-deformation curves represent the results of two tests of one beam composed of 30 mm steel fibers in Figure 15. The rehabilitated beam has a greater bending stiffness, which is denoted by the steeper slope. Neither graph exhibits a decrease in load after the elastic limit. Specifically, the bending stiffness of the beam while testing just to the point of when cracking started is 3,046 lb/mm and the bending stiffness of the beam after being reinforced with basalt fiber is 3,667 lb/mm. With external flexural reinforcement, the elastic limit increases and occurs at a larger midspan deformation. The elastic limit for testing to first crack is 3,028 lb and occurred at a midspan deformation of 0.99 mm, whereas after being reinforced with basalt fiber, the elastic limit is 4,227 lb, and occurs at a midspan deformation of 1.31 mm.

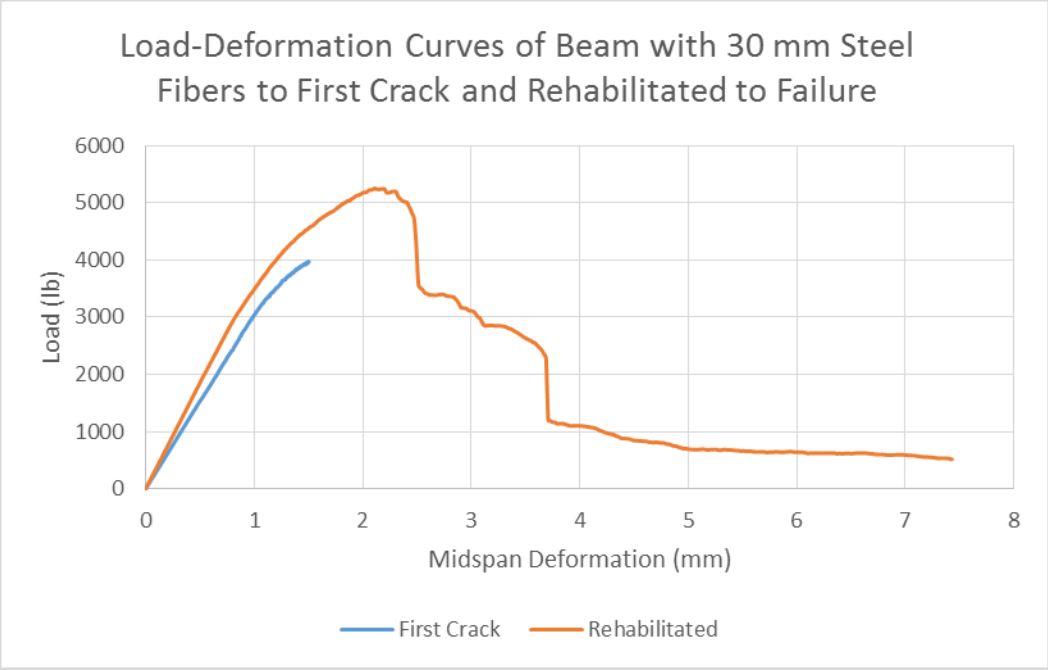


Figure 15: Load-Deformation Curves of Beam with 30 mm Steel Fibers Tested to First Crack and to Failure with the Addition of External Flexural Reinforcement

(a)

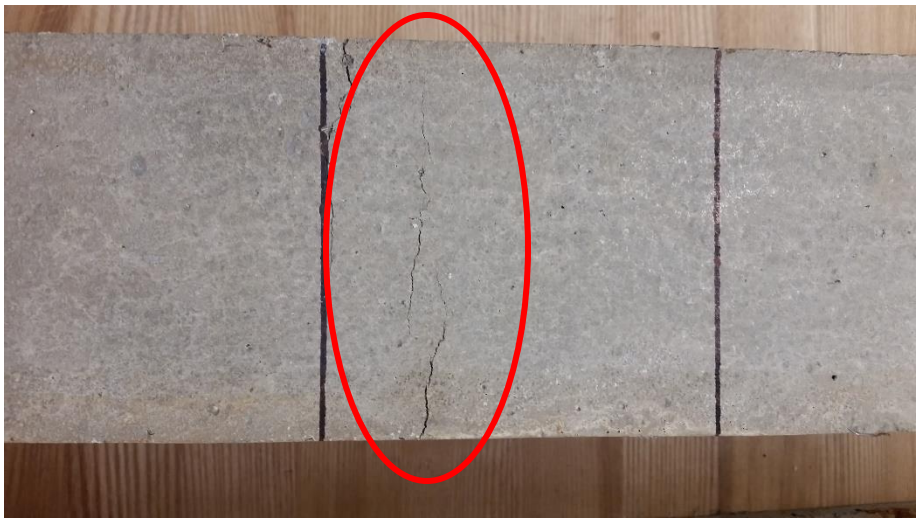

(b)

Figure 16: 6&30MM-0323-AL4 Tested to First Crack (a) Side view; (b) Bottom view

Figure 16 shows the extent of cracking of 6&30MM-0323-AL4. The two load-deformation curves represent the results of two tests of one beam composed of 6 mm & 30 mm steel fibers in Figure 17. As can be seen in the graph, the bending stiffnesses of both load-deformation curves are close to one another. Specifically, the bending stiffness of the beam while testing just to the point of when cracking started is 4,190 lb/mm and the bending stiffness of the beam after being reinforced with basalt fiber is 4,109 lb/mm. After testing to first crack, it is shown that the elastic limit is lower, and occurs at a smaller midspan deformation than the beam reinforced with basalt fiber. There is a decrease in load after the elastic limit when the beam is tested to first crack, but because the load does not increase afterwards, it is inconclusive as to whether the peak of this curve corresponds to the elastic limit or ultimate load. The elastic limit for testing to first crack is 2,700 lb and occurred at a midspan deformation of 0.66 mm, whereas after being reinforced with basalt fiber, the elastic limit is 4,213 lb and occurs at a midspan deformation of 1.13 mm.

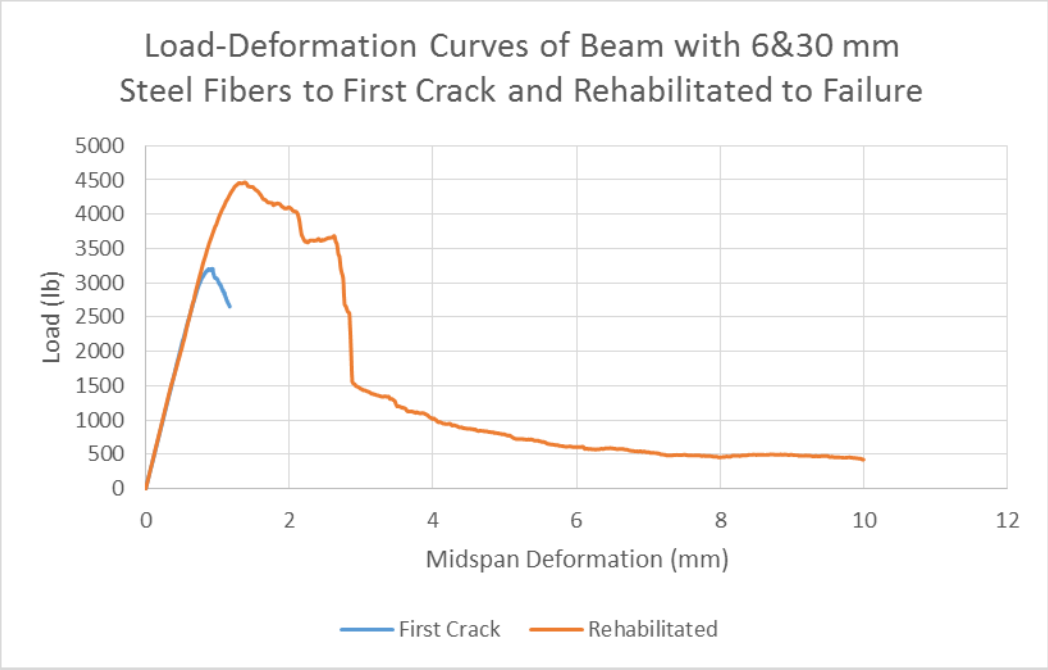


Figure 17: Load-Deformation Curves of Beam with 6 mm & 30 mm Steel Fibers Tested to First Crack and to Failure with the Addition of External Flexural Reinforcement


(a)

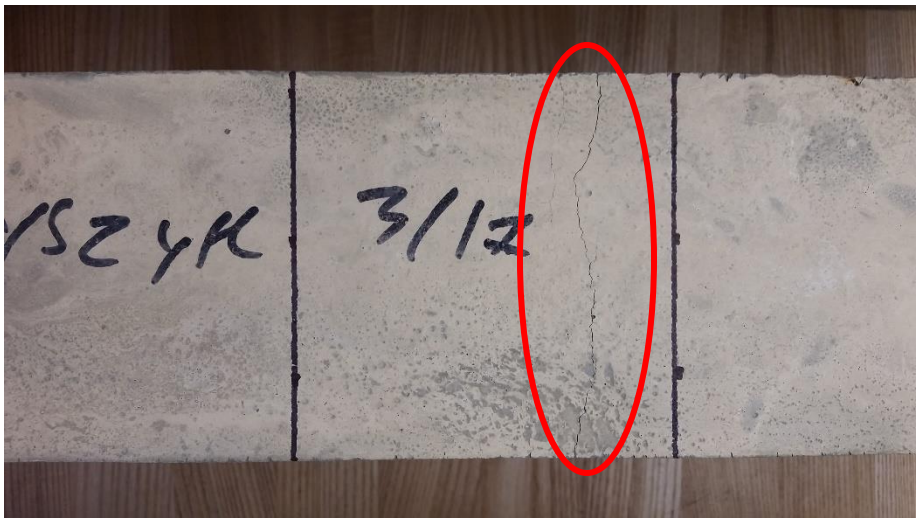

(b)

Figure 18: 13MM-0317-FRP4 Tested to First Crack (a) Side view; (b) Bottom view

Figure 18 shows the extent of cracking of 13MM-0317-FRP4. The two load-deformation curves represent the results of two tests of one beam composed of 13 mm steel fibers in Figure 19. The bending stiffnesses of both load-deformation curves are close to one another. The bending stiffness of the beam while testing just to the point of when cracking started is 2,558 lb/mm and the bending stiffness of the beam after being reinforced with basalt fiber is 2,796 lb/mm. Neither graph shows a decrease in load after the elastic limit. After testing to first crack, it is shown that the elastic limit is lower, and occurs at a smaller midspan deformation than the elastic limit after being reinforced with basalt fiber. The elastic limit for testing to first crack is 1,780 lb, and occurrs at a midspan deformation of 0.71 mm, whereas after being reinforced with basalt fiber, the elastic limit is 2,811 lb, and occurs at a midspan deformation of 1.08 mm.

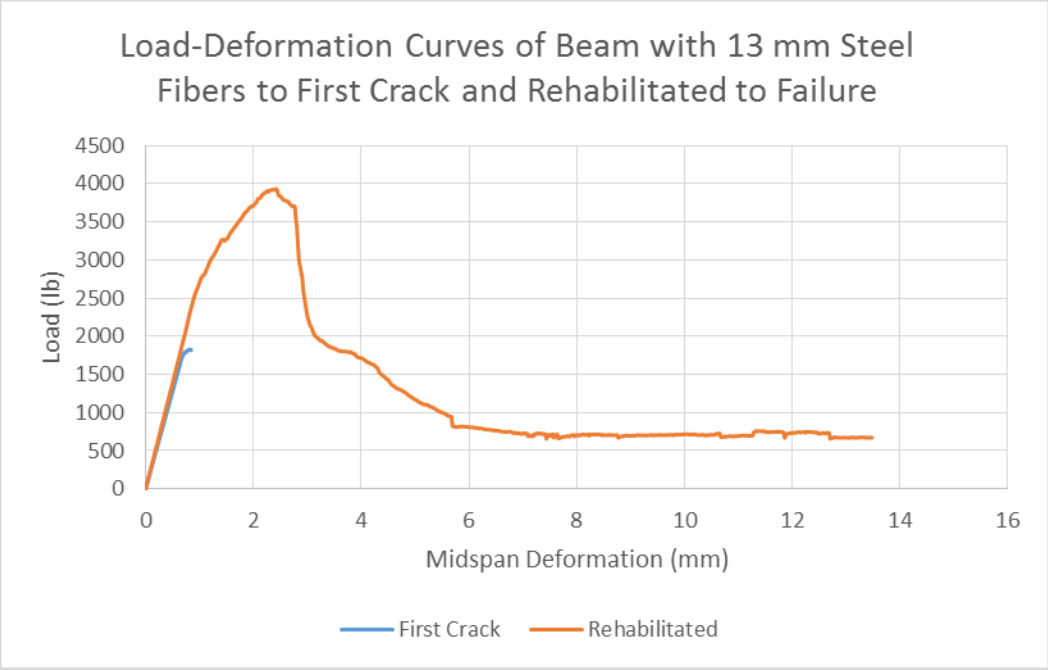


Figure 19: Load-Deformation Curves of Beam with 13 mm Steel Fibers Tested to First Crack and to Failure with the Addition of External Flexural Reinforcement


(a)

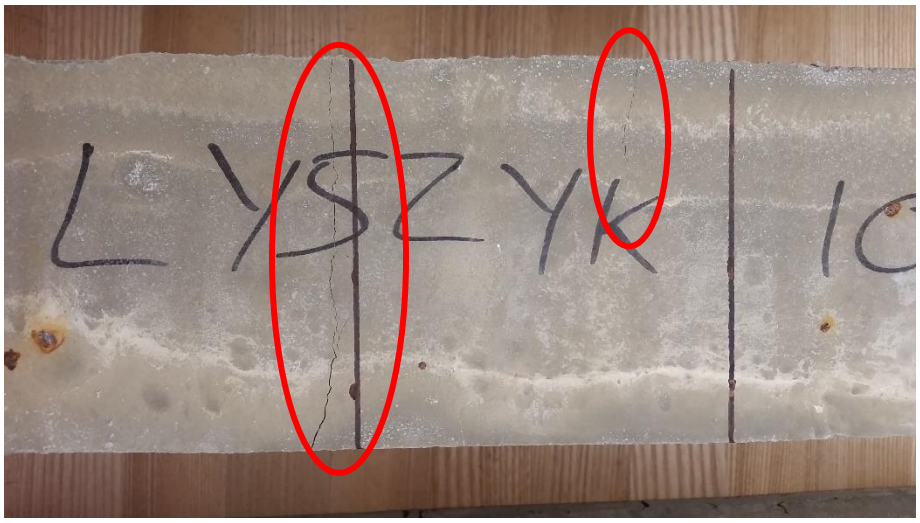

(b)

Figure 20: 50MM-1008-AL4 Tested to First Crack (a) Side view; (b) Bottom view

Figure 20 shows the extent of cracking of 50MM-1008-AL4. The two load-deformation curves represent the results of two tests of one beam composed of 50 mm steel fibers in Figure 21. The rehabilitated beam has a greater bending stiffness, which is denoted by the steeper slope. The bending stiffness of the beam while testing just to the point of when cracking started is 3,489 lb/mm, and the bending stiffness of the beam after being reinforced with basalt fiber is 4,534 lb/mm. After the elastic limit, there is a small decrease in load when the beam is tested to first crack. This phenomenon is non-existent once the beam is reinforced with basalt fiber on its tensile flange. The beam with external flexural reinforcement has a greater elastic limit and correpsonding midspan deformation. The elastic limit for testing to first crack is 1,837 lb, and occurrs at a midspan deformation of 0.53 mm, whereas after being reinforced with basalt fiber, the elastic limit

is 3,193 lb, and occurs at a midspan deformation of 0.71 mm.

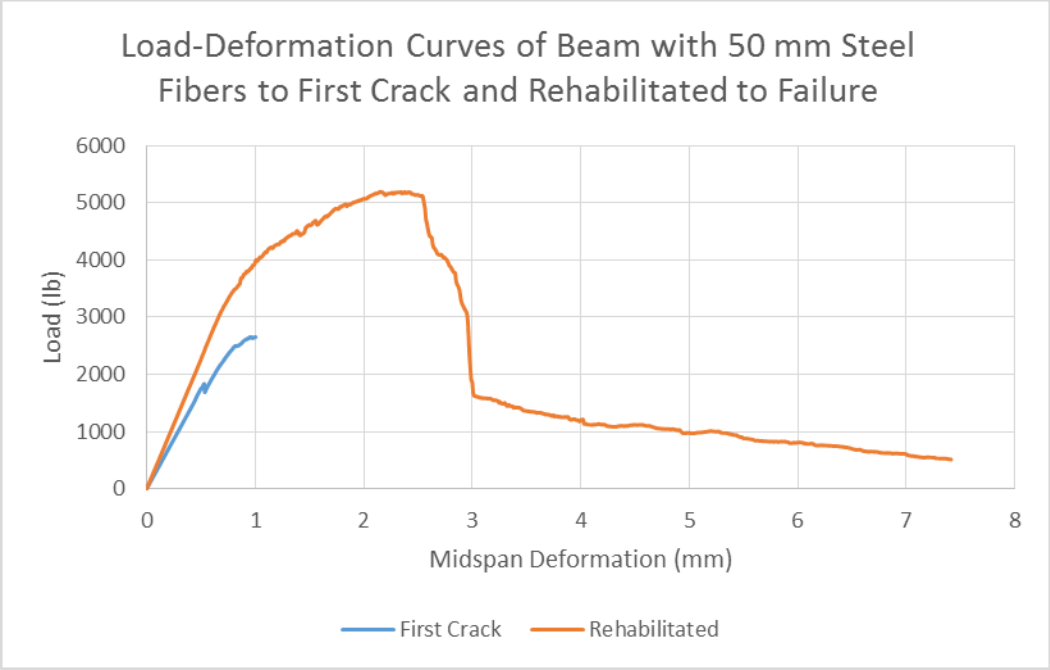


Figure 21: Load-Deformation Curves of Beam with 50 mm Steel Fibers Tested to First Crack and to Failure with the Addition of External Flexural Reinforcement

(a)

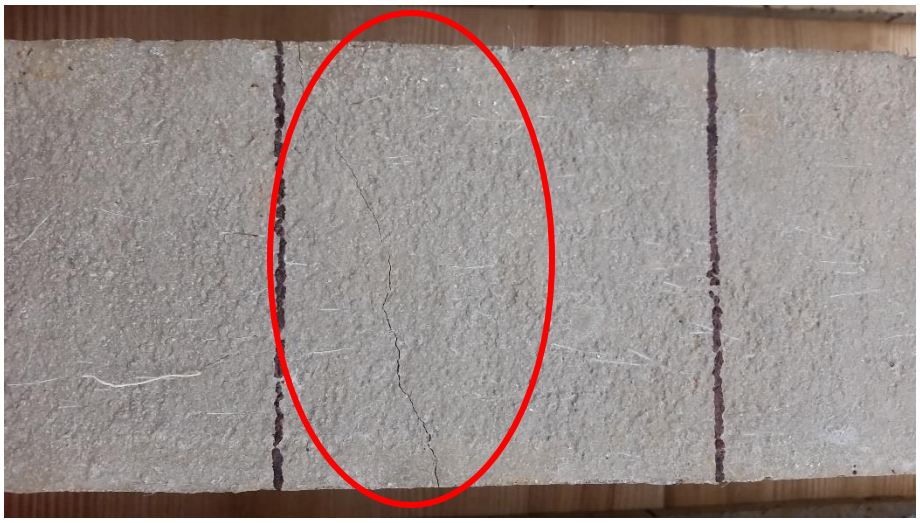

(b)

Figure 22: 13&50MM-0318-AL6 Tested to First Crack (a) Side view; (b) Bottom view

Figure 22 shows the extent of cracking of 13&50MM-0318-AL6. The two load-deformation curves represent the results of two tests of one beam composed of 13 mm & 50 mm steel fibers in Figure 23. The rehabilitated beam has a greater bending stiffness, which is denoted by the steeper slope. Specifically, the bending stiffness of the beam while testing just to the point of when cracking started is 2,267 lb/mm, and the bending stiffness of the beam after being reinforced with basalt fiber is 2,800 lb/mm. After the beam has been reinforced with basalt fiber, the elastic limit is increased, yet the corresponding midspan deformation of both curves are similar. Furthermore, both curves shows a decrease in load at similar deformations. The elastic limit for testing to first crack is 1,914 lb and occurred at a midspan deformation of 0.83 mm, whereas after being reinforced with basalt fiber, the elastic limit is 2,566 lb, and occurs at a midspan

deformation of 0.93 mm.

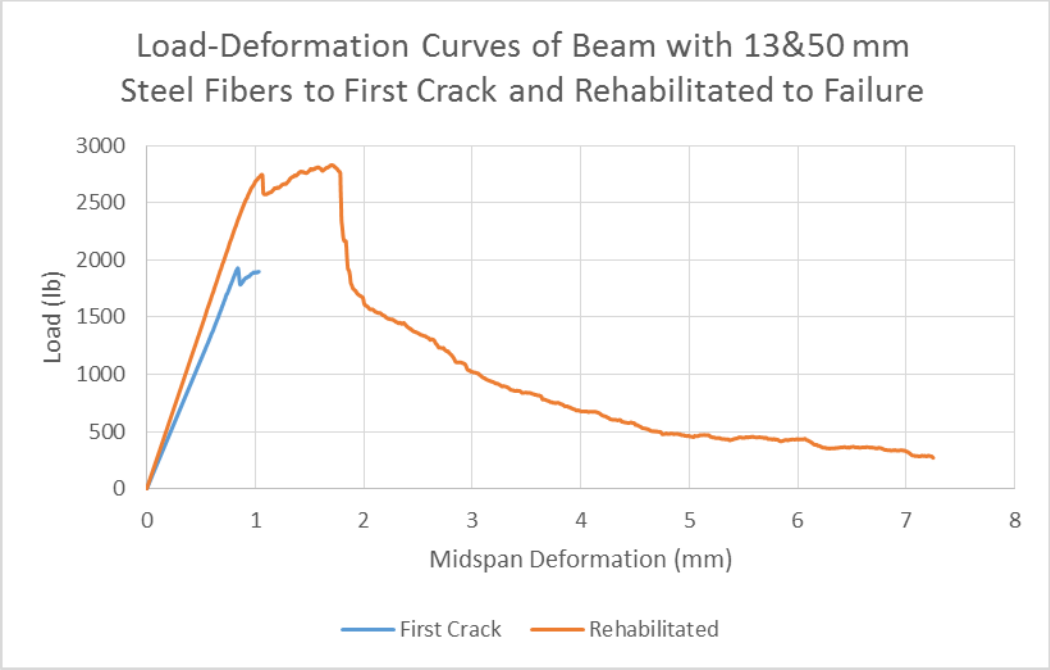


Figure 23: Load-Deformation Curves of Beam with 13 mm & 50 mm Steel Fibers Tested to First Crack and to Failure with the Addition of External Flexural Reinforcement

### 3.3 Beams with External Flexural Reinforcement Tested to Failure

The beams represented in this section are 6MM-0323-FRP6, 13MM-0317-FRP5, 6&30MM-0323-AL5, 13&50MM-0318-AL4, 30MM-1124-AL6 and 50MM-1008-AL4. After having been tested to first crack, all beams were externally reinforced with basalt fiber and tested to failure. Figure 24 shows these beams at end of testing. The age of the beam with 6 mm fibers, 13 mm fibers, 6 mm & 30 mm fibers, 13 mm & 50 mm fibers, 30 mm fibers, and 50 mm fibers were 153 days, 159 days, 153 days, 158 days, 272 days and 319 days, respectively. It should be noted that due to the fact that some previous beams failed in shear as opposed to flexure, not all the beams had the same width of basalt fiber attached to the tension flange at the time of testing. The basalt fiber attached to 13MM-0317-FRP5, 30MM-1124-AL6 and 50MM-1008-AL4 had a width of 3 inches, whereas the basalt fiber attached to 6MM-0323-FRP6, 6&30MM-0323-AL5 and 13&50MM-

0318-AL4 had a width of 2 ½ inches, 2 inches and 2 ½ inches, respectively. All of these six beams failed in flexure, apart from 13MM-0317-FRP5, which failed in shear. The following graphs illustrate load-deformation curves generated by the flexure tests. Each graph depicts test results from either two or three beams for comparison.


(a)


(b)

(c)

(d)

(e)


(f)

Figure 24: Beams Tested to Failure with External Flexural Reinforcement (a) 6MM-0323-FRP6; (b) 13MM-0317-FRP5; (c) 6&30MM-0323-AL5; (d) 13&50MM-0318-AL4; (e) 30MM-1124-AL6; (f) 50MM-1008-AL4

The load-deformation curves in Figure 25 are of two beams with different fiber types and one beam with both fiber types that are present in the other two beams. Beam 30MM-1124-AL6 has the highest ultimate load, and the other beams have similar ultimate loads. The midspan deformation at the ultimate load of 30MM-1124-AL6 is the greatest, whereas the midspan deformations at the ultimate load of 6MM-0323-FRP6 is the least. The elastic limit and midspan deflection at the elastic limit follow the same trend among the three beams as the ultimate load and midspan deformation at the ultimate load. Beams 6MM-0323-FRP6 and 30MM-1124-AL6 have similar bending stiffnesses, and 6&30MM-0323-AL5 has the lowest bending stiffness. In any of the three graphs, there is no decrease in load after the elastic limit. All beams exhibit a parabolic shape around ultimate load, and experience a sharp drop after the peak, though 30MM-1124-AL6 seems to level out before continuing to drop. All beams have a smooth

leveling of load towards end of testing, and support similar loads at this stage. Beam 6&30MM-0323-AL5 deforms the greatest, whereas 6MM-0323-FRP6 deforms the least.

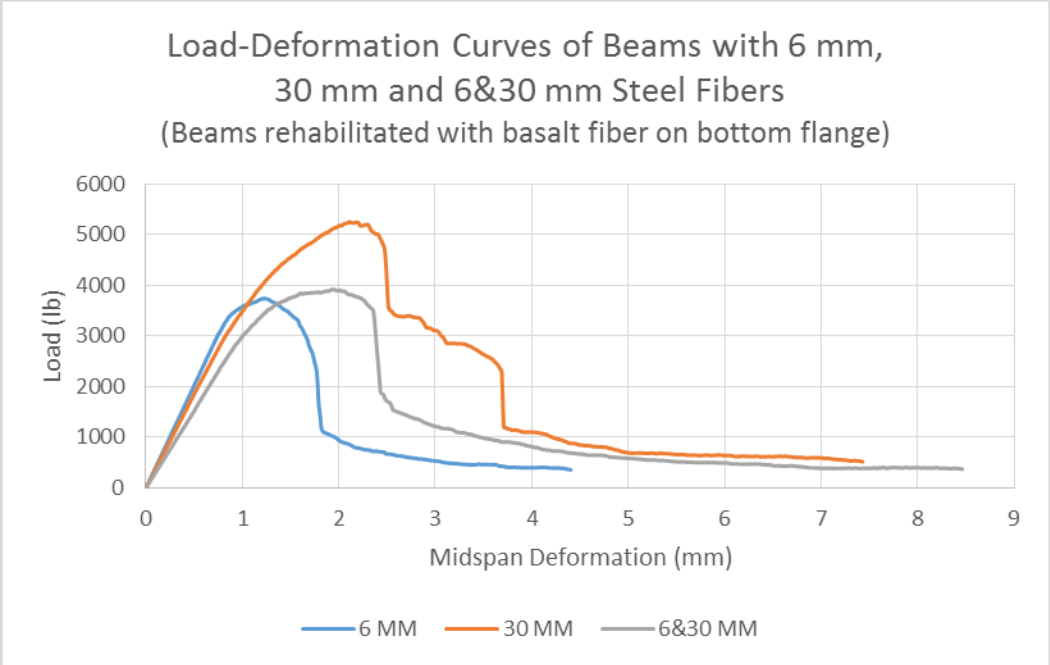


Figure 25: Load-Deformation Curves of Externally Reinforced Beams with 6 mm, 30 mm and 6 mm & 30 mm Steel Fibers

The load-deformation curves in Figure 26 are of two beams with different fiber types and one beam with both fiber types that are present in the other two beams. Beam 50MM-1008-AL4 has the highest ultimate load and 13&50MM-0318-AL4 has the lowest ultimate load. The midspan deformation at the ultimate load of 13MM-0317-FRP5 is the greatest, whereas the midspan deformatione at the ultimate load of 50MM-1008-AL4 is the least. Beam 50MM-1008-AL4 has the greatest elastic limit, whereas 13MM-0317-FRP5 has the lowest elastic limit. Regarding the midspan deformation at the elastic limit, 13MM-0317-FRP5 has the largest deformation, whereas 50MM-1008-AL4 has the smallest deformation. Beam 50MM-1008-AL4 has the highest bending stiffness, and 13MM-0317-FRP5 has the lowest bending stiffness. There is no decrease in load after elastic limit in any of the graphs. All graphs tend to curve and plateau, but a perfect

parabola is not formed. However, 13MM-0317-FRP5 most resembles a parabola around the ultimate load. Beams 13MM-0317-FRP5 and 13&50MM-0318-AL4 both experience a sharp drop in load after the ultimate before leveling out. This also occurs with 50MM-1008-AL4, but some load is resisted temporarily before continuing to drop. During the last phase of testing, 13MM-0317-FRP5 and 50MM-1008-AL4 have almost identical slopes, and support similar loads towards the end, yet 13MM-0317-FRP5 deforms the most. At this stage, 13&50MM-0318-AL4 slopes at a rate similar to the other two beams, but supports a smaller load and deforms the least.

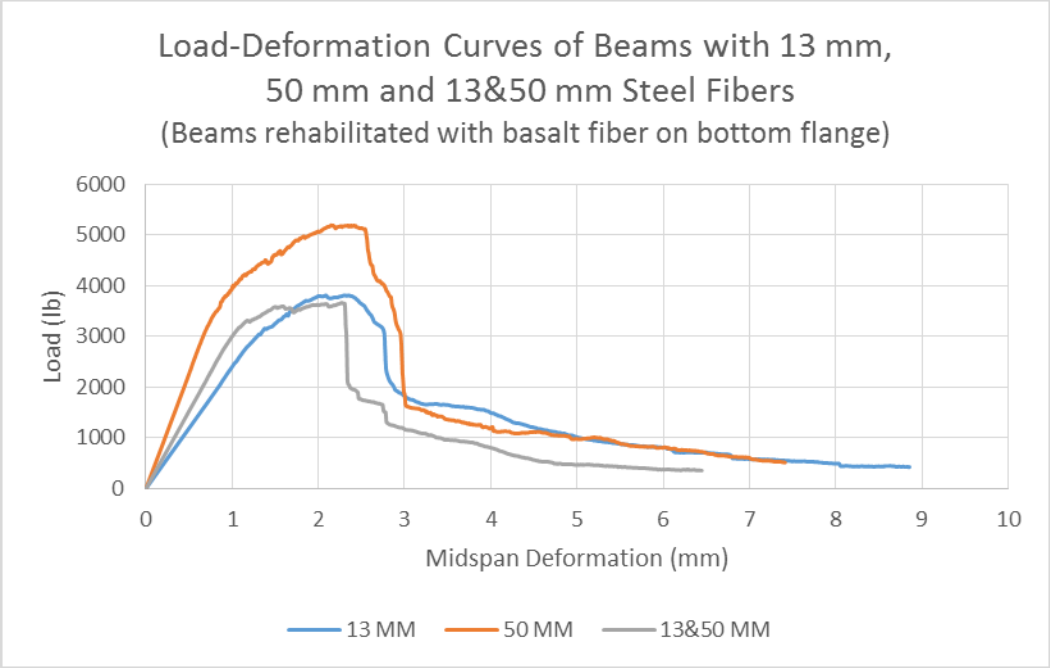


Figure 26: Load-Deformation Curves of Externally Reinforced Beams with 13 mm, 50 mm and 13 mm & 50 mm Steel Fibers

Figure 27 depicts load-deformation curves of two beams with straight steel fibers. The ultimate loads of both beams are close to one another, yet the midspan deformation at the ultimate load is larger for 13MM-0317-FRP5 than 6MM-0323-FRP6. Beam 6MM-0323-FRP6 has a greater elastic limit yet a smaller corresponding midspan deformation than 13MM-0317-FRP5. Beam 6MM-0323-FRP6 has a greater bending stiffness than

13MM-0317-FRP5. In either graph, there is no significant decrease in load after the elastic limit. Both beams form a line resembling a parabola around the ultimate load. The width of 13MM-0317-FRP5's graph is larger than that of 6MM-0323-FRP6. There is a sharp decrease in both graphs, but 6MM-0323-FRP6 has a deeper drop than 13MM-0317-FRP5. Both beams level out towards the end and support similar loads, though 13MM-0317-FRP5 deforms much more.

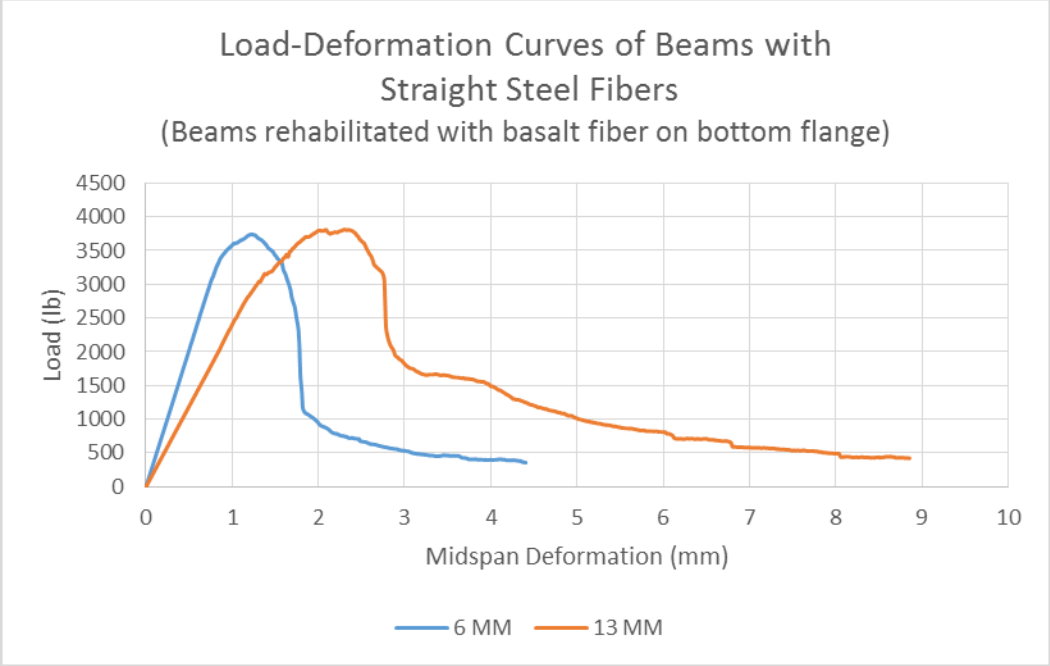


Figure 27: Load-Deformation Curves of Externally Reinforced Beams with Straight Steel Fibers

Figure 28 depicts load-deformation curves of two beams with hooked end fibers. The ultimate loads of both beams are close to one another, yet the midspan deformation at the ultimate load is larger for 50MM-1008-AL4 than 30MM-1124-AL6. Beam 30MM-1124-AL6 has a greater elastic limit and corresponding midspan deformation than 50MM-1008-AL4. Beam 50MM-1008-AL4 has a greater bending stiffness than 30MM-1124-AL6. There is no significant drop in load after the elastic limit in either graph. The graph for 30MM-1124-AL6 forms more a parabola, whereas the graph for 50MM-1008-

AL4 curves and flattens out around the ultimate load. Both beams experience a sharp decrease in load, a phase of resisting some load, and a continuation of the sharp decrease in load. Beam 30MM-1124-AL6 resists load longer than 50MM-1008-AL4 between the two sharp drops. Both beams level off and support similar loads at the end of testing. Beam 30MM-1124-AL6 deforms more than 50MM-1008-AL4, and 50MM-1008-AL4 begins its leveling off phase earlier than 30MM-1124-AL6.

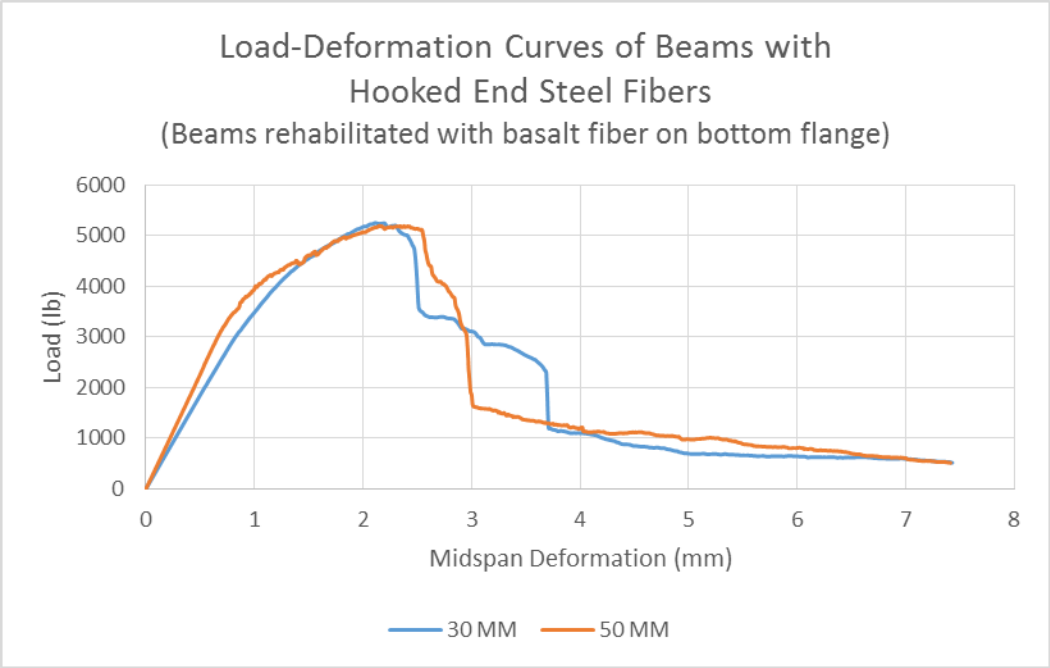


Figure 28: Load-Deformation Curves of Externally Reinforced Beams with Hooked End Steel Fibers

Figure 29 depicts load-deformation curves of two beams with hybrid or multiple fiber types. Beam 6&30MM-0323-AL5 has a larger ultimate load, yet smaller corresponding midspan deformation than 13&50MM-0318-AL4. Beam 6&30MM-0323-AL5 has a greater elastic limit and corresponding midspan deformation than 13&50MM-0318-AL4. Both beams have almost identical bending stiffnesses. There is no decrease in load after the elastic limit in either graph. Both graphs are almost identical in size and shape except for a few differences. Around the ultimate, 6&30MM-0323-AL5 forms a

parabola, whereas 13&50MM-0318-AL4 tends to flatten out more. Both beams have a sharp decrease in load, yet 13&50MM-0318-AL4 resists some load before the graph continues to drop. The slopes of both graphs during leveling off are similar as is the load both beams support in this phase. Beam 6&30MM-0323-AL5 deforms more than 13&50MM-0318-AL4.

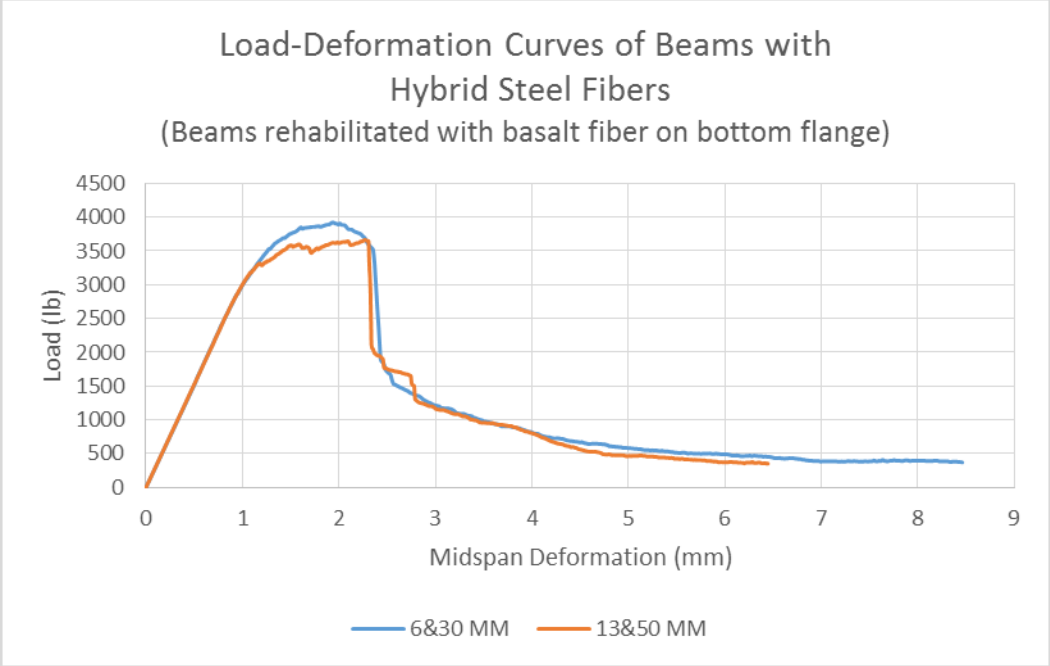


Figure 29: Load-Deformation Curves of Externally Reinforced Beams with Hybrid Steel Fibers

Load-deformation curves for 6MM-0323-FRP6, 50MM-1008-AL4 and 13&50MM-0318-AL4 are shown in Figure 30. Beam 50MM-1008-AL4 has the highest ultimate load, whereas 6MM-0323-FRP6 and 13&50MM-0318-AL4 have similar ultimate loads. Beam 13&50MM-0318-AL4 has the largest midspan deformation at the ultimate load, and 6MM-0323-FRP6 has the smallest midspan deformation at the ultimate load. Beam 6MM-0323-FRP6 has the highest elastic limit, whereas 13&50MM-0318-AL4 has the lowest elastic limit. At the elastic limit, 13&50MM-0318-AL4 has the greatest midspan deformation and 50MM-1008-AL4 has the smallest midspan

deformation. Beams 6MM-0323-FRP6 and 50MM-1008-AL4 have similar bending stiffnesses, whereas 13&50MM-0318-AL4 has the lowest bending stiffness. There is no decrease in load after the elastic limit in either graph. At the peak, 6MM-0323-FRP6 forms a parabolic shape, 13&50MM-0318-AL4 flattens out, and 50MM-1008-AL4 seems to does not really form a parabola or flatten out. All graphs have a sharp decrease in load after the peak, though 13&50MM-0318-AL4 experiences the sharpest drop. During the leveling off of the load, 50MM-1008-AL4 supports the greatest load and deforms the most, whereas 6MM-0323-FRP6 supports the least load and deforms the least.

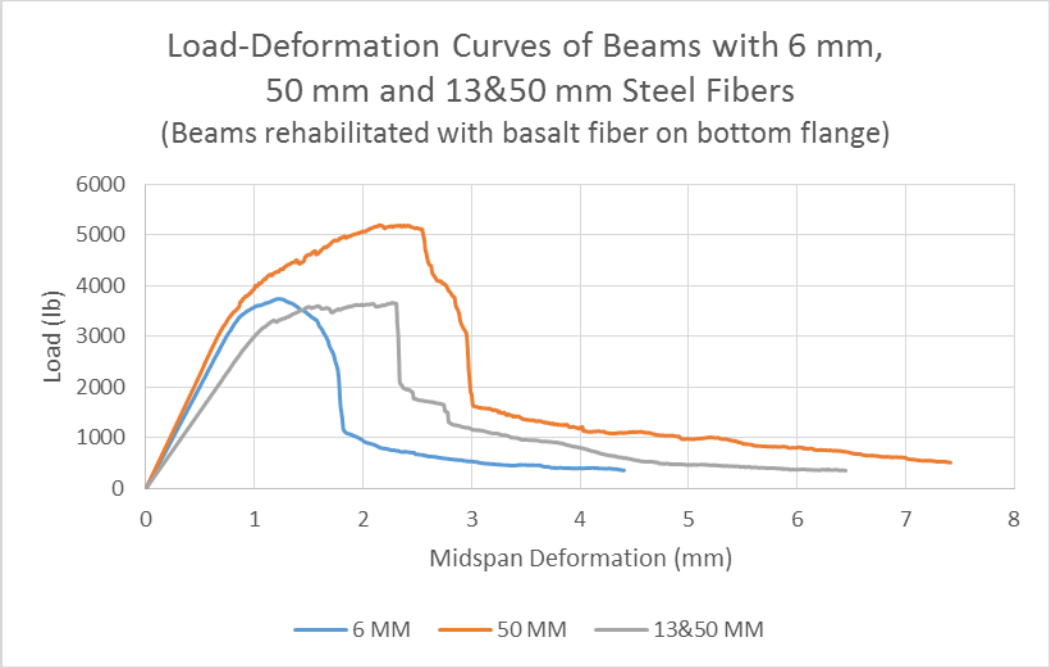


Figure 30: Load-Deformation Curves of Externally Reinforced Beams with 6 mm, 50 mm and 13 mm & 50 mm Steel Fibers

Load-deformation curves for 30MM-1124-AL6, 13MM-0317-FRP5 and 13&50MM-0318-AL4 are shown in Figure 31. Beam 30MM-1124-AL6 has the highest ultimate load, whereas 13&50MM-0318-AL4 has an ultimate load slightly less than that of 13MM-0317-FRP5. Beam 13MM-0317-FRP5 has the largest midspan deformation at the ultimate load, and 30MM-1124-AL6 has the smallest midspan deformation at the

ultimate load. Beam 30MM-1124-AL6 has the highest elastic limit, whereas 13MM-0317-FRP5 has the lowest elastic limit. Beam 13MM-0317-FRP5 has the largest midspan deformation at the elastic limit, whereas 13&50MM-0318-AL4 has the smallest midspan deformation at the elastic limit. Beam 30MM-1124-AL6 has the highest bending stiffness, whereas 13MM-0317-FRP5 has the lowest bending stiffness. There is no decrease in load after the elastic limit in either graph. Beam 13MM-0317-FRP5 and 30MM-1124-AL6 resemble a parabola around the ultimate load, whereas 13&50MM-0318-AL4 flattens out more. All graphs experience a sharp decrease in load after the ultimate load, though 30MM-1124-AL6 temporarily resists load before continuing to decrease. Beams 13MM-0317-FRP5 and 30MM-1124-AL6 have almost identical slopes while the load is leveling off. Beams 13MM-0317-FRP5 and 30MM-1124-AL6 support similar loads towards the end of testing, and 13MM-0317-FRP5 experiences the greatest deformation. Beam 13&50MM-0318-AL4 deforms the least and supports the least load towards the end of testing.

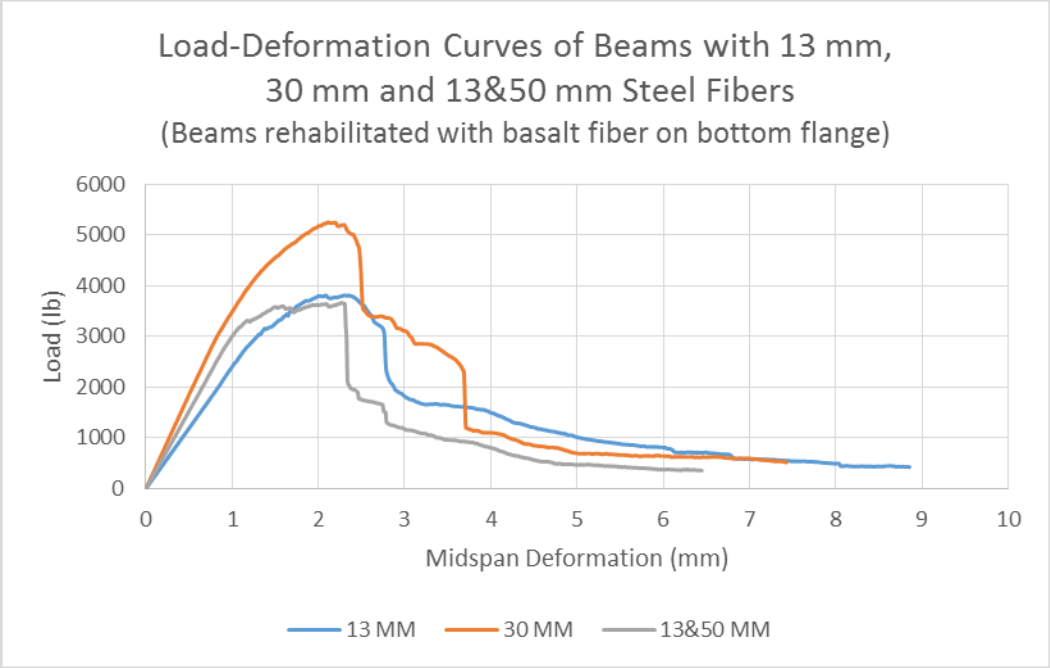


Figure 31: Load-Deformation Curves of Externally Reinforced Beams with 13 mm, 30 mm and 13 mm & 50 mm Steel Fibers

Load-deformation curves for 6&30MM-0323-AL5, 13MM-0317-FRP5 and 50MM-1008-AL4 are shown in Figure 32. Beam 50MM-1008-AL4 has the highest ultimate load, whereas 13MM-0317-FRP5 and 6&30MM-0323-AL5 have similar ultimate loads. Beam 13MM-0317-FRP5 has the largest midspan deformation at the ultimate load, and 6&30MM-0323-AL5 has the smallest midspan deformation at the ultimate load. Beam 6&30MM-0323-AL5 has the highest elastic limit, whereas 13MM-0317-FRP5 has the lowest elastic limit. At the elastic limit, 13MM-0317-FRP5 has the largest midspan deformation and 50MM-1008-AL4 has the smallest midspan deformation. Beam 50MM-1008-AL4 has the highest bending stiffness, whereas 13MM-0317-FRP5 has the lowest bending stiffness. There is no decrease in load after the elastic limit in any of the graphs. Beams 13MM-0317-FRP5 and 6&30MM-0323-AL5 form a parabola around the ultimate load, whereas 50MM-1008-AL4 depicts a curve that flattens out at the apex before rapidly decreasing. All graphs exhibit a rapid decrease in load after

the ultimate, though 50MM-1008-AL4 temporarily resists some load before the load rapidly drops again. Beams 13MM-0317-FRP5 and 50MM-1008-AL4 have almost identical slopes in the last phase of testing. All beams support similar loads in this phase. Out of all three beams 13MM-0317-FRP5 deforms the most, and 50MM-1008-AL4 deforms the least.

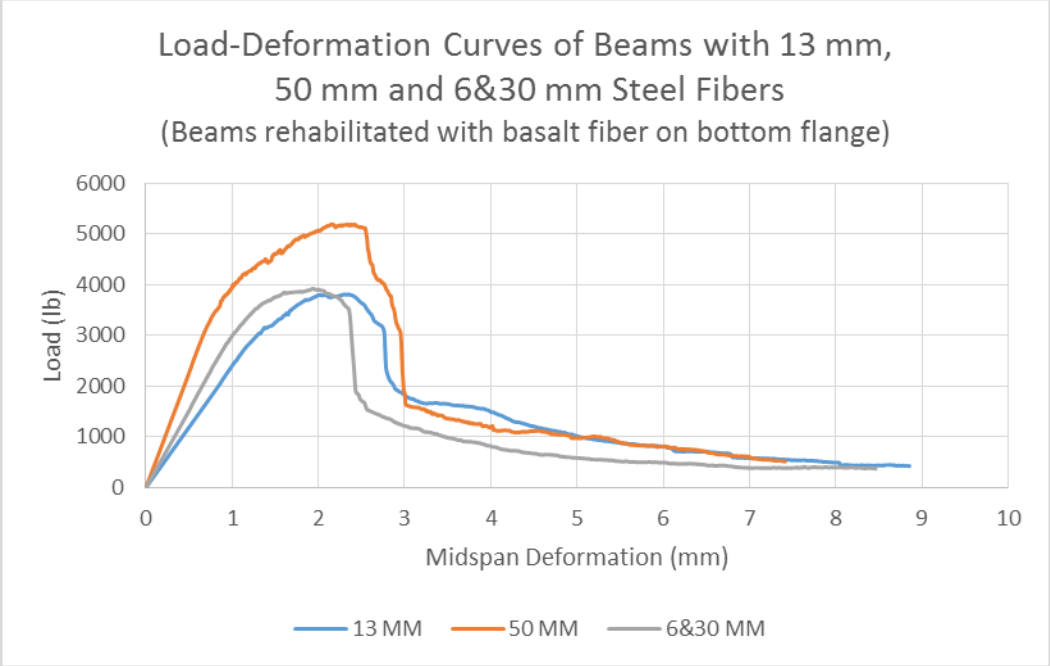


Figure 32: Load-Deformation Curves of Externally Reinforced Beams with 13 mm, 50 mm and 6 mm & 30 mm Steel Fibers

Table 5 shows a summary of the mechanical properties obtained from the flexural tests for all the beams tested with external flexural reinforcement. The first column tabulates the ultimate load of each beam. The beams that have the greatest ultimate load to the least strength in terms of fiber combinations are as follows: 30 mm steel fibers, 50 mm steel fibers, 6 mm & 30 mm steel fibers, 6 mm steel fibers, 13 mm steel fibers and 13 mm & 50 mm steel fibers. The second column tabulates the midpan deformation or deflection at the ultimate load of each beam. At the ultimate load, the beams that have the greatest deflection load to the least deflection in terms of fiber combinations are as

follows: 13 mm steel fibers, 30 mm steel fibers, 50 mm steel fibers, 13 mm & 50 mm steel fibers, 6 mm steel fibers and 6 mm & 30 mm steel fibers. The third column tabulates the elastic limit of each beam. The beams that have the greatest elastic limit to the least elastic limit in terms of fiber combinations are as follows: 30 mm steel fibers, 6 mm & 30 mm steel fibers, 6 mm steel fibers, 13 mm steel fibers, 50 mm steel fibers and 13 mm & 50 mm steel fibers. The fourth column tabulates what is the midpan deformation or deflection at the elastic limit of each beam. At the elastic limit, the beams that have the greatest deflection load to the least deflection in terms of fiber combinations are as follows: 30 mm steel fibers, 13 mm steel fibers, 6 mm & 30 mm steel fibers, 13 mm & 50 mm steel fibers, 6 mm steel fibers and 50 mm steel fibers. The fifth column tabulates the bending stiffness each beam. The beams that have the greatest bending stiffness to the least bending stiffness in terms of fiber combinations are as follows: 50 mm steel fibers, 6 mm steel fibers, 6 mm & 30 mm steel fibers, 30 mm steel fibers, 13 mm & 50 mm steel fibers and 13 mm steel fibers.

Table 5: Mechanical Properties Summary of Beams with External Flexural Reinforcement

| Specimen | Ultimate Load (lb) | Deflection at Ultimate (mm) | Elastic Limit (lb) | Deflection at Elastic Limit (mm) | Bending Stiffness (lb/mm) |
|---|---|---|---|---|---|
| 6MM-0323-AL4 | 4,666.9 | 2.624 | 3,366.5 | 0.957 | 3,703.3 |
| 6MM-0323-FRP5 | 3,523.9 | 1.503 | 3,030.3 | 0.919 | 3,350.7 |
| 6MM-0323-FRP6 | 3,741.8 | 1.234 | 3,387.2 | 0.865 | 4,049.2 |
| 13MM-0317-FRP4 | 3,934.1 | 2.413 | 2,811.1 | 1.083 | 2,796.2 |
| 13MM-0317-FRP5 | 3,814.1 | 2.308 | 3,158.2 | 1.377 | 2,398.2 |
| 13MM-0317-FRP6 | 3,747.2 | 2.958 | 2,827.0 | 1.001 | 2,939.3 |
| 30MM-1024-AL4 | 4,523.3 | 2.197 | 3,166.3 | 1.037 | 3,126.1 |
| 30MM-1024-AL5 | 5,410.8 | 2.125 | 4,707.5 | 1.564 | 3,063.3 |
| 30MM-1124-AL6 | 5,256.0 | 2.115 | 4,227.2 | 1.307 | 3,666.5 |
| 50MM-1008-AL4 | 5,196.6 | 2.15 | 3,192.9 | 0.711 | 4,539.9 |
| 50MM-1124-AL5 | 3,525.0 | 2.092 | 2,616.3 | 0.805 | 3,314.8 |
| 6&30MM-0323-AL4 | 4,466.6 | 1.388 | 4,213.2 | 1.134 | 4,108.5 |
| 6&30MM-0323-AL5 | 3,921.3 | 1.929 | 3,493.0 | 1.255 | 3,066.7 |
| 6&30MM-0401-AL6 | 3,830.7 | 1.51 | 3,275.4 | 0.971 | 3,433.6 |

| | | | | | |
|---|---|---|---|---|---|
| 13&50MM-0318-AL4 | 3,665.3 | 2.272 | 3,183.1 | 1.093 | 3,059.8 |
| 13&50MM-0318-AL5 | 3,553.2 | 1.828 | 2,896.9 | 0.967 | 3,055.9 |
| 13&50MM-0318-AL6 | 2,831.6 | 1.708 | 2,565.8 | 0.933 | 2,800.1 |

Table 6 lists the areas of various regions as well as the accumulative areas of the load-deformation curves obtained from the flexural tests for all the beams tested with external flexural reinforcement. The first column tabulates the area of the elastic region of each beam. In the elastic region, the beams that have the greatest area to the least area in terms of fiber combinations are as follows: 30 mm steel fibers, 6 mm & 30 mm steel fibers, 13 mm steel fibers, 6 mm steel fibers, 13 mm & 50 mm steel fibers and 50 mm steel fibers. The second column tabulates the area under the load-deformation curve between the elastic limit and ultimate load of each beam. Between the elastic limit and ultimate load, the beams that have the greatest area to the least area in terms of fiber combinations are as follows: 50 mm steel fibers, 13 mm steel fibers, 30 mm steel fibers, 6 mm steel fibers, 13 mm & 50 mm steel fibers and 6 mm & 30 mm steel fibers. The third column tabulates the post-ultimate area under the load-deformation curve of each beam. The beams that have the greatest post-ulitmate area to the least post-ultimate area in terms of fiber combinations are as follows: 13 mm steel fibers, 6 mm & 30 mm steel fibers, 30 mm steel fibers, 13 mm & 50 mm steel fibers, 50 mm steel fibers and 6 mm steel fibers. The fourth column tabulates the accumulative area under the load-deformation curve of each beam. The beams with the greatest accumulative area to the least accumulative area in terms of fiber combinations are as follows: 13 mm steel fibers, 30 mm steel fibers, 6 mm & 30 mm steel fibers, 50 mm steel fibers, 13 mm & 50 mm steel fibers and 6 mm steel fibers.

Table 6: Area under Load-Deformation Curves of Beams with External Flexural Reinforcement

| Specimen | Area of Elastic Region (lb-mm) | Area between Elastic Limit and Ultimate Load (lb-mm) | Area of Post-Ultimate Region (lb-mm) | Accumulative Area (lb-mm) |
|---|---|---|---|---|
| 6MM-0323-AL4 | 1,688.5 | 6,845.3 | 7,661.6 | 16,195.3 |
| 6MM-0323-FRP5 | 1,404.3 | 1,950.4 | 3,261.2 | 6,616.0 |
| 6MM-0323-FRP6 | 1,508.1 | 1,329.3 | 3,348.5 | 6,186.0 |
| 13MM-0317-FRP4 | 1,621.5 | 4,639.8 | 11,655.3 | 17,916.7 |
| 13MM-0317-FRP5 | 2,249.1 | 3,337.6 | 7,459.2 | 13,046.0 |
| 13MM-0317-FRP6 | 1,460.4 | 6,776.3 | 5,610.0 | 13,846.7 |
| 30MM-1024-AL4 | 1,676.0 | 4,663.9 | 7,099.6 | 13,439.4 |
| 30MM-1024-AL5 | 3,731.7 | 2,884.9 | 6,008.4 | 12,625.0 |
| 30MM-1124-AL6 | 3,013.2 | 3,891.6 | 8,289.2 | 15,194.0 |
| 50MM-1008-AL4 | 1,144.3 | 6,394.1 | 8,082.0 | 15,620.4 |
| 50MM-1124-AL5 | 1,072.3 | 4,182.8 | 2,551.5 | 7,806.5 |
| 6&30MM-0323-AL4 | 2,594.2 | 1,115.0 | 10,672.0 | 14,381.2 |
| 6&30MM-0323-AL5 | 2,353.5 | 2,542.1 | 5,875.6 | 10,771.2 |
| 6&30MM-0401-AL6 | 1,618.9 | 1,960.0 | 7,720.1 | 11,299.1 |
| 13&50MM-0318-AL4 | 1,814.3 | 4,149.5 | 3,442.3 | 9,406.1 |
| 13&50MM-0318-AL5 | 1,426.3 | 2,868.8 | 8,907.3 | 13,202.4 |
| 13&50MM-0318-AL6 | 1,219.0 | 2,101.9 | 4,252.3 | 7,573.2 |

### 3.4 Beams with and without External Flexural Reinforcement Tested to Failure

This section utilizes graphs of the load-deformation curves to illustrate the effect of external flexural reinforcement. Each graph depicts test results of two beams tested to failure with and without external flexural reinforcement. The beams represented in this section are those found in Sections 3.1 and 3.3.

Two load-deformation curves for 6MM-0323-AL2 and 6MM-0323-FRP6 are depicted in Figure 33. After being rehabilitated with basalt fiber, the ultimate load 6MM-0323-FRP6 is larger than the ultimate load of 6MM-0323-AL2. The difference between the midspan deformations at theultimate load of the two beams is less drastic than the difference of the ultimate loads themselves. As with the ultimate load, the elastic limit and the corresponding midspan deformation of 6MM-0323-FRP6 are larger than those of 6MM-0323-AL2. The bending stiffness of 6MM-0323-FRP6 is larger than the bending

stiffness of 6MM-0323-AL2. In contrast to 6MM-0323-AL2, there is a steep drop in the load-deformation curve of 6MM-0323-FRP6 beyond the ultimate load. Beam 6MM-0323-AL2 displays a decrease in load after the elastic limit. Around the ultimate load, a parabola forms for each beam, though 6MM-0323-FRP6 has a sharper peak. Beam 6MM-0323-FRP6 has a steep drop after the ultimate load, whereas the post-ultimate slope of 6MM-0323-AL2 similar to its slope in the elastic region. Towards the end of testing, 6MM-0323-FRP6 levels off more, has greater maximum deformation, and supports a greater load than 6MM-0323-AL2.

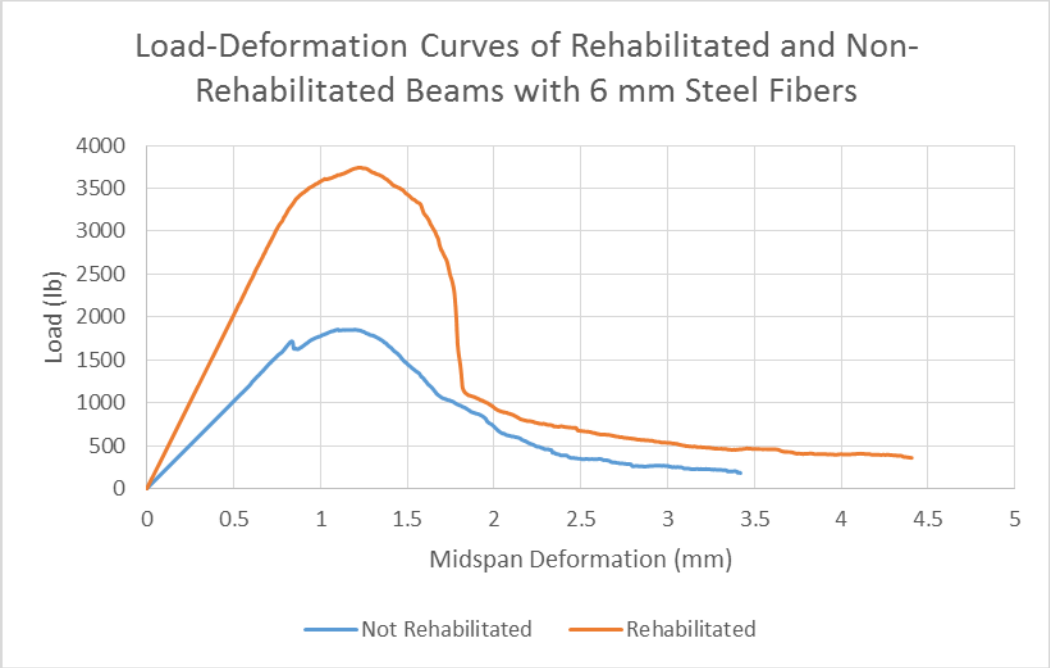


Figure 33: Load-Deformation Curves of Beams with 6 mm Steel fibers with and without External Reinforcement

Two load-deformation curves for 30MM-1029-AL1 and 30MM-1124-AL6 are depicted in Figure 34. After being rehabilitated with basalt fiber, the ultimate load and corresponding midspan deformation of 30MM-1124-AL6 is larger than those of 30MM-1029-AL1. As with the ultimate load, the elastic limit and the midspan deformation at the elastic limit of 30MM-1124-AL6 are larger than those of 30MM-1029-AL1. The bending

stiffness 30MM-1124-AL6 is larger than the bending stiffness of 30MM-1029-AL1. Neither graph shows a decrease in load after the elastic limit. Around the ultimate load, 30MM-1029-AL1 exhibits a sharp peak, whereas 30MM-1124-AL6 is more reminiscent to a parabola. The post-ultimate slope of 30MM-1029-AL1 is similar to its slope in the elastic region, whereas 30MM-1124-AL6's post-ultimate slope includes two sharp drops in load. Both graphs level out towards the end, though 30MM-1124-AL6 supports a greater load and deforms more than 30MM-1029-AL1.

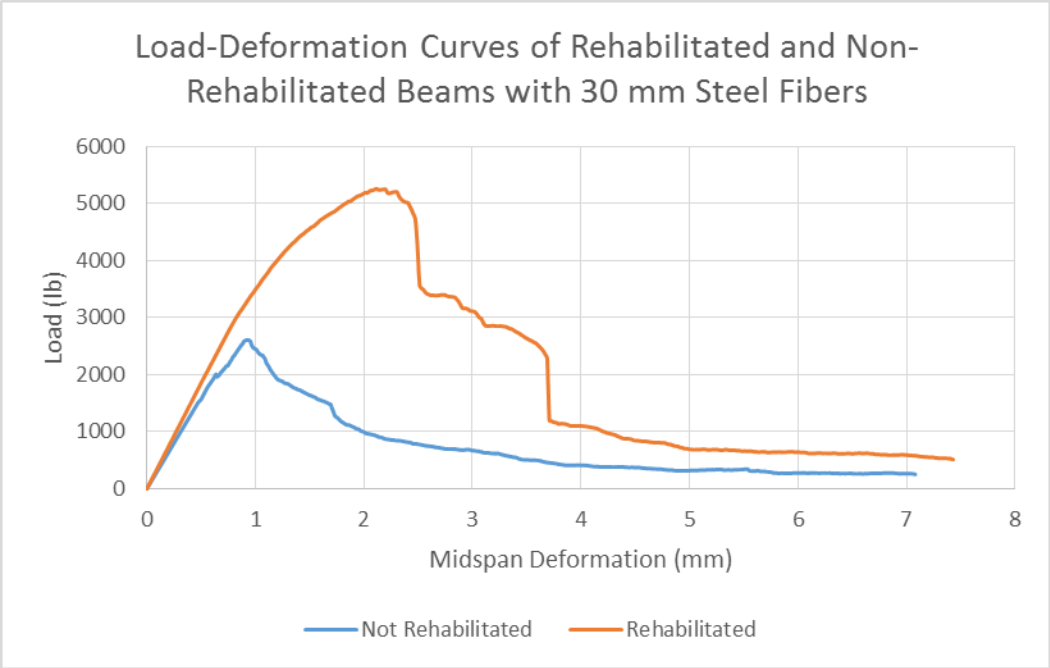


Figure 34: Load-Deformation Curves of Beams with 30 mm Steel fibers with and without External Reinforcement

Two load-deformation curves for 6&30MM-0401-AL1 and 6&30MM-0323-AL5 are depicted in Figure 35. After being rehabilitated with basalt fiber, the ultimate load of 6&30MM-0323-AL5 is greater than the ultimate load of 6&30MM-0401-AL1. The midspan deformation at ultimate load of 6&30MM-0323-AL5 is larger than that of 6&30MM-0401-AL1. The elastic limit and corresponding midspan deformation of 6&30MM-0323-AL5 are larger than those of 6&30MM-0401-AL1. The bending stiffness

of both beams are similar to one another. In both curves, there is no decrease in load after the elastic limit. Around the ultimate, 6&30MM-0401-AL1 has a relatively small parabolic shape, whereas 6&30MM-0323-AL5 has a more pronounced parabolic shape. The post-ultimate slope of 6&30MM-0401-AL1 is similar to its slope in the elastic region, whereas there is a sharp decrease in load after the ultimate load for 6&30MM-0323-AL5. During the leveling off of the load towards the end of testing, both beams share similar slopes and support similar loads. Beam 6&30MM-0323-AL5 experiences greater deformation than 6&30MM-0401-AL1.

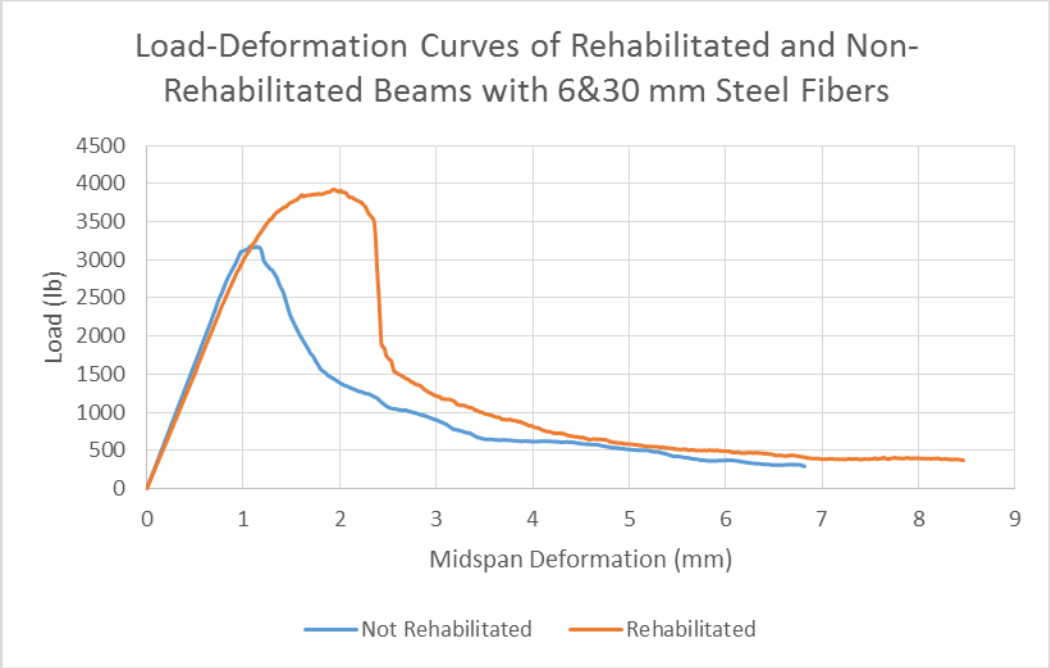


Figure 35: Load-Deformation Curves of Beams with 6 mm & 30 mm Steel fibers with and without External Reinforcement

Two load-deformation curves for 13MM-0317-FRP3 and 13MM-0317-FRP5 are depicted in Figure 36. The ultimate load and corresponding midspan deformation of 13MM-0317-FRP5 are larger than those of 13MM-0317-FRP3. The elastic limit and corresponding midspan deformation for 13MM-0317-FRP5 are larger than those of 13MM-0317-FRP3. The bending stiffness of 13MM-0317-FRP5 is less than the bending

stiffness of 13MM-0317-FRP3. There is a slight decrease in load after the elastic limit for 13MM-0317-FRP3, but this is not evident for 13MM-0317-FRP5. The graph for 13MM-0317-FRP5 is reminiscent to a parabola around the ultimate load, whereas the graph for 13MM-0317-FRP3 curves up to a sharp peak before the load begins to drop. There is a sharp drop in load for 13MM-0317-FRP5 after the ultimate. Beam 13MM-0317-FRP5 supports a greater load and deformation than 13MM-0317-FRP3 towards the end of testing.

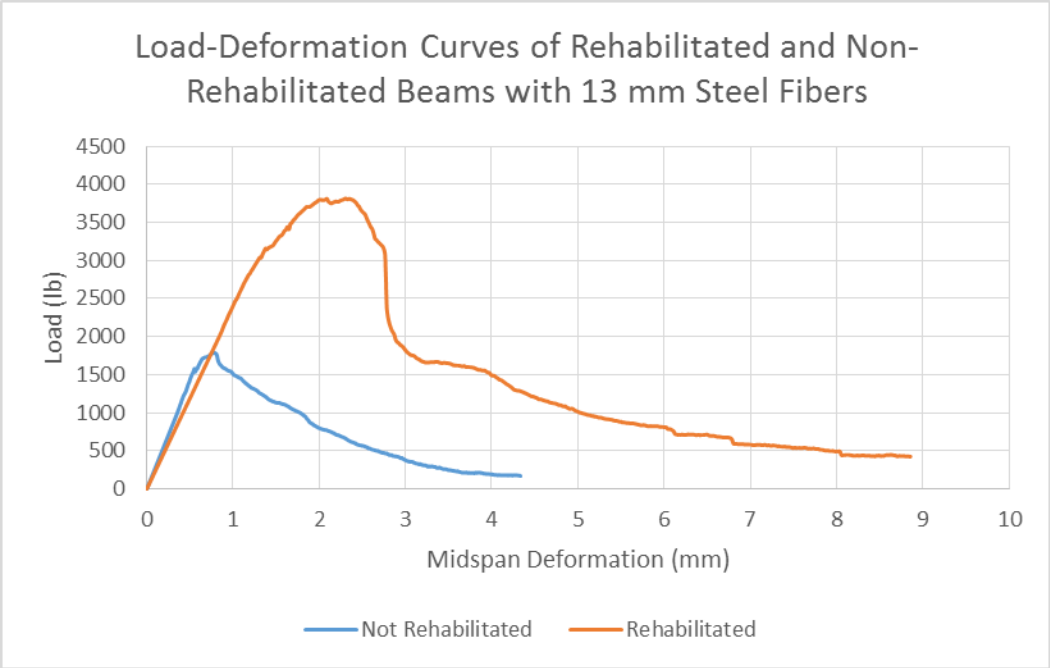


Figure 36: Load-Deformation Curves of Beams with 13 mm Steel fibers with and without External Reinforcement

Two load-deformation curves for 50MM-1015-AL1 and 50MM-1008-AL4 are depicted in Figure 37. Beam 50MM-1008-AL4 has a greater ultimate load and corresponding midspan deformation than 50MM-1015-AL1. Beam 50MM-1008-AL4 has a greater elastic limit, corresponding deformation and bending stiffness. Neither beam shows a clear decrease in load after the elastic limit. Apart from the ultimate load, 50MM-1015-AL1 shows a relatively flat line at the peak, whereas 50MM-1008-AL4

gradually curves all the up to the peak. The post-ultimate slope of 50MM-1015-AL1 is similar to the slope of its elastic region, whereas 50MM-1008-AL4 experiences a sharp drop in load after the ultimate load. Both beams exhibit leveling off in the last phase of testing, though 50MM-1008-AL4 supports a greater load and deforms more than 50MM-1015-AL1.

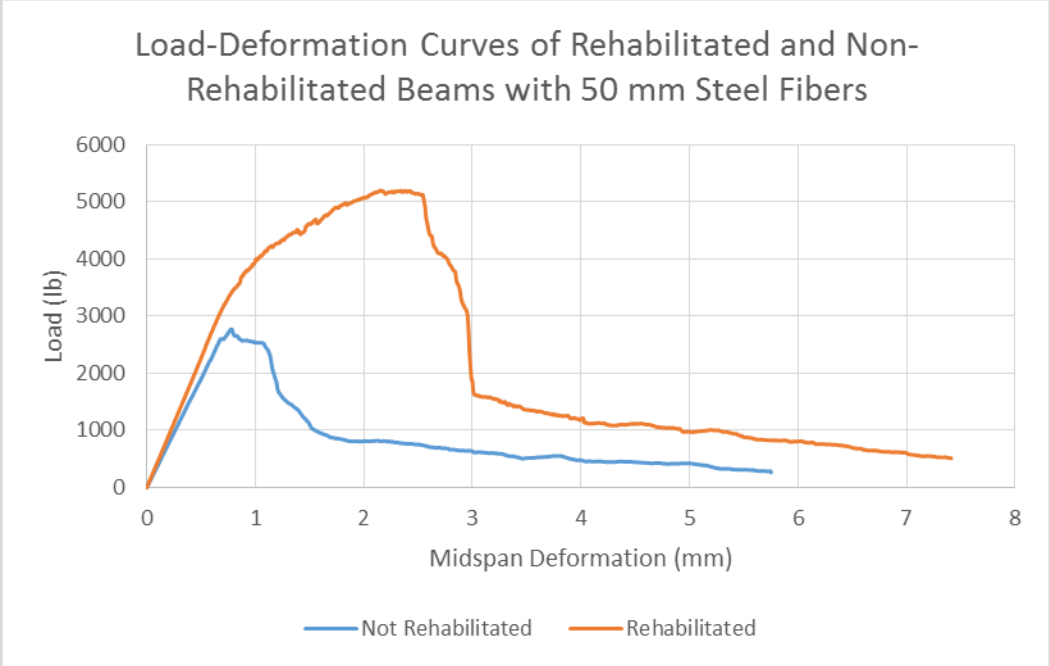


Figure 37: Load-Deformation Curves of Beams with 50 mm Steel fibers with and without External Reinforcement

Two load-deformation curves for 13&50MM-0318-AL1 and 13&50MM-0318-AL4 are depicted in Figure 38. Beam 13&50MM-0318-AL4 has a greater ultimate load and corresponding midspan deformation than 13&50MM-0318-AL1. The elastic limit and its corresponding midspan deformation is greater for 13&50MM-0318-AL4. Beam 13&50MM-0318-AL4 has a greater bending stiffness than 13&50MM-0318-AL1. Beam 13&50MM-0318-AL1 exhibits a decrease in load after the elastic limit, which is not seen in 13&50MM-0318-AL4. Although both graphs are not very smooth around the peak, 13&50MM-0318-AL1 forms somewhat closer a parabola, whereas 13&50MM-0318-

AL4 tends to flatten out more. There is a sharp drop with 13&50MM-0318-AL4 after the ultimate load, whereas the post-ultimate slope of 13&50MM-0318-AL1 is much more gradual. Beam 13&50MM-0318-AL1 experiences a longer period of leveling off than 13&50MM-0318-AL4, as well as supports a greater load and deforms more towards the end of testing.

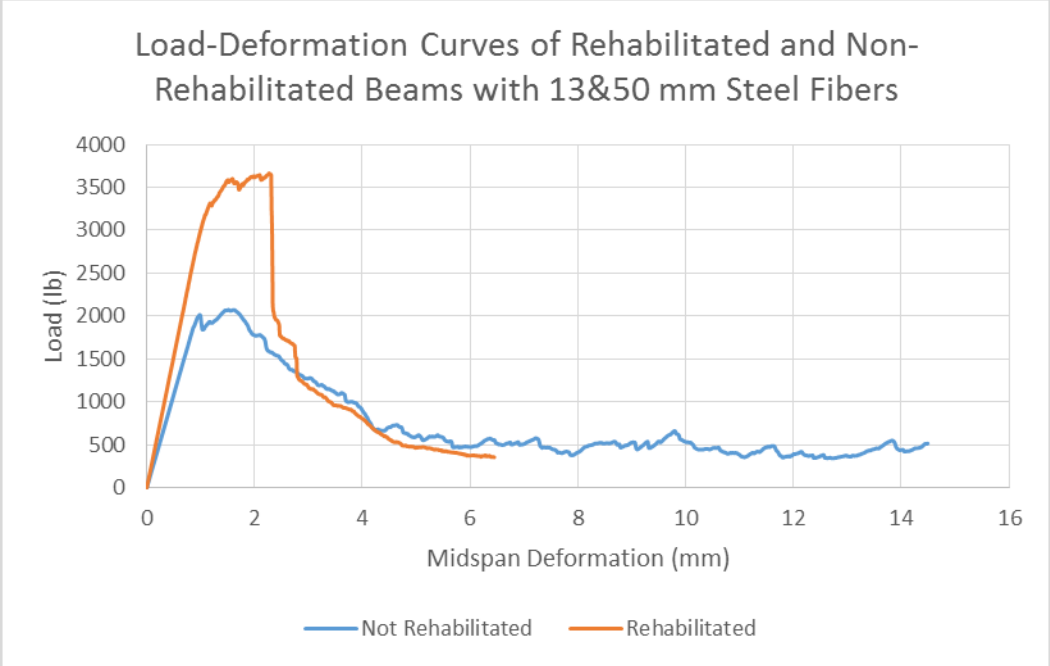


Figure 38: Load-Deformation Curves of Beams with 13 mm & 50 mm Steel fibers with and without External Reinforcement

### 3.5 Flexural Behavior Summary

Table 7 shows the load at the elastic limit and ultimate load for all the beams tested. Included are beams with and without external basalt fiber flexural reinforcement. The fifth column in Table 7 shows the percentage of the ultimate load at which the elastic load limit was observed in a given row. For the beams with 6 mm, 13 mm and 50 mm steel fibers, the introduction of flexural reinforcement lowers the percentage of the ultimate load which the elastic load limit was observed. The opposite is true for the beams with 30 mm, 6 & 30 mm and 13 & 50 mm steel fibers. With the addition of

external flexural reinforcement, the maximum midspan deformation does increase for some of the specimens. The specimens that experience an increase of maximum midspan deformation due to the addition of external flexural reinforcement include beams with 6 mm, 13 mm, 30 mm and 6 & 30 mm steel fibers. The opposite is true for the beams with 50 mm mm and 13 & 50 mm steel fibers where the maximum deformation tends to decrease with the addition of flexural reinforcement.

Table 7: Elastic Limit – Ultimate Load Ratio and Maximum Deformation

| Specimen | Flexural Reinforcement | Elastic Limit (lb) | Ultimate Load (lb) | Elastic Limit: Ultimate Load | Max δ (mm) |
|---|---|---|---|---|---|
| 6MM-0401-AL1 | No | 2,448.7 | 2,692.1 | 91.0 % | 3.422 |
| 6MM-0323-AL2 | No | 1,718.6 | 1,854.6 | 92.7 % | 3.419 |
| 6MM-0323-AL3 | No | 1,835.9 | 1,970.6 | 93.2 % | 4.41 |
| 6MM-0323-AL4 | Yes | 3,366.5 | 4,666.9 | 72.1 % | 7.928 |
| 6MM-0323-FRP5 | Yes | 3,030.3 | 3,523.9 | 86.0 % | 3.996 |
| 6MM-0323-FRP6 | Yes | 3,387.2 | 3,741.8 | 90.5 % | 4.405 |
| 13MM-0317-FRP1 | No | 1,938.7 | 2,020.5 | 96.0 % | 4.361 |
| 13MM-0317-FRP2 | No | 924.6 | 1,339.0 | 69.1 % | 6.896 |
| 13MM-0317-FRP3 | No | 1,579.6 | 1,787.8 | 88.4 % | 4.334 |
| 13MM-0317-FRP4 | Yes | 2,811.1 | 3,934.1 | 71.5 % | 13.48 |
| 13MM-0317-FRP5 | Yes | 3,158.2 | 3,814.1 | 82.8 % | 8.857 |
| 13MM-0317-FRP6 | Yes | 2,827.0 | 3,747.2 | 75.4 % | 7.679 |
| 30MM-1029-AL1 | No | 2,007.7 | 2,607.6 | 77.0 % | 7.081 |
| 30MM-1029-AL2 | No | 1,706.0 | 2,175.6 | 78.4 % | 6.929 |
| 30MM-1029-AL3 | No | 1,042.4 | 3,078.5 | 33.9 % | 4.62 |
| 30MM-1024-AL4 | Yes | 3,166.3 | 4,523.3 | 70.0 % | 9.245 |
| 30MM-1024-AL5 | Yes | 4,707.5 | 5,410.8 | 87.0 % | 5.641 |
| 30MM-1124-AL6 | Yes | 4,227.2 | 5,256.0 | 80.4 % | 7.43 |
| 50MM-1015-AL1 | No | 2,592.3 | 2,771.5 | 93.5 % | 5.752 |
| 50MM-1015-AL2 | No | 1,356.4 | 2,247.9 | 60.3 % | 8.249 |
| 50MM-1015-AL3 | No | 2,775.9 | 2,984.0 | 93.0 % | 4.774 |
| 50MM-1008-AL4 | Yes | 3,192.9 | 5,196.6 | 61.4 % | 7.413 |
| 50MM-1124-AL5 | Yes | 2,616.3 | 3,525.0 | 74.2 % | 4.768 |
| 6&30MM-0401-AL1 | No | 2,924.6 | 3,183.1 | 91.9 % | 6.818 |
| 6&30MM-0323-AL2 | No | 3,175.9 | 3,737.0 | 85.0 % | 6.482 |
| 6&30MM-0323-AL3 | No | 1,793.7 | 1,996.8 | 89.8 % | 12.666 |
| 6&30MM-0323-AL4 | Yes | 4,213.2 | 4,466.6 | 94.3 % | 9.991 |
| 6&30MM-0323-AL5 | Yes | 3,493.0 | 3,921.3 | 89.1 % | 8.463 |
| 6&30MM-0401-AL6 | Yes | 3,275.4 | 3,830.7 | 85.5 % | 8.561 |
| 13&50MM-0318-AL1 | No | 1,987.3 | 2,072.8 | 95.9 % | 14.492 |
| 13&50MM-0318-AL2 | No | 1,447.6 | 2,060.8 | 70.2 % | 7.823 |
| 13&50MM-0318-AL3 | No | 1,783.1 | 2,583.5 | 69.0 % | 6.089 |
| 13&50MM-0318-AL4 | Yes | 3,183.1 | 3,665.3 | 86.8 % | 6.447 |
| 13&50MM-0318-AL5 | Yes | 2,896.9 | 3,553.2 | 81.5 % | 12.447 |
| 13&50MM-0318-AL6 | Yes | 2,565.8 | 2,831.6 | 90.6 % | 7.248 |

Table 8 depicts the average ultimate load values of beams of a certain fiber type with and without external basalt fiber flexural reinforcement. With the addition of external basalt flexural reinforcement, the beams experienced a greater ultimate load. This increase in ultimate load is represented as a percent increase with respect to the average ultimate load of the beams without flexural reinforcement. The ultimate load of the beams increased from 45% to 73% with the addition of external flexural reinforcement. The beams with 13 mm steel fibers experienced the smallest increase of ultimate load, whereas the beams with 6 mm & 30 mm steel fibers experienced the greatest increase of ultimate load.

Table 8: Effect of External Flexural Reinforcement on Ultimate Load

| Fiber Combination | Average Ultimate Load without External Flexural Reinforcement (lb) | Average Ultimate Load with External Flexural Reinforcement (lb) | Percent Increase of Ultimate Load Due to Flexural Reinforcement |
|---|---|---|---|
| 6 MM | 2,172.4 | 3,977.5 | 55% |
| 13 MM | 1,715.7 | 3,831.8 | 45% |
| 30 MM | 2,620.6 | 5,063.3 | 52% |
| 50 MM | 2,667.8 | 4,360.8 | 61% |
| 6&30 MM | 2,972.3 | 4,072.9 | 73% |
| 13&50 MM | 2,239.0 | 3,350.0 | 67% |

Table 9 shows the average partial and accumulative areas under the load-deformation curves of beams of a certain fiber type with and without external flexural reinforcement. This area represents the fracture toughness or the fracture energy of the beam. With the addition of external flexural reinforcement, the beams generally experienced an increase of area under the load-deformation curve. The increase of the area under the load-deformation curve of the elastic region, between the elastic limit and ultimate load, after the ultimate load and accumulative area are represented as percent increases. The fracture energy area of the elastic region of the beams increased from 62%

to 365% with the aid of external flexural reinforcement. The beams with 30 mm steel fibers experienced the largest increase of area in the elastic region, whereas the beams with 6 mm & 30 mm as well as 6 mm steel fibers experienced the smallest increase of area in the elastic region. The area under the load-deformation curve between the elastic limit and the ultimate load of the beams increased from 152% to 1,736% with the aid of external flexural reinforcement. The beams with 13 mm steel fibers experienced the largest increase of area in the elastic region, whereas the beams with 6 mm & 30 mm steel fibers experienced the smallest increase of area in the elastic region. With the aid of external flexural reinforcement, the beams with 13 mm steel fibers showed to have the greatest increase in area of the post-ultimate region, which in this case was 173%. Contrary to the other regions, the beams with 13 mm & 50 mm steel fibers experienced a decrease of 8% area in the post-ultimate region. The accumulative area under the load-deformation curve of the beams increased from 0% to 304% with the aid of external flexural reinforcement. The beams with 13 mm steel fibers experienced the largest increase of accumulative area under the load-deformation curve, whereas the beams with 6 mm & 30 mm steel fibers experienced the smallest increase of accumulative area under the load-deformation curve.

Table 9: Effect of External Flexural Reinforcement on Area under Load-Deformation Curve

| Fiber Combination | Average Area under Curve without External Flexural Reinforcement (lb) | Average Area under Curve with External Flexural Reinforcement (lb) | Percent Increase of Ultimate Load Due to Flexural Reinforcement |
|---|---|---|---|
| **ELASTIC REGION** | | | |
| 6 MM | 948.6 | 1,533.7 | 62% |
| 13 MM | 411.2 | 1,777.0 | 332% |
| 30 MM | 603.4 | 2,806.9 | 365% |
| 50 MM | 773.6 | 1,108.3 | 43% |
| 6&30 MM | 1,352.2 | 2,188.9 | 62% |
| 13&50 MM | 682.8 | 1,486.5 | 118% |
| **BETWEEN ELASTIC LIMIT AND ULTIMATE LOAD** | | | |
| 6 MM | 502.1 | 3,375.0 | 572% |
| 13 MM | 267.9 | 4,917.9 | 1,736% |
| 30 MM | 983.1 | 3,813.5 | 288% |
| 50 MM | 654.5 | 5,288.4 | 708% |
| 6&30 MM | 744.4 | 1,872.4 | 152% |
| 13&50 MM | 1,086.5 | 3,040.1 | 180% |
| **POST-ULTIMATE REGION** | | | |
| 6 MM | 1,936.5 | 4,757.1 | 146% |
| 13 MM | 3,021.9 | 8,241.5 | 173% |
| 30 MM | 3,307.0 | 7,132.4 | 116% |
| 50 MM | 3,452.1 | 5,316.8 | 54% |
| 6&30 MM | 5,498.2 | 8,089.3 | 47% |
| 13&50 MM | 6,021.7 | 5,534.0 | -8% |
| **ACCUMULATIVE** | | | |
| 6 MM | 3,387.2 | 9,665.8 | 185% |
| 13 MM | 3,701.0 | 14,936.4 | 304% |
| 30 MM | 4,893.4 | 13,752.8 | 181% |
| 50 MM | 4,880.2 | 11,713.5 | 140% |
| 6&30 MM | 12,150.5 | 12,150.5 | 0% |
| 13&50 MM | 7,791.0 | 10,060.6 | 29% |

# CHAPTER 5: DISCUSSION

## 1. Compression Tests

In the compression tests, two sets of concrete cylinders were tested to determine the compressive strengths and the compressive elastic modulus of the various mixes. The first set of cylinders that were tested to determine the compressive strengths had an age of 28 days. The second set of cylinders that were tested to determine the compressive elastic moduli had an age of 70 days. Although the age of concrete for both sets differed from one another, the cylinders within one set all had the same age. As this is the case, this issue should have negligible effect on the results, since this study investigates the difference of mechanical properties between mixes, and not the correlation between the compressive strength and compressive elastic modulus. The only parameter in the compression tests was the steel fiber combination present in each mix. When comparing the mechanical properties of the specimens, the average value is taken into account, and not the value of individual specimens.

The mixes with the greatest compressive strength to the mixes with the least compressive strength are as follows: 6 mm and 30 mm steel fibers, 13 mm and 50 mm steel fibers, 50 mm steel fibers, 30 mm steel fibers, 6 mm steel fibers and 13 mm steel fibers. The difference between the greatest and least compressive strengths was 2,016 psi. The various fiber combinations can be divided into three groups: straight steel fibers, hooked end steel fibers and hybrid steel fibers. The hybrid steel fibers contains both straight steel fibers and hooked end steel fibers. With these three groups in mind, it is evident the concrete with hybrid steel fibers had the greatest compressive strengths, the concrete with hooked end steel fibers had the intermediate compressive strengths and the concrete with straight steel fibers had the least compressive strengths.

In regards to the three groups, the concrete with the hybrid fibers resulted in the greatest compressive strengths due to the fact that voids created by the larger fibers were filled with the small fibers. The amount of the steel fibers alone is not a factor in ranking the compressive strengths in this study, otherwise the concrete with 5% volume of hooked end steel fibers would have a greater compressive strength than the concrete with 3.8% volume of 6 mm and 30 mm steel fibers and the concrete with 2.8% volume of 13 mm and 50 mm steel fibers. The concrete with hooked end steel fibers had greater compressive strengths than the concrete with straight steel fibers because the fiber volumes of the hooked end steel fibers were greater than the fiber volumes of the straight steel fibers. The concrete with hooked end steel fibers included 5% volume of 50 mm steel fibers and 3% volume of 30 mm steel fibers, whereas the concrete with straight steel fibers included 2% volume of 6 mm steel fibers and 1% volume of 13 mm steel fibers. The fact that the hooked end steel fibers are larger in size than the straight steel fibers might indicate that a greater fiber size increases the compressive strength, however, this presumption loses validity when taking into account that the concrete with 6 mm and 30 mm steel fibers had a greater compressive strength than the concrete with 13 mm and 50 mm steel fibers, and the concrete with 6 mm steel fibers had a greater compressive strength than the concrete with 13 mm steel fibers.

It is also noteworthy to examine the compressive strength ranking in each fiber group. In the group with hybrid steel fibers, the concrete with 6 mm and 30 mm steel fibers had a greater compressive strength than the concrete with 13 mm and 50 mm steel fibers because the concrete with 6 mm and 13 mm steel fibers had a greater fiber volume. The fiber volume of 6 mm and 30 mm steel fibers was 3.8%, whereas the fiber volume of

13 mm and 50 mm steel fibers was 2.8%. In the group with hooked end steel fibers, the concrete with 50 mm steel fibers had a greater compressive strength than the concrete with 30 mm steel fibers because the concrete with 50 mm steel fibers had a greater fiber volume. The fiber volume of 50 mm steel fibers was 5%, whereas the fiber volume of 30 mm steel fibers was 3%. In the group with straight steel fibers, the concrete with 6 mm steel fibers had a greater compressive strength than the concrete with 13 mm steel fibers because the concrete with 6 mm steel fibers had a greater fiber volume. The fiber volume of 6 mm steel fibers was 2%, whereas the fiber volume of 13 mm steel fibers was 1%.

The mixes with the greatest compressive elastic modulus to the mixes with the least compressive elastic modulus are as follows: 13 mm and 50 mm steel fibers, 6 mm and 30 mm steel fibers, 6 mm steel fibers, 13 mm steel fibers, 30 mm steel fibers and 50 mm steel fibers. The difference between the greatest and least compressive elastic moduli was 297 ksi. The concrete with hybrid steel fibers had the greatest compressive elastic moduli, the concrete with straight steel fibers had the intermediate compressive elastic moduli and the concrete with hooked end steel fibers had the least compressive elastic moduli.

In regards to the three groups, the amount of the steel fibers alone is not a factor in ranking the compressive elastic moduli in this study. The increase either in size of steel fibers or the fiber volume did not affect the compressive elastic modulus. This is indeed true otherwise the concrete with a greater fiber volume and greater size such as those present in the hooked end steel fiber group would have a greater compressive elastic modulus than the straight steel fiber group. One similarity between the concrete with hybrid steel fibers and the concrete with straight steel fibers alone is both contain fibers

that were mixed with the concrete prior to casting. In contrast, the hooked end steel fibers were preplaced in the mold. By having the fibers mixed with the concrete, the fibers were more likely to be more uniformly distributed throughout the concrete. After placing the hooked end steel fibers into the molds, the fibers at times would move during vibration of the concrete. In casting cylinders, it is possible that the amount of hooked end steel fibers and concrete added were not perfectly proportionate to one another throughout the mold. It is hypothesized that the hooked end steel fibers would be concentrated in some areas and sparser in other areas of the molds. This would cause the hooked end steel fibers to be less uniformly distributed than the straight steel fibers. The explanation as to why the hybrid fibers resulted in greater elastic moduli than the straight steel fibers is due to the fact that voids created by the larger fibers were filled with the small fibers.

To further enforce the reasoning on what affects and what does not affect the compressive elastic modulus, each group should be closer examined. Although the concrete with 13 mm and 50 mm steel fibers had a greater compressive elastic modulus than the concrete with 6 mm and 30 mm steel fibers, both essentially had the same compressive elastic modulus as their average values differed only by 1 ksi. Within the group with straight steel fibers, the concrete with 6 mm steel fibers had a greater compressive elastic modulus than the concrete with 13 mm steel fibers. A possible reasoning behind this is that either a smaller size of fibers or a lower fiber volume within the concrete attributes to a greater compressive elastic modulus. However, this reasoning is invalid since neither trend is consistent within the group with hybrid steel fibers and the group with hooked end steel fibers. The 13 mm and 50 mm steel fibers were larger in size than the 6 mm and 30 mm steel fibers, and the concrete with 13 mm and 50 mm steel

fibers had a lower fiber volume compared to the concrete with 6 mm and 30 mm steel fibers. Similarly to the group with straight steel fibers, the 30 mm steel fibers were smaller in size than the 50 mm steel fibers, yet the concrete with 30 mm steel fibers had a lower fiber volume than the concrete with 50 mm steel fibers. It may be hypothesized that reasoning behind the ranking of compressive elastic modulus follows that of the three groups of fibers. Neither the size of the fibers nor the fiber volume attributes to the compressive elastic modulus, but rather the uniformity of the fibers.

With the results of the compressive strengths and compressive elastic moduli, it is advisable to determine whether there is a relationship between the two mechanical properties in this study. An observation made consulting the results is that the ranking of the specimens according to compressive strength did not match the ranking of the specimens according to compressive elastic modulus. This also occurred in Catagay et. al's (2010) study, and it was concluded that there is not much correlation between compressive strength and compressive elastic modulus of steel-fiber reinforced concrete. The same conclusion can be proposed with this study, otherwise the ranking of these two mechanical properties would mirror one another.

**2. Flexural Tests**

In the flexural tests, two sets of concrete beams were tested to failure. The first set of beams were tested without external flexural reinforcement on the tension flange. The second set of beams were tested with external flexural reinforcement on the tension flange. Unlike, the cylinders, the beams tested did not all have the same age. Nonetheless, the effect of the age shall be discussed, in order to reinforce the aforementioned assumption. Although the age of concrete for most of the beams differed from one

another, the age of the concrete should not have an effect on the mechanical properties of the beams, as all beams were tested much later than 28 days, and theoretically the strengths stayed relatively constant. Specifically, the youngest age of the beams was 96 days. Both sets of beams had the same parameters, yet as the second set of beams were tested with external flexural reinforcement, the second set of beams had a few additional parameters. The mutual parameters of both sets of beams were the age, fiber volume, fiber size and shear reinforcement. The additional parameters of the beams with external flexural reinforcement were the width of the external flexural reinforcement on the tension flange and failure type, as some beams failed in shear due to an excessive flexural capacity and as a result other beams had their external flexural reinforcement reduced. When comparing the mechanical properties of the specimens, the average value is taken into account, and not the value of individual specimens.

**2.1 Beams without External Flexural Reinforcement**

The mixes with the highest ultimate load to the mixes with the lowest ultimate load are as follows: 6 mm and 30 mm steel fibers, 50 mm steel fibers, 30 mm steel fibers, 13 mm and 50 mm steel fibers, 6 mm steel fibers and 13 mm steel fibers. The difference between the highest and lowest ultimate loads was 1,257 lb. The percent volume of fibers had an effect on the ranking of the beams in regards to ultimate load. The ranking from highest fiber volume to lowest fiber volume is almost identical with that of the ranking of the ultimate load, with exception to the beams with 13 mm and 50 mm steel fibers. Comparing the rankings of the beams of a certain fiber content helps illustrate the fact that a greater fiber volume results in a beam experiencing a greater ultimate load. The fiber size does not seem to have a visible effect on the ultimate load of the beams,

otherwise the beams with 13 mm and 50 mm steel fibers would have experienced a greater ultimate load than the beams with 30 mm steel fibers.

As mentioned before, the age of the concrete plates that make up the beams do not affect the ultimate load of the beams. Since concrete strength is known to increase with time, it should have an effect on the ultimate load, however, if this was indeed the case then the beams with 50 mm steel fibers would have had a greater ultimate load than the beams with 6 mm and 30 mm steel fibers. If by any chance the age of the concrete does have an effect on the ultimate load, then it is substantially overshadowed by effect of fiber volume of the beams.

All except three beams had aluminum angles as shear reinforcement. The other three beams had basalt fiber as shear reinforcement. Due to the fact that all three beams of similar fiber type only had one type of shear reinforcement, there is no way to compare the aluminum angles and basalt fibers within a group of beams with a certain fiber content. Nevertheless, the only effect the shear reinforcement would have had on the beams would be the shear strength of the beams, but since these beams failed in flexure, the shear reinforcement does not affect the ultimate load in this case.

As for the other mechanical properties measured in this study such as the midspan deformation at the ultimate load, the elastic limit, midspan deformation at the elastic limit and the bending stiffness of the beams it remains inconclusive as to why the beams performed differently to one another. Through comparing the ranking of the different fiber combinations for these properties, there is no trend that can be seen that would explain why some beams experienced a certain load and corresponding midspan deformation compared to other beams.

**2.2 Beams with External Flexural Reinforcement**

The mixes with the highest ultimate load to the mixes with the lowest ultimate load are as follows: 30 mm steel fibers, 50 mm steel fibers, 6 mm and 30 mm steel fibers, 6 mm steel fibers, 13 mm steel fibers and 13 mm and 50 mm steel fibers. The difference between the highest and lowest ultimate load was 1,713 lb. The fiber volume had an effect on the ranking of the beams in regards to ultimate load. The ranking from highest fiber volume to lowest fiber volume is almost identical with that of the ranking of the ultimate load, with exception to the beams with 13 mm and 50 mm steel fibers. Comparing the rankings of the beams of a certain fiber content helps illustrate the fact that a greater fiber volume results in a beam with a greater ultimate load. The fiber size does not seem to have a visible effect on the ultimate load of the beams, otherwise the beams with 13 mm and 50 mm steel fibers would have experienced a greater ultimate load than the beams with 30 mm steel fibers. The beams with 50 mm steel fibers and 30 mm steel fibers experienced the greatest ultimate loads as their external flexural reinforcement was 3 inches wide, whereas the width of the external flexural reinforcement of the remaining beams was reduced to ensure a flexural failure. With this in mind, comparing the beams with similar widths of external flexural reinforcement, the ranking of the beams with the greatest to least ultimate loads is similar to the ranking of the beams without external flexural reinforcement. Another factor that had a role in possibly affecting the ranking of the beams in regards to ultimate load is how the beams failed. Three beams with external flexural reinforcement failed in shear, as opposed to flexure. These three beams included one beam with 6 mm steel fibers and two beams with 13 mm steel fibers. These beams failed in shear as their 3-inch wide external

flexural reinforcement made them too strong in flexure, and thus they were subjugated to a shear failure. When these beams are not considered as part of the average ultimate load for the fiber type they belong to, there is little to no change in the ranking, and hence the failure type has negligible effect on the ranking of the beams in terms of ultimate load in this study.

As mentioned before, the age of the concrete plates that make up the beams do not affect the ultimate load of the beams. Since concrete strength is known to increase with time, it should have an effect on the ultimate load, however, if this was indeed the case then the beams with 13 mm steel fibers would have had a greater ultimate load than the beams with 6 mm steel fibers. If by any chance the age of the concrete does have an effect on the ultimate load, then it is substantially overshadowed by effect of fiber volume of the beams.

All except five beams had aluminum angles as shear reinforcement. The other five beams had basalt fiber as shear reinforcement. Three of the beams with basalt fiber as shear reinforcement composed of 13 mm steel fibers, and as state before, due to the fact that all three beams of similar fiber type only had one type of shear reinforcement, there is no way to compare the performance of aluminum angles and basalt fibers among the beams with 13 mm steel fibers. However, three beams with 6 mm steel fibers included two beams with basalt fiber as shear reinforcement and one beam with aluminum angles as shear reinforcement. The one beam with aluminum angles had a much different ultimate load than the other two beams, but it was not because of the shear reinforcement, but rather that one beam failed in shear and had external flexural reinforcement 3 inches in width. The other two beams had their external flexural

reinforcement reduced from 3 inches to ensure a flexural failure, and thus had a lower ultimate load. Nevertheless, the only effect the shear reinforcement would have on the beams would be the shear strength of the beams, but since the beams were to fail in flexure, the shear reinforcement does not affect the ultimate load in this case.

As for the other mechanical properties measured in this study such as the midspan deformation at the ultimate load, the elastic limit, midspan deformation at the elastic limit and the bending stiffness of the beams it remains inconclusive as to why the beams performed differently to one another. Through comparing the ranking of the different fiber combinations for these properties, there is no trend that can be seen that would explain why some beams experienced a certain load and corresponding midspan deformation compared to other beams.

### 2.3 Load-deformation Curves of Beams with and without External Flexural Reinforcement

The load-deformation curves of the beams without external flexural reinforcement differed from those with external flexural reinforcement. Three main differences were observed between the two types of graphs. First, the load-deformation curves of the beams without external flexural reinforcement experienced a sudden drop in load after the elastic limit was reached, and then the curve continued to rise until the ultimate load was reached. The load-deformation curves of the beams with external flexural reinforcement showed no drop in load immediately after the elastic limit. In a stress-strain curve, the sudden drop after the elastic limit would correspond to the upper and lower yield points, and comparing the different curves in regards to this phenomenon is similar to comparing mild steel with aluminum. It is proposed that the basalt fiber on the

tension flange adds ductility to the beam, as materials with more ductility, such as aluminum, continuously transition into the plastic region as opposed to mild steel, which experiences upper and lower yield points. Secondly, the curves differed in shape and slope around the ultimate load. For the beams without external flexural reinforcement, whose load-deformation curves formed a relatively sharp apex around the ultimate load, the addition of external flexural reinforcement caused the load-deformation curves to form a parabola around the ultimate load. Similarly, for the beams without external flexural reinforcement, whose load-deformation curves formed a parabola around the ultimate load, the addition of external flexural reinforcement caused the load-deformation curves to flatten around the ultimate load. In both instances, the slope of the load-deformation curves around the ultimate load decreases with external flexural reinforcement. What occurred when the slope decreased before and after the ultimate load was that the beams were deforming more at a smaller load increment compared to the beams without external flexural reinforcement. This phenomenon leads to the conclusion that the basalt fiber increases the ductility of the beams. Lastly, the slope of the curves differed from one another after the ultimate load was reached. Beams that did not have external flexural reinforcement had load-deformation curves whose post-ultimate slope mimicked the slope of the load-deformation curve in the elastic region. In contrast, the post-ultimate slope of the load-deformation curves of beams with external flexural reinforcement were relatively large as the curves showed a sharp drop sometime after the ultimate load was reached. The sharp drop in load coincided with the failure of the basalt fibers on the tension flange of the beam, and as soon as the basalt fibers failed, the beams were no longer able to resist load. This shows that the post-ultimate behavior

of the beams rely heavily on the external flexural reinforcement, as the sharp decrease in load does not occur until the sole failure of the basalt fiber.

**2.4 Effect of External Flexural Reinforcement**

The external flexural reinforcement increased the average ultimate load of the beams from 45% to 73%. The beams ranked from greatest to least percent increase in ultimate load are as follows: 6 mm and 30 mm steel fibers, 13 mm and 50 mm steel fibers, 50 mm steel fibers, 6 mm steel fibers, 30 mm steel fibers and 13 mm steel fibers. Similar to the reasoning why certain beams experienced a greater ultimate load than others, the beams with a greater fiber volume generally tended to experience a greater percent increase in ultimate load. There were two exceptions however. The beams with 50 mm steel fibers, though greater in fiber volume, experienced a smaller percent increase of ultimate load compared to the beams with hybrid fibers. Additionally, the percent increase was larger for the beams with 6 mm steel fibers than the beams with 13 mm.

The ratio of the elastic limit to the ultimate load tends to decrease for beams with 6 mm steel fibers, 13 mm steel fibers and 50 mm steel fibers after incorporating the external flexural reinforcement. This decrease is a result of a greater difference in load between the elastic limit and ultimate load, and thus the plastic region is increased as it takes a greater load and deformation for the beams to reach ultimate once the elastic limit is achieved. The ratio of the elastic limit to the ultimate load tends to increase for beams with 30 mm steel fibers, 6 mm and 30 mm steel fibers and 13 mm and 50 mm steel fibers after incorporating the external flexural reinforcement. This increase is a result of a smaller difference in load between the elastic limit and ultimate load, thus the plastic

region is increased as it takes a smaller load and deformation for the beams to reach ultimate once the elastic limit is achieved.

The area under the load-deformation curve is related to the energy absorption of the beams. It is clear to see that the area under the load-deformation curves increased with the addition of external flexural reinforcement. Generally, the largest increase in area was in the plastic region between the elastic limit and the ultimate load. This signifies that the external flexural reinforcement was mainly effective in facilitating the beams to undergo more load and plastic deformation before reaching the ultimate load.

# CHAPTER 6: CONCLUSION AND RECOMMENDATIONS

## 1. Conclusion

Based on the results and discussion of the experimental investigation of this study, the following conclusions can be made:

- Built-up I-beams made with hybrid fibers SIFCON plates can be fabricated to support loads.
- It is possible to connect the SIFCON plates using an organic epoxy resin with aluminum angles and an inorganic epoxy with basalt fibers.
- The 1/8 in thick SIFCON plates were too slender to fabricate and work with to make the built-up I-beams.
- It was difficult to fabricate monolithic I-Beam using a three dimensional mold so as to avoid building individual plates and connecting them because the long fibers could not be uniformly distributed in the web and the flanges.
- Flexural behavior of built-up I-beams made from plates with hybrid-fiber was superior to those made from plates with one fiber type.
- Built-up I-beams reinforced with basalt fabrics at the bottom had higher flexural strength and ductility compared to unreinforced built-up I-beams.
- There is little correlation between the compressive strength and elastic modulus of concrete cylinders made with hybrid fibers.
- Concrete made with hybrid fibers of 50 mm hooked steel fibers and straight brass coated fibers had higher compressive strengths than concrete made with only straight steel fibers or with only hooked end steel fibers.
- Specimens with pre-placed steel fibers had higher elastic moduli compared to those specimens with fibers mix with concrete.

- The specimens with hybrid steel fibers show the higher elastic moduli due to the straight steel fibers filling the voids created by the larger hooked end steel fibers.
- Fibers that are more uniformly distributed within concrete had higher elastic modulus.
- Built-up beams reinforced with basalt fiber fabrics acting as external flexural reinforcement showed higher stiffness. The failure of the beams with external flexural reinforcement is reached only when the basalt fabric fails.

**2. Recommendations for Future Research**

The statements below are recommendations for future research and for improving this study.

- Fabricate and test three-dimensional monolithic I-beam and compare them to built-up I-beams.
- Determine tensile strength and tensile elastic modulus using a direct tension test.
- Fabricate and test built-up box beams made of SIFCON plates.
- Investigate further the use of the basalt fabrics for retrofit of built-up I-beams.
- Perform analytical study to for built-up beam design with and without basalt fabric.

## REFERENCES

ASTM C31. 2016. “Standard Practice for Making and Curing Concrete Test Specimens in the Field.” American Society for Testing and Materials.

ASTM C469. 2014. “Standard Test Method for Static Modulus of Elasticity and Poisson’s Ratio of Concrete in Compression.” American Society for Testing and Materials.

Abu-Obeidah, Adi Salman. 2012. “Behavior of Shear Deficient Reinforced Concrete Beams with Externally Bonded Aluminum Plates.” *Thesis*. Sharjah, United Arab Emirates: American University of Sharjah, June.

Ali, Nageh Mohammed, Xin Wang, Zhishen Wu and Ahmed Yehia Hassanein. 2015. “Basalt fiber reinforced polymer grids as an external reinforcement for reinforced concrete structures.” *Reinforced Plastics & Composites* 1615-1627.

Balaji, S. and G.S. Thirugnanam. 2013. “Flexural strengthening of reinforced concrete beams using precast SIFCON laminates.” *Journal of Structural Engineering* 262-267.

Cagatay, Ismail H. and Riza Dincer. 2011. “Modeling of concrete containing steel fibers: toughness and mechanical properties.” *Computers and Concrete* 357-369.

Caggiano, Antonio, Marco Cremona, Ciro Faella, Carmine Lima and Enzo Martinelli. 2012. “Fracture behavior of concrete beams reinforced with mixed long/short steel fibers.” *Construction and Building Materials* 832-840.

Jain, Kranti and Bhupinder Singh. 2013. “Flexural performance criteria for steel fibre reinforced concrete – an experimental investigation.” *Journal of Structural Engineering* 486-495.

Kotatkova, Jaroslava and Pavel Reiterman. 2014. “Effects of Different Types of Steel Fibers on the Mechanical Properties of High Strength Concrete.” *Advanced Materials Research* 80-84.

Liu, Kang. 2014. “Experimental Study on the Ductility of Beams with SIFCON Blocks.” *Applied Mechanics and Materials* 41-44.

Marar, Khaled, Ozgur Eren and Hooman Roughani. 2016. “The Influence of Amount and Aspect Ratio of Fibers on Shear Behaviour of Steel Fiber Reinforced Concrete.” *KSCE Journal of Civil Engineering* 1-7.

Nanni, Antonio. 1992. “PROPERTIES OF ARAMID-FIBER REINFORCED CONCRETE AND SIFCON.” *Journal of Materials in Civil Engineering* 1-15.

Ni, Kun, Yun Xin Shi, Yi Ning Ding, Yan Gang Zhang, Jing Bin Shi and Wei Liu. 2015. “Influence of Aspect Ratio of Hooked End Steel Fiber on Flexural Behavior of Fiber Reinforced Concrete.” *Key Engineering Materials* 560-564.

Pajak, M. and T. Ponikiewski. 2013. “Flexural behavior of self-compacting concrete reinforced with different types of steel fibers.” *Construction and Building Materials* 397-408.

Rahim, Mustaqqim Abdul, Zuhayr Md Ghazaly, Raja Nurazira Raja Mamat, Muhammed Azizi Azizan, Nur Fitriah Isa and Shahiron Shahidan. 2016. “Experimental Study of Slurry Infiltrated Fiber Reinforced Concrete.” *Materials Science Form* 363-366.

Shen, Deijan, Shucheng Deng, Jinyang Zhang, Wei Wang and Guoqing Jiang. 2015. “Behavior of reinforced concrete box beam with initial cracks repaired with basalt fiber-reinforced polymer sheet.” *Reinforced Plastics & Composites* 1540-1554.

Sashidhar, C., H. Sudarsana Rao, K. Gnaneswara and N.V. Ramana. 2011. “Flexural behavior of SIFCON produced with low tensile strength steel fibre.” *The Indian Concrete Journal* 37-41.

Shahidan, Shahiron, Mustaqqim Abdul Rahim, Nik Suharliza, Nik Zol, Muhammad Azizi Azizan and Isham Ismail. 2015. “Properties Of Steel Fiber Reinforcement Concrete With Different Characteristic Of Steel Fiber.” *Applied Mechanics and Materials* 28-32.

Shannag, M.J., S. Barakat and F. Jaber. 2001. “Structural repair of shear-deficient reinforced concrete beams using SIFCON.” *Magazine of Concrete Research* 391-403.

Sharma, Dr. H. K., V. P. Singh and Mukesh Kumar. 2008. “STRUCTURAL OPTIMIZATION AND PERFORMANCE OF SIFCON PLATES.” *7th WSEAS Int. Conference on APPLIED COMPUTER & APPLIED COMPUTATIONAL SCIENCE* 787-792.

Sim, Jongsung, Cheolwoo Park and Do Young Moon. 2015. “Characteristics of basalt fiber as a strengthening material for concrete structures.” *Composites Part B: Engineering* 504-512.

Thirugnanam, G.S., P. Govindan and A. Sethurathnam. 2001. “Ductile behavior of SIFCON structural members.” *Journal of Structural Engineering* 27-32.

Uygunoglu, Tayfun. 2008. “Investigation of microstructure and flexural behavior of steel-fiber reinforced concrete.” *Materials and Structures* 1441-1449.